Calcium Signals in the murine Zona Glomerulosa

vorgelegt von

M. Sc.

Hoang An Dinh

an der Fakultät II – Mathematik und Naturwissenschaften

der Technischen Universität Berlin

zur Erlangung des akademischen Grades

Doktorin der Naturwissenschaften

- Dr. rer. nat. -

genehmigte Dissertation

Promotionsausschuss:

Vorsitzende: Prof. Dr. Franziska Heß
Gutachter: Prof. Dr. Thomas Friedrich
Gutachter: Prof. Dr. Andrew Plested
Gutachter: Dr. Gabriel Stölting

Tag der wissenschaftlichen Aussprache: 02. Februar 2024

Berlin 2024

Zusammenfassung

In der Zona glomerulosa (ZG) der Nebenniere spielt Kalzium eine zentrale Rolle bei der Stimulation der Aldosteronproduktion. Aldosteron ist ein Stereoidhormon, welches die Salz-Wasser-Homöostase und somit den Blutdruck reguliert. Spannungsabhängige Kalziumkanäle sind entscheidend für die Kontrolle der intrazellulären Kalziumkonzentration ($[Ca^{2+}]_i$) in ZG-Zellen.

Die Stimulation von ZG-Zellen durch die primären Stimuli Angiotensin II (Ang II) oder Kalium führt zu Oszillationen sowohl im Membranpotential als auch in der $[Ca^{2+}]_i$. Dieser Anstieg in der $[Ca^{2+}]_i$ ist das Signal für die Aldosteronsynthese.

Die unverzichtbare Rolle des T-Typ Kalziumkanals $Ca_V3.2$ für die Erzeugung von Membranpotentialoszillationen wurde postuliert, seine genaue Rolle bei der Erhöhung der $[Ca^{2+}]_i$ ist jedoch noch nicht vollständig geklärt. Sollte $Ca_V3.2$ auch für Oszillationen in der $[Ca^{2+}]_i$ erforderlich sein, wie er es für die Generierung der Membranpotentialoszillationen ist, erwartet man bei einer Deletion des $Ca_V3.2$ eine Abnahme der Aldosteronspiegels.

Mäuse, die $Ca_V3.2$ nicht exprimieren, zeigten jedoch keine Veränderungen der Aldosteronspiegel, was auf das Vorhandensein zusätzlicher Kalziumeinstromwege hinweist. Um diese Wege in $Ca_V3.2$-defizienten Mäusen zu untersuchen, wurden Kalzium-Imaging, RNA-Sequenzierung und Whole-Cell Patch-Clamp-Aufzeichnungen durchgeführt.

In Abwesenheit von $Ca_V3.2$ blieben die Kalziumoszillationen in ZG-Zellen bestehen. Diese wurden durch L-Typ Kalziumkanäle vermittelt. Die akute Hemmung der T-Typ Kalziumkanäle führte zu einer unvollständigen Unterdrückung des Ang II-vermittelten Kalziumeinstroms in ZG-Zellen von Wildtyp-Tieren. Stattdessen zeigte eine Untergruppe von Zellen immer noch einen oszillierenden Kalziumeinstrom, der über L-Typ Kalziumkanäle vermittelt wurde. Darüber hinaus induziert Ang II ausschließlich durch die Rekrutierung von T- und L-Typ Kalziumkanälen und ohne Beteiligung intrazellulärer Kalziumspeicher die Erhöhungen der $[Ca^{2+}]_i$.

Diese Ergebnisse zeigen, dass sowohl T- als auch L-Typ Kalziumkanäle eine entscheidende Rolle bei der Regulation des Kalziumeinstroms in ZG-Zellen unter physiologischen Bedingungen spielen. Dies hat bedeutende Implikationen für pharmakologische Interventionen und stellt die Hypothese in Frage, dass die alleinige Hemmung von T-Typ Kalziumkanälen die Aldosteronsynthese effektiv senken könnte. Unsere Ergebnisse lassen vermuten, dass die alleinige Inhibition von T-Typ Kalziumkanälen zu einem kompensatorischen Kalziumeinstrom über L-Typ Kanäle führen würde.

In menschlichen ZG-Zellen werden primär T-Typ und L-Typ Kalziumkanäle exprimiert. Mutationen in diesen Kanälen sind mit primärem Aldosteronismus (PA) assoziiert, einer Erkrankung, die weltweit etwa 50 Millionen Menschen betrifft. PA ist durch eine übermäßige Aldosteronproduktion gekennzeichnet, die zu Bluthochdruck führt. Bei Patienten mit PA wurden Mutationen in den Genen *CACNA1H* (kodiert den $Ca_V3.2$ Kanal) und *CACNA1D* (kodiert den L-Typ Kalziumkanal $Ca_V1.3$) identifiziert. Diese Mutationen tragen zu einem erhöhten Kalziumeinstrom und erhöhten Aldosteronspiegeln bei.

In dieser Arbeit wurden die Auswirkungen einer der Mutationen im *CACNA1H* Gen auf die Kalziumsignale in ZG-Zellen mit Hilfe eines Mausmodells untersucht. Diese Mäuse weisen die Mutation M1560V/+ im *Cacna1h* Gen auf, die mit PA assoziiert ist.

ZG-Zellen dieser Tiere zeigten ein erhöhtes $[Ca^{2+}]_i$. Dies lässt vermuten, dass in diesem Fall eine spezifische Blockade des $Ca_V3.2$-Kanals das Potenzial hätte, die Kalziumspiegel zu senken und den pathologischen Phänotyp zu lindern.

Das *Cacna1d*$^{I772M/+}$-Mausmodell spiegelt den menschlichen Phänotyp von PA wider, einschließlich erhöhter $[Ca^{2+}]_i$ und Aldosteronspiegel sowie neurologischen Auffälligkeiten. Die Behandlung dieser Mäuse mit dem L-Typ-Kanal-Inhibitor Isradipin führte zu einer Verringerung der $[Ca^{2+}]_i$, einer Abnahme des Aldosteronspiegels und einer Verbesserung der motorischen Funktion.

Diese Ergebnisse legen nahe, dass Patienten mit PA aufgrund von Mutationen in Kalziumkanälen von einer Behandlung mit kanalspezifischen Inhibitoren profitieren könnten.

Bei erhöhter Aldosteronsynthese ohne spezifische Kalziumkanal-Mutation würde jedoch die Inhibition eines einzelnen Kanaltyps, T-Typ oder L-Typ, den Aldosteronspiegel langfristig nicht effektiv senken, da jeder Kanaltyp in Abwesenheit des anderen die Kalziumaktivität vermitteln kann. Diese Erkenntnisse zur Rolle von Kalziumkanälen in ZG-Zellen haben wichtige Auswirkungen auf die Entwicklung zielgerichteter therapeutischer Strategien, die das Ziel haben, die Aldosteronproduktion zu reduzieren.

Abstract

Within the adrenal gland's zona glomerulosa (ZG), calcium plays a central role in stimulating aldosterone production, a hormone critical for maintaining salt-water balance and blood pressure regulation. Voltage-gated calcium channels (VGCCs) are key components responsible for controlling intracellular calcium levels ($[Ca^{2+}]_i$) in ZG cells. Stimulation of ZG cells by angiotensin II (Ang II) or potassium elicits oscillations in both membrane potential and $[Ca^{2+}]_i$ providing the signal for aldosterone synthesis.

While the involvement of the T-type VGCC $Ca_V3.2$ in generating membrane potential oscillations has been suggested, its precise role in elevating $[Ca^{2+}]_i$ remains incompletely understood.

If $Ca_V3.2$ is also needed for oscillations of $[Ca^{2+}]_i$ as it is for the membrane potential, one would expect a decrease in aldosterone levels.

However, mice lacking the $Ca_V3.2$ did not display altered aldosterone levels, indicating the presence of additional calcium influx pathways.

To investigate these pathways in $Ca_V3.2$-deficient mice, a range of techniques, including calcium imaging, RNA-sequencing, and whole-cell patch-clamp recordings, was employed.

Surprisingly, calcium oscillations persisted in the absence of $Ca_V3.2$ and were mediated by L-type calcium channels. Acute inhibition of T-type calcium channels did not fully abolish Ang II-mediated calcium influx in wild-type ZG cells. Instead, a subset of cells still exhibited oscillatory calcium influx via L-type calcium channels. Furthermore, Ang II induces increases in $[Ca^{2+}]_i$ within ZG cells exclusively through the recruitment of T- and L-type calcium channels, without involvement of intracellular calcium stores.

These findings emphasize the vital roles played by both T-type and L-type calcium channels in regulating calcium influx in ZG cells under physiological conditions. These observations also have significant implications for pharmacological interventions, challenging the notion that inhibiting T-type calcium channels alone can effectively lower aldosterone synthesis, as compensatory calcium influx via L-type channels would occur.

In human ZG cells, T-type and L-type calcium channels are the predominantly expressed VGGCs, and mutations in these channels are associated with primary aldosteronism (PA), a condition characterized by excessive aldosterone production leading to hypertension and cardiovascular risks and impacting approximately 50 million individuals globally. Mutations in *CACNA1H* (encoding $Ca_V3.2$) and *CACNA1D* (encoding $Ca_V1.3$, L-type VGCC) genes have been identified in PA patients, contributing to increased calcium influx and elevated aldosterone levels.

This work further investigated the impact of two mutations in these channels on cal-

cium signaling. Calcium imaging in ZG cells of *Cacna1h*$^{M1560V/+}$ mice, displayed heightened $[Ca^{2+}]_i$, suggesting the potential of specific $Ca_V3.2$ channel blockade to lower calcium levels and alleviate the pathological phenotype.

The *Cacna1d*$^{I772M/+}$ mouse model closely mirrors the human phenotype of PA, including elevated $[Ca^{2+}]_i$ and aldosterone, along with neurological abnormalities.

Treatment of these mice with the L-type channel inhibitor isradipine resulted in reduced $[Ca^{2+}]_i$, decreased aldosterone production, and improved motor function.

These findings suggest that patients with PA due to mutations in VGGCs may benefit from treatment with channel-specific inhibitors.

However, in cases of elevated aldosterone synthesis without a specific VGCC mutation, a single-channel inhibition, whether T-type or L-type, may not suffice to effectively lower aldosterone levels, as each channel sustains calcium activity in the absence of the other. These insights into calcium channel regulation in ZG cells have important implications for developing targeted therapeutic strategies.

Contents

1 Introduction

1.1 The role of calcium in biological systems

Calcium plays a pivotal role in transmitting signals to nearly all critical cellular functions, including secretion, muscle contraction and gene-regulatory events[1]. Due to its indispensable role in cellular processes, unregulated spatial and temporal fluctuations of calcium within cells can lead to a spectrum of severe cellular dysfunctions, ultimately resulting in cell death[2,3].

Calcium ions (Ca^{2+}) act as intracellular messengers. Therefore, the intracellular Ca^{2+} concentration ($[Ca^{2+}]_i$) needs to be rigorously controlled at low basal levels to avoid excessive energy expenditure required for the modulation of the $[Ca^{2+}]_i$. A large array of proteins has evolved to facilitate the transportation or reversible binding of calcium ions regulating the $[Ca^{2+}]_i$ within cells. Due to the distinctive coordination chemistry of calcium, it is possible to sustain very low intracellular concentrations of this ion, enabling it to function effectively as a signaling molecule.

In this context, calcium demonstrates a notable advantage over other coexisting divalent metals, particularly magnesium, which was significantly more abundant in the primordial seawater where life originated[4]. The inherent flexibility in calcium's coordination properties allowed it to be it highly amenable to interaction with sites characterized by irregular geometries, such as those presented by complex biomolecules, e.g. proteins[5]. Ca^{2+} typically features coordination numbers ranging from 6 to 8, which can be extended up to 12, and a variable bond length and angle[3].

In contrast, magnesium's smaller ionic radius (0.65 Å compared to calcium's 0.99 Å, Table 1) and substantially lower polarizability requires a fixed octahedral geometry involving six coordinating ligands with minimal variability in bond lengths. As a result, coordinating ligands are less prone to accommodate magnesium due to its lack of coordination flexibility[3,6].

Table 1. *Comparison of ion radii[6].*

Compound	ionic radius [Å]
Na^+	0.95
Cl^-	1.81
K^+	1.33
Ca^{2+}	0.99
Mg^{2+}	0.65
Zn^{2+}	0.74

The advantages of the coordination chemistry of calcium facilitate the modulation of its intracellular concentration enabling it to function as a signal carrier. The reduction in cellular calcium levels is a requisite for the effective execution of signalling processes.

Typically, the cytosol of most cells maintains a free calcium concentration within the range of low-to-mid nmol/l, which is about 10 000 times lower than the extracellular environment where calcium concentrations range from 2.1 to 2.6 mmol/l[5,7–9]. However, certain intracellular organelles known as "Ca^{2+} stores" possess the ability to accumulate calcium and uphold a higher $[Ca^{2+}]_i$ compared to the cytoplasm (typically within the range of 100 µmol/l to 5 mmol/l)[10,11]. The endoplasmic reticulum represents the main internal reservoir for calcium storage.

Diverse cellular stimuli, including events like membrane depolarization or the presence of extracellular signaling molecules, induce elevations of $[Ca^{2+}]_i$ from their low-nanomolar baseline to 1 µmol/l or higher, thereby generating a calcium signal. The return to low $[Ca^{2+}]_i$ mainly relies on the actions of the plasma membrane calcium transport ATPase[12] and the Na^{2+}/Ca^{2+}-exchanger transporting Ca^{2+} across the plasma membrane[13] as well as the sarcoendoplasmic reticulum calcium ATPase replenishing calcium stores in the endoplasmic reticulum/sarcoplasmic reticulum[12]. These proteins are capable of sensing and becoming activated by Ca^{2+}, thereby ensuring homeostatic control of $[Ca^{2+}]_i$.

Besides proteins that facilitate the translocation of Ca^{2+} across cellular membranes (e.g. calcium channels and transporters), low $[Ca^{2+}]_i$ is also maintained by proteins that buffer Ca^{2+} through direct binding (primarily proteins harboring a Ca^{2+}-binding EF-hand motif, e.g. calmodulin[14] and calcineurin[15]). Besides their buffering role, these proteins are also able to convey and process calcium-mediated information. Enzymes, for instance, exhibit alter-

ations in their catalytic activity upon Ca^{2+} binding, thus propagating the signal downstream.

Calcium plays a pivotal role in regulating almost every facet of cellular functions, including processes such as secretion, gene expression, muscle contraction, and metabolism[1]. Unregulated elevations in $[Ca^{2+}]_i$ would compromise the proper functioning of these cellular processes. Therefore, it is imperative to guarantee both spatial and temporal regulation of $[Ca^{2+}]_i$.

1.2 Voltage-gated calcium channels

Voltage-gated calcium channels (VGCCs) play a crucial role in many physiological processes in excitable as well as non-excitable cells. VGGCs can be found in various tissues throughout the body, including the brain, kidneys, muscle, pancreas and other endocrine tissues[16]. Upon membrane potential depolarization, VGCCs are activated and become permeable. The typical concentration gradient between extra- and intracellular Ca^{2+} levels generates an influx of calcium along its electrochemical gradient. This increase in intracellular calcium initiates various events in a variety of cell types including the release of hormones[17–19] and neuro-transmitters[20,21], the calcium-dependent transcription of many genes[22,23] as well as spontaneous pacemaker activity[24,25].

VGCCs are complex proteins comprising a pore-forming α_1-subunit and up to four auxiliary subunits (α_2, β, γ, and δ, Fig. 1)[26]. The α_1-subunit is the largest subunit (~200 kDa) and is ancestrally and structurally most closely related to the pore-forming subunits of voltage-gated sodium (Na_v) and potassium channels. All three channel types belong to a large super family of (cat-)ion channel proteins consisting 143 members[27].

The pore-forming subunits of both Ca^{2+} and Na^+ channels are composed of four homologous transmembrane (TM) domains in a single polypeptide chain (Fig. 2)[28]. Each of the domains comprises six TM helices (S1-S6) plus a pore loop (p-loop) motif between segments S5 and S6 forming the conduction pore and ensuring selectivity for calcium ions[29]. The S4 segment constitutes positively charged residues that are crucial for voltage sensitivity allowing the channel to open in response to membrane depolarization[30].

The three linkers between the four TM domains are facing the cytoplasm. These loops as well as the intracellular amino- and carboxy-termini serve as important interaction sites for channel regulation mediated by second messengers[31].

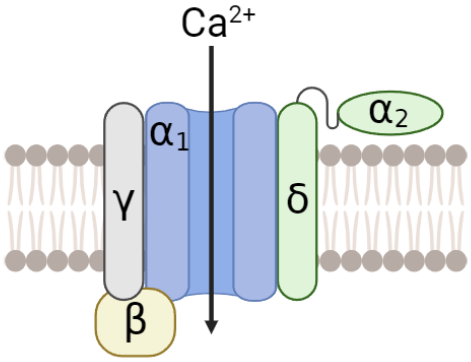

Figure 1. The general structure of VGCCs. *They are heteromultimers comprising a pore-forming α_1-subunit plus up to four auxiliary subunits (α_2, β, γ, and δ), which modulate the biophysical properties of the α_1-subunit. $Ca_V1.x$ and $Ca_V2.x$ α_1-subunits require association with the auxiliary subunits to form functional channel proteins. $Ca_V3.x$ α_1-subunits can function as channel monomers.*

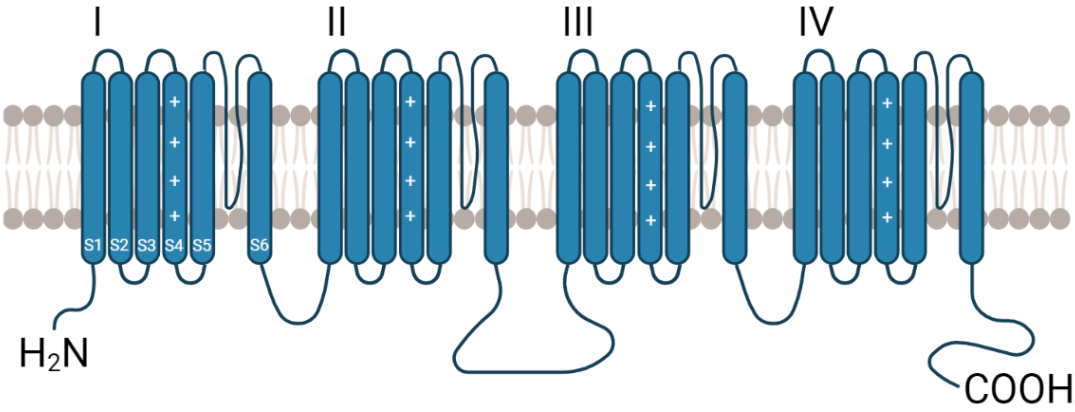

Figure 2. Transmembrane topology model of the α_1-subunit of VGCCs. *Transmembrane (TM) domains I–IV and segments S1–S6 are indicated. The voltage sensing S4 helix is highlighted.*

Through phylogenetic and protein family analyses the most likely evolutionary path of the voltage gated ion channel superfamily has been deduced[32]. It is assumed that the structure of the 6 TM helices within a TM domain evolved from a basic motif comprising two TM helices and a loop (Fig. 3A)[33]. This basic structure is though to be the precursor of the S5 and S6 helices within a TM domain.

Further evolution added four TM helices including the positively charge S4 helix responsible for voltage sensitivity. The S1-S4 motive can also be found in other voltage-sensing proteins, e.g. voltage-sensor-containing phosphatase Ci-VSP[34] and voltage-gated proton channel H_V1[35]. The addition of the four TM helices gave rise to the 6 core helices of a TM domain observed in the bacterial sodium channel NaChBac[36] and voltage-gated potassium channels[37] (Fig. 3B).

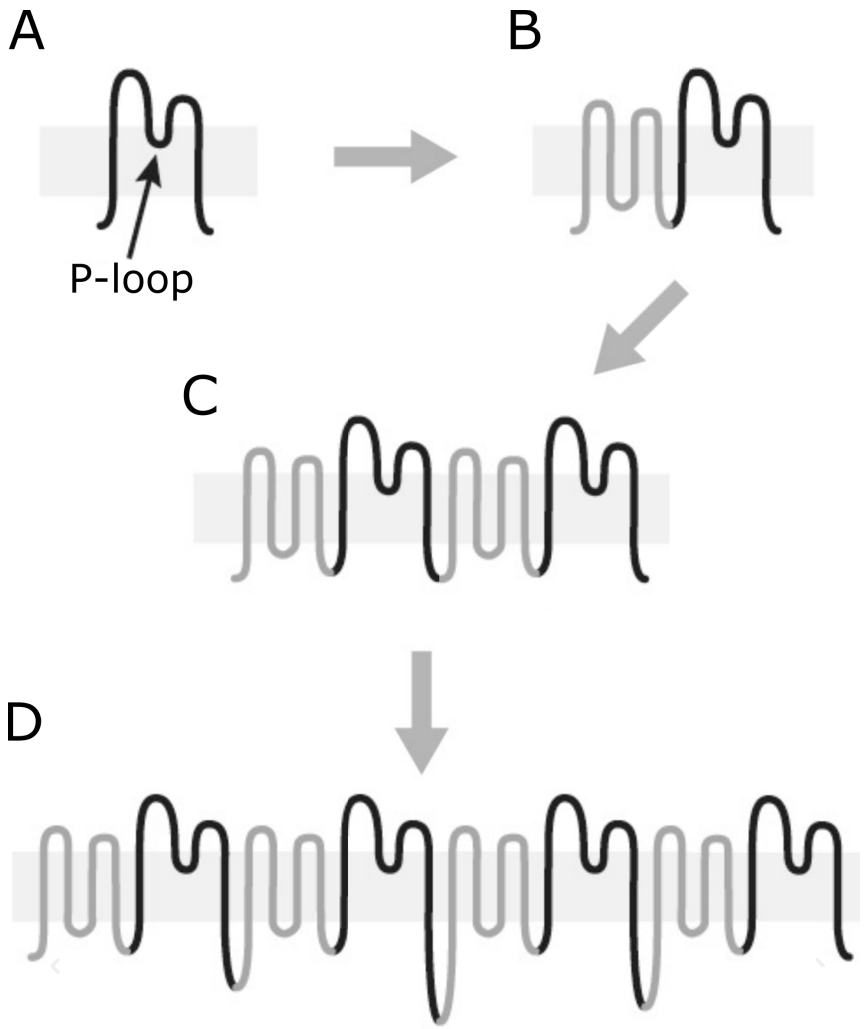

Figure 3. Evolution of the fundamental α_1-subunit structure of VGCCs. ***(A)*** *Evolution of the pore-forming subunit of VGCCs structure is thought to have started with a configuration featuring two TM segments coupled with a P-loop motif.* ***(B)*** *This was followed by the addition of a voltage-sensing helix being part of a segment comprising four TM helices.* ***(C-D)*** *Based on sequence similarity analysis, it is postulated that the development of the 4x6 TM structure in VGCCs can be attributed to two successive gene duplication events. Adapted from*[32]*.*

Duplications first gave rise to the two TM domain-comprising channels (like two-pore channels, Fig. 3C) and then to the four TM domain-spanning channel structures found in Na_v and voltage-gated Ca^{2+} channels (Ca_v) (Fig. 3D)[38,39]. Several ion channel types and motifs identified in eukaryotes can be found in prokaryotes. Therefore, the evolution of many ancestral ion channel types, including Na_v and Ca_v, appears to have taken place early in ancestral prokaryotes highlighting their importance[40,41].

In mammals, the family of the pore-forming α_1-subunits comprises ten members (en-

coded by genes *CACNA1A* to -*I* and -*S*), which can be divided into three subfamilies, the Ca_V1, Ca_V2 and Ca_V3 channels, based on their electrophysiological and pharmacological properties (Fig. 4)[28].

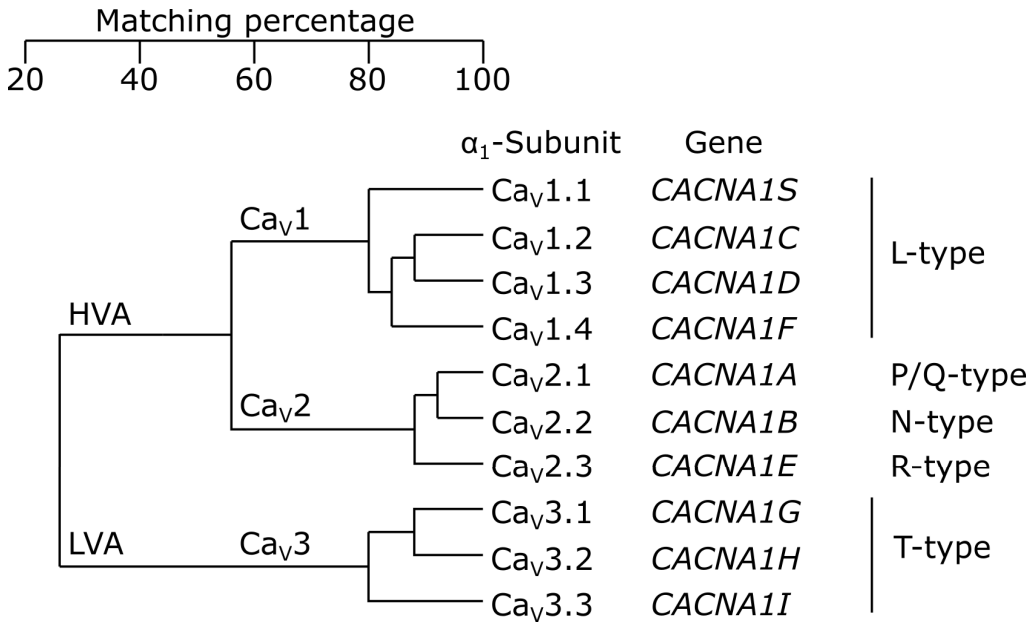

Figure 4. Evolutionary tree of the α_1-subunits of VGCCs. *The tree is based on an aligment of the putative membrane-spanning regions and pore loops of the human channels. The scale represents the percentage of identity between the α_1-subunits of VGCCs. Low-voltage-activated (LVA, Ca_V3 or T-type subfamily) VGCCs seem to have evolved separately from an ancestral Ca^{2+} channel prior to the split of the high-voltage-activated (HVA) channel family into Ca_V1 (L-type subfamily) and Ca_V2 subfamilies. Adapted from[42].*

Ca_V1 and Ca_V2 calcium channels are classified as high voltage-activated (HVA) as they require larger membrane depolarizations to open than the low-voltage activated (LVA) Ca_V3 calcium channels[43,44].

The Ca_V1 family includes four channels ($Ca_V1.1$ to $Ca_V1.4$). They were classified as **L**-type calcium channels due their **l**arger single-channel conductance (approx. 2-3 times greater than Ca_V3) and slower inactivation kinetics resulting in **l**arger **l**ong-lasting calcium currents compared to Ca_V3 channels[28,45]. L-type calcium channels can be distinguished from other HVA channels by their larger sensitivity to dihydropyridines (DHPs).

The Ca_V2 family comprises P/Q- ($Ca_V2.1$), N- ($Ca_V2.2$) and R-type ($Ca_V2.3$) channels. The $Ca_V2.1$ and 2.2 channels were identified due to their insensitivity to DHPs but sensitivity to agatoxin and conotoxin, respectively[46]. The R-type ($Ca_V2.3$) calcium currents are

resistant to DHPs and the P/Q- and N-type to channel toxins.

Members of the Ca_V3 family ($Ca_V3.1$-$Ca_V3.3$) were termed as **T**-type calcium channels as they exhibit small single-channel conductances and fast inactivation kinetics leading to smaller ("**t**iny") **t**ransient calcium currents compared to L-type Ca_V1 channels[47,48]. Ca_V3 channels are relatively insensitive to DHPs as well as to the toxins that block Ca_V2 channels[42].

$Ca_V1.x$ and $Ca_V2.x$ calcium channels require association with the auxiliary subunits in order to form properly functioning channels[49]. In contrast, $Ca_V3.x$ channels function as α_1 subunit monomers[50]. All ten $\alpha_1$subunits are known to undergo alternative splicing which gives rise to additional functional diversity[51]. The auxiliary subunits also form splice variants, thus fine-tuning the biophysical properties of the calcium channels[26].

As tight control over $[Ca^{2+}]_i$ is crucial (see Section 1.1), even minor dysregulation of VGCC activity can cause various diseases. This ranges from cardiovascular disorders to neurological and psychiatric conditions such as epilepsy and autism[52–54].

1.3 The zona glomerulosa and aldosterone

The adrenal glands are paired endocrine glands found above the kidneys (Fig. 5)[55]. Each gland is encased by a capsule and comprises an outer cortex producing steroid hormones from the same precursor cholesterol and an inner medulla producing catecholamines. The adrenal cortex itself is further divided into three layers: the outermost zona glomerulosa (ZG), the zona fasciculata (ZF) and the innermost zona reticularis (ZR) (Fig. 5).

The ZG lies directly below the capsule and comprises densely packed cell clusters (glomeruli) and is responsible for the production of aldosterone. The ZF consists of cells arranged in parallel columns synthesizing cortisol in humans and corticosterone in rodents. The ZR, which is found in humans and other mammals but not in mice and rats, is responsible for androgen synthesis.

In young (8 days of age postnatal) female and male mice an additional zone is present between the ZF of the cortex and the inner medulla[56]. This zone is termed X-zone and disappears in male mice during puberty (before 40 days of age)[57]. In female mice the X-zone undergoes regression at 5–15 days of their first pregnancy[58]. Without pregnancy, the X-zone in female mice regresses gradually between 3 and 7 months of life. It is suggested

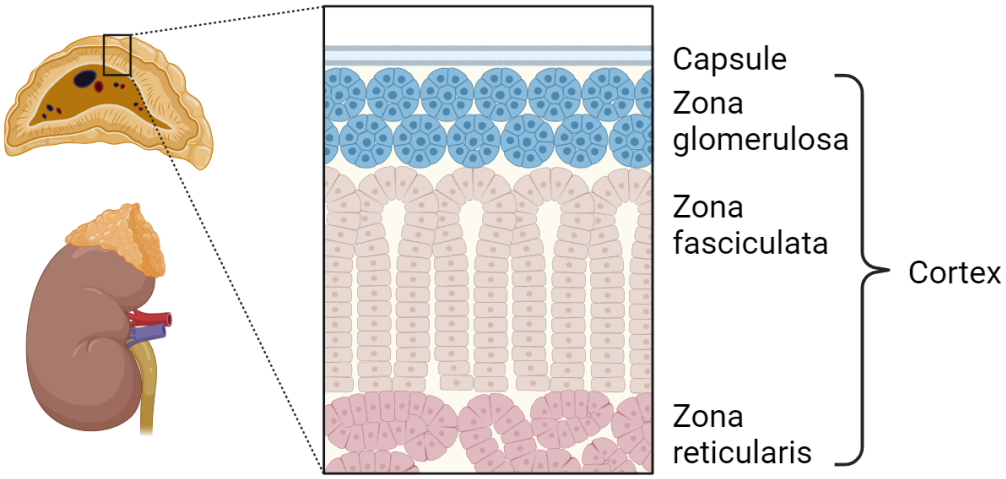

Figure 5. Location of the adrenal gland its outer layers. *The adrenal glands are located above the kidneys. The adrenal cortex consists of three cell layers, the zona glomerulosa (producing aldosterone), zona fasciculata (producing either cortisol in humans or corticosterone in mice) and in humans the zona reticularis (producing androgens).*

that this zone and the fetal zone in humans represent analogous structures, as they share molecular, functional and phenotypic characteristics[59].

The fetal zone in humans disappears within the first two to three weeks after birth[60]. It was proposed that the X-zone serves similar functions as the outer cortical zones but is not the main site of steroid hormone production[56].

In human ZG cells, T- and L-type are the predominantly expressed VGCCs[52,61–63]. Among the Ca_V3 familiy, $Ca_V3.2$ has been found to be the most highly expressed sub-type and besides this channel, only $Ca_V3.1$ showed relevant mRNA levels in the ZG[63]. Among the L-type VGCCs, mainly $Ca_V1.2$ and 1.3 are expressed[52,63] while no mRNA of $Ca_V1.1$ and $Ca_V1.4$ were detected[63]. In ZG cells, differences in VGCCs vary little between species. Studies of rodent[64,65] and bovine[66] ZG cells demonstrated the presence of both T- and L-type channels with $Ca_V3.2$ being the main T-type channel component[67].

Aldosterone plays a crucial role in the maintenance of electrolyte and fluid balance, thus regulating blood pressure[68]. The aldosterone production in the ZG is mainly controlled by two physiological stimuli: reduction of extracellular fluid volume and elevated serum potassium levels (hyperkalemia). Upon volume depletion, renin is released from the kidney leading to the production of the peptide hormone angiotensin II (Ang II) (Fig. 6)[69,70].

The stimulation of ZG cells with Ang II or increases in extracellular K^+ is transduced into a signal for aldosterone synthesis via a depolarization of the cells from a their resting membrane potential (primarily maintained by potassium channels at approximately -75 mV

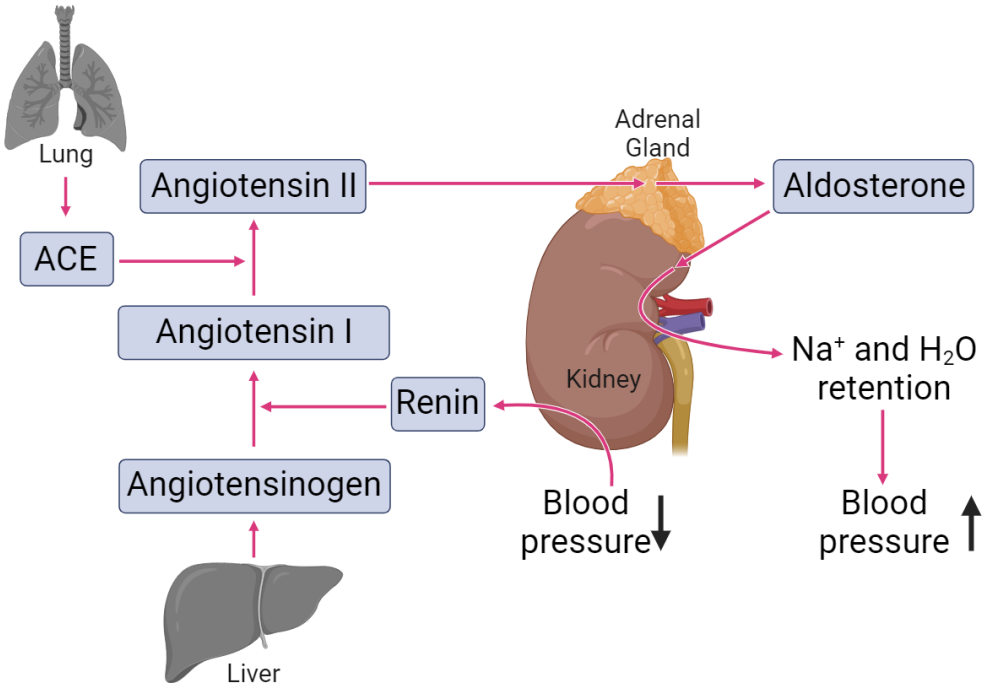

Figure 6. Schematic representation of the Renin-Angiotensin-Aldosterone System (RAAS). *A drop in blood pressure activates the RAAS leading to the conversion of Angiotensinogen to Angiotensin I, the precursor of Ang II. Subsequently, Ang II is generated from Ang I by the angiotensin-converting enzyme (ACE, produced mainly in the lung) and stimulates aldosterone synthesis in the adrenal gland. Aldosterone acts on the kidney promoting sodium and water reabsorption and potassium excretion*[69,70]*.*

(Fig. 7)[25,55,71]. This leads to the influx of Ca^{2+} through VGCCs, which controls key events in the aldosterone production.

The mechanism of Ang II-induced increases in $[Ca^{2+}]_i$ involves its binding to the G protein-coupled angiotensin II type 1 receptor (AT1R). This activates phospholipase C (PLC), which cleaves phosphatidylinositol-4,5-bisphosphat (PIP_2) into inositol trisphosphate (IP_3) and diacylglycerol (DAG). This results in the inhibition of background potassium channels thus leading to depolarization and activation of VGCCs[72,73]. Additionally, the release of Ca^{2+} from intracellular stores is supposedly triggered by IP_3 increasing $[Ca^{2+}]_i$ and subsequently promoting aldosterone production[74]. Increases in extracellular K^+ levels directly depolarize ZG cells initiating calcium influx[71].

Calcium is required for the activation of transcription factors that promote the expression of the *STAR* (encoding the steroidogenic acute regulatory protein, StAR) and *CYP11B2* genes (encoding the aldosterone synthase). One of the rate-limiting steps during aldosterone synthesis is the transport of cholesterol to the inner mitochondrial membrane, which

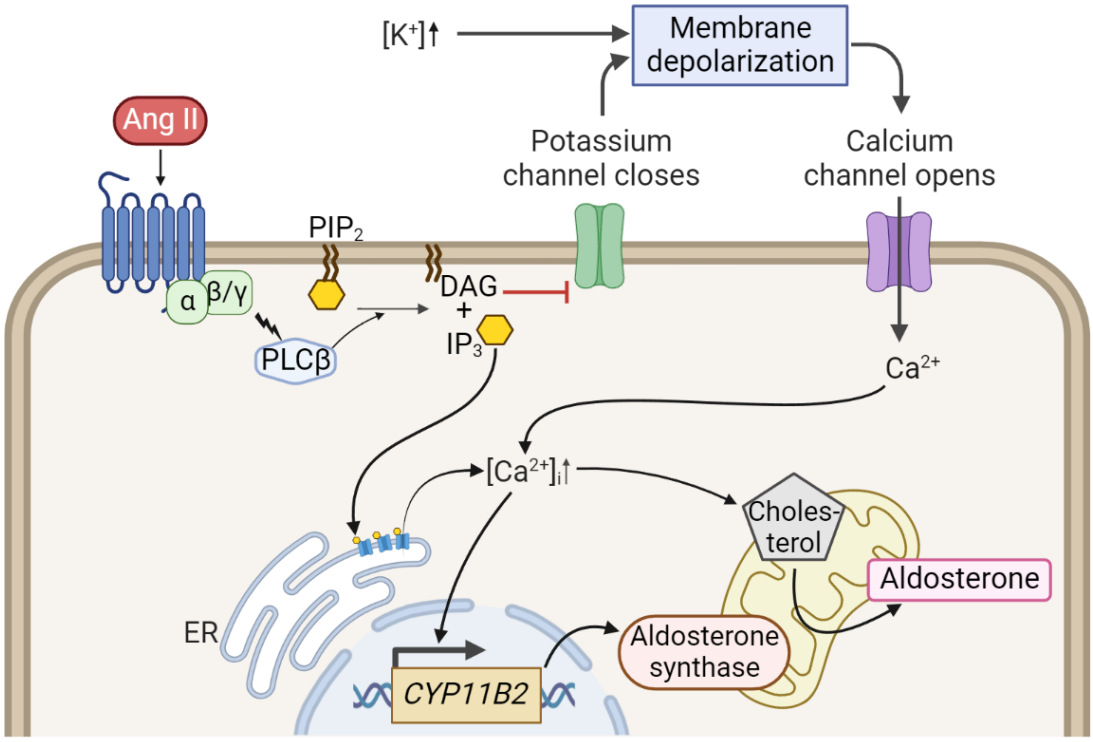

Figure 7. Calcium signaling in ZG cells. *Increases in $[Ca^{2+}]_i$ can take place through activation of VGCCs and binding of ang II to its G protein-coupled receptor. Both mechanisms lead to a deploarization of the cell membrane. Additionally, increases in extracellular K+ levels directly depolarize the cell. Ang II triggerd formation of IP3 release can also lead to increases in $[Ca^{2+}]_i$ via opening of Ca^{2+} stores (e.g. the ER). The rise in $[Ca^{2+}]_i$ promotes the transcription of the aldosterone synthase (gene CYP11B2) and facilitates the transport of cholesterol into the mitochondria, where it is converted to aldosterone. Taken from*[75].

is facilitated by the StAR protein.

Cholesterol is then converted to aldosterone through a series of enzymatic steps with the aldosterone synthase catalyzing the last rate-limiting step (Fig. 8).

Calcium is also needed for the regeneration of NAD^+ to NADH, which is correlated with the rate of aldosterone production[77]. It is therefore crucial to control the $[Ca^{2+}]_i$ withhin ZG cells in order to achieve tight regulation of the aldosterone synthesis.

1.4 The $Ca_V3.2$ calcium channel in the zona glomerulosa

The $Ca_V3.2$ calcium channel is a T-type calcium channel and is encoded by the *CACNA1H* gene located on chromosome 16[78]. Both activation and inactivation of T-type calcium chan-

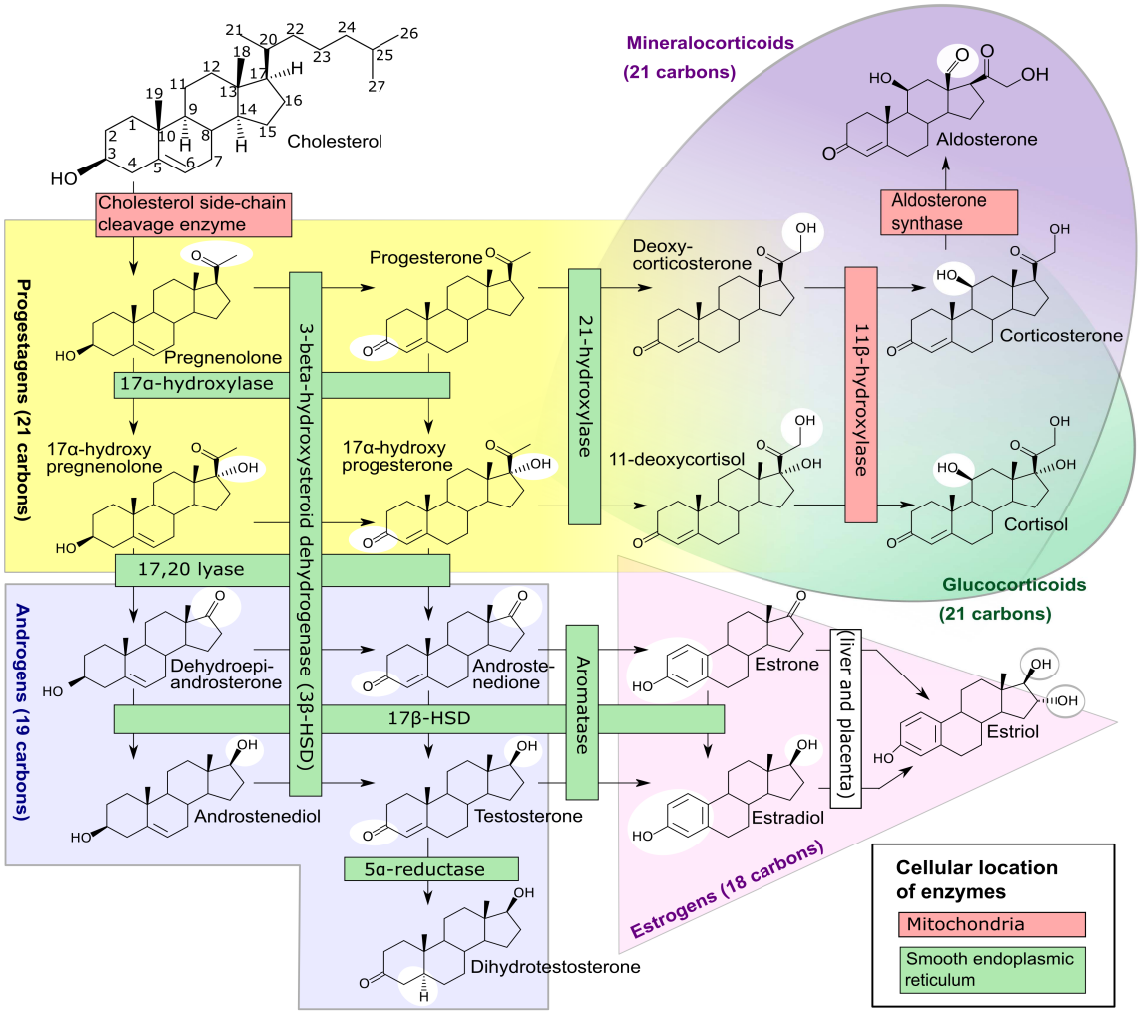

Figure 8. The enzymes, substrates and products in human steroidogenesis and their cellular location. *The steroid hormones are grouped in their major classes: progestagens, mineralocorticoids, glucocorticoids, androgens and estrogens. Adapted from*[76].

nels, including $Ca_V3.2$, are strongly voltage dependent. Activation of the $Ca_V3.2$ channel, being a LVA calcium channel, typically starts at -70mV[48]. In contrast, HVA channels of the Ca_V1 and Ca_V2 families need higher depolarizations (above -40 mV) to be opened (Fig. 9A).

Steady-state inactivation curves of $Ca_V3.2$ range from no inactivation at -80 mV to complete inactivation at -40 mV (Fig. 9B, dashed green line). The overlap of the activation and inactivation curves define the so called "window current". Within this voltage range (approximately between -65 and -40 mV for $Ca_V3.2$) channels can be activated but not be completely inactivated. This leads to a steady-state rather then a transient calcium influx[48,78].

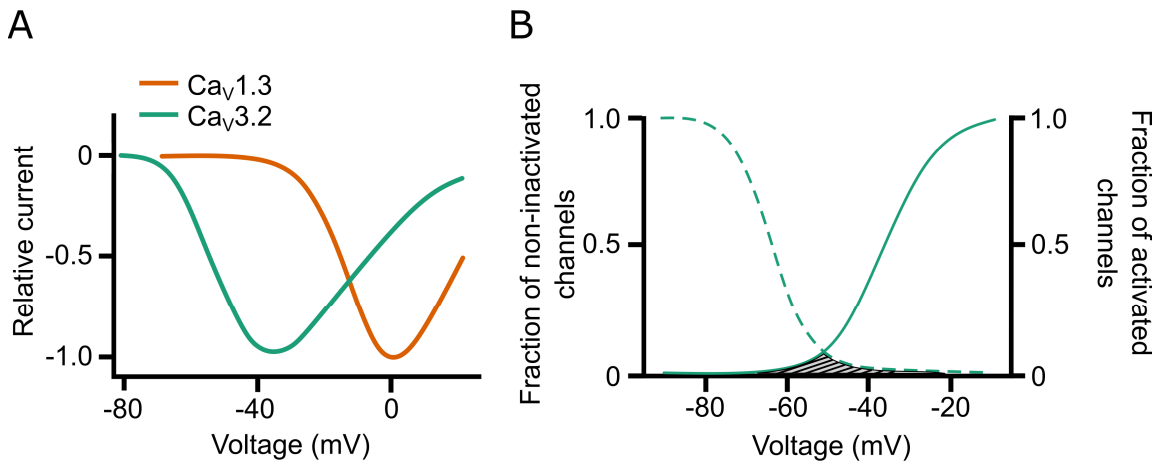

Figure 9. Current-voltage relationships and the window current (A) *Examplary current-voltage relationships of T-type channel $Ca_V3.2$ (green) and L-type channel $Ca_V1.3$ (orange) demonstrating the difference in voltage dependence.* ***(B)*** *The overlap of the activation (solid line) and inactivation (dashed line) curves of $Ca_V3.2$ produces the window current between -65 and -40 mV (hatched area). This plot is based on*[62]

.

The $Ca_V3.2$ channel, being a low-voltage activated channel, activates at membrane voltages positive to -70 mV, which is close to the resting membrane potential of ZG cells (~80mV). Therefore, small depolarizations may already suffice to open $Ca_V3.2$ which leads to the influx of calcium further depolarizing the ZG cells. This biophysical characteristic of the $Ca_V3.2$ has been proposed to mediate membrane potential oscillations[25].

These oscillations exhibited an intermediate frequency (~1 Hz) that correlates to the level of stimulation with K^+ and Ang II (Fig. 10A and B)[25]. The individual depolarizations showed a uniform shape like those of action potentials.

Exposure of these cells to Ni^{2+}, a T-type calcium channel inhibitor, silenced all oscillatory activity suggesting an important contribution of this channel class in generating these depolarizations (Fig. 10C and D)[25].

Since $Ca_V3.2$ is the main sub-type of the HVA calcium channels expressed in the ZG, it was hypothesized that the activation of $Ca_V3.2$ channels underlies the fast depolarizing phase of the ZG cell oscillation cycle (Fig. 11)[25]. However, $Ca_V3.2$ channels are most likely not able to drive the depolarization from a resting membrane potential by itself, considering that the $Ca_V3.2$-mediated current was less than 11% of the current that would be necessary (26 pA) to raise the membrane potential from –80 to –64 mV[25].

This suggests that other conductances must play a role at the start of an oscillatory

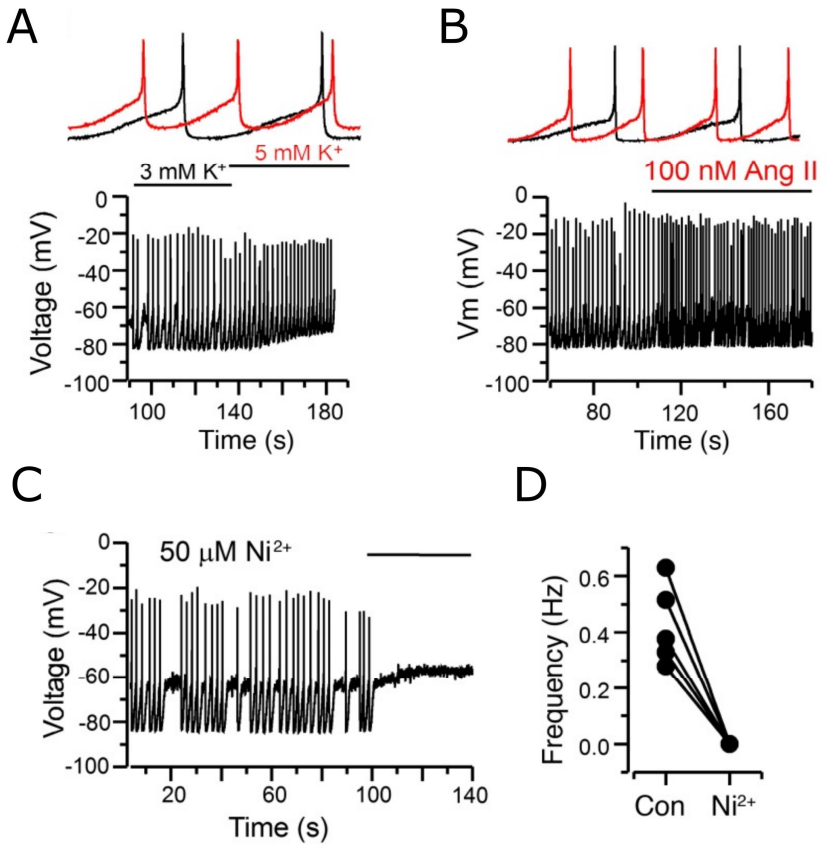

Figure 10. ZG cells exhibit oscillatory behavior. ***(A)*** *Representative current clamp recordings of ZG cells in buffer containing 3 and 5 mM K^+.* ***(B)*** *Representative current clamp recording of a cell spontaneously oscillating before and during exposure to 100 nM Ang II. Expanded traces in A and B are calculated average cycles from same voltage recordings.* ***(C)*** *Representative cell with periodic oscillations, before and after exposure to 50 µM Ni_2^+ (T-type calcium channel inhibitor).* ***(D)*** *Mean oscillation frequency was abolished by Ni^{2+} in all recorded cells (n = 6). Taken from[25].*

cycle. These ion channels would mediate the initial depolarization needed for the opening of LVA channel, i.e $Ca_V3.2$. $Ca_V3.2$ channels would then further depolarize the membrane potential facilitating the opening of HVA channels like $Ca_V1.3$.

The increase in Ca^{2+} levels would recruit Ca^{2+}-activated K^+ channels returning the membrane potential back to the resting potential thereby allowing the start of another oscillatory cycle (Fig. 11).

Furthermore, it was shown, that ZG cells not only exhibit oscillations in the membrane potential but also show oscillatory influx of calcium into the ZG cell with a similar frequency as observed in the membrane voltage (Fig. 12A)[80–82].

When stimulated with physiological concentrations of Ang II, these oscillations in $[Ca^{2+}]_i$

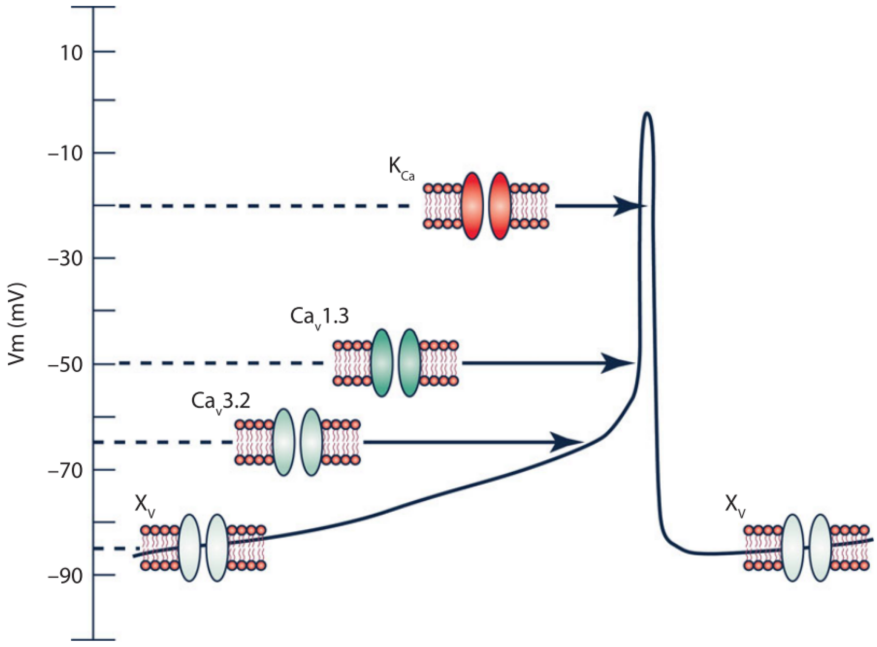

Figure 11. A proposed model of a oscillatory cycle within ZG cells. *At the start of an oscillatory cycle at the resting potential, depolarizing conductance(s) (X_v) elicit the opening of LVA $Ca_V3.2$ channels. These further depolarize the membrane potential allowing the opening of HVA channels (e.g. $Ca_V1.3$). Influx of Ca^{2+} activates Ca^{2+}-dependent K^+ channels that hyperpolarize the membrane potential back to resting conditions allowing another oscillatory cycle. Taken from*[79].

are, unlike the electrical signals, not continuous but grouped into "burst of calcium spikes" that are separated by pauses with no oscillations (no activity)[80–82]. Elevating the level of Ang II stimulation increases the number and length of the bursts leading to higher $[Ca^{2+}]_i$ (Fig. 12B)[81,82].

It was suggested that the $Ca_V3.2$ channel plays a critical role in generating these oscillations as the electrical oscillations were abolished in ZG cells upon specific $Ca_V3.2$ inhibition with Ni^{2+}[25]. Accordingly, the authors were able to elicit voltage oscillations in human adrenal tumor cells (H295R) upon transfection of *CACNA1H*, which are not present in untransfected cells[25]. Inhibition of L-type calcium or sodium channels did not alter voltage oscillations[25]. Additionally, it was suggested before that specific inhibition of T-type VGCCs might provide a potential strategy to pharmacologically lower aldosterone production[17].

These investigations propose a fundamental role for $Ca_V3.2$ channels in eliciting voltage oscillations, which are most likely the foundation of oscillatory calcium influx within ZG cells. Nevertheless, with regard to aldosterone production, it is the calcium signals rather than alterations in voltage that represent the crucial determinant. The function of the $Ca_V3.2$

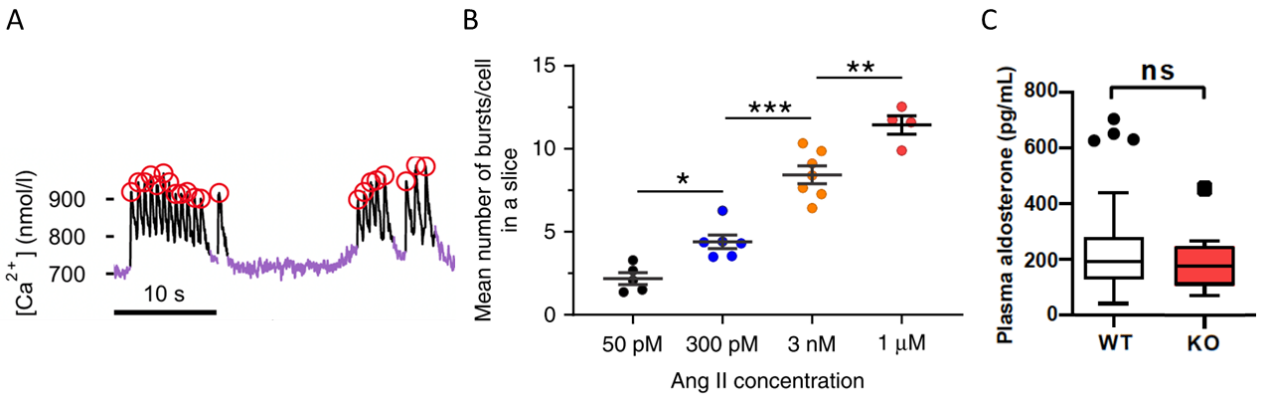

Figure 12. ZG cells exhibit oscillatory influx resembling the membrane voltage oscillation. ***(A)*** *The changes in $[Ca^{2+}]_i$ of one representative cell at 5 mmol/l K^+ and 1 nmmol/l Ang II) is shown. Red circles highlight the peaks of calcium spikes that are group into bursts. Purple colored parts of the signal represent phases without soiking activity and represent baseline concentrations. Adapted from[83].* ***(B)*** *Number of bursts per cell is dependent on Ang II concentration. Means ± SEM are shown (Bonferroni's test: 50 pM vs 300pM (*P = 0.029); 300pM vs 3 nM (***P < 0.0001); 3 nM vs 1 µM (***P < 0.0001). Adapted from[82].* ***(C)*** *Plasma aldosterone is not significantly changed in mice lacking $Ca_V3.2$ (KO: n = 13; P = 0.895; Kruskal–Wallis test and Dunn's MCP). Adapted from[83].*

calcium channel in calcium signaling within ZG cells remains unclear, but it is likely to be a significant one, as voltage oscillations are likely to underlie calcium oscillations.

If $Ca_V3.2$ were exclusively responsible for Ca^{2+} signaling as it was suggested for voltage oscillations, it would be anticipated that the loss of $Ca_V3.2$ would result in reduced levels of aldosterone. However, contrary to this hypothesis, mice deficient of $Ca_V3.2$ did not demonstrate changed aldosterone or renin levels in comparison to wild-type mice (Fig. 12C)[83,84]. Furthermore, when $Ca_V3.2$-deficient mice were infused with Ang II the increase in mean arterial blood pressure was indistinguishable from those observed in wild-type mice[84].

These studies mainly focused on systemic effects in KO mice. Compensatory secondary mechanisms (e.g., activation of the renin-angiotensin system or upregulation of other calcium influx pathways in the ZG) may have mitigated the loss of the $Ca_V3.2$ channel. Therefore, this study aimed to investigate the mechanisms regulating calcium influx in the ZG of $Ca_V3.2$-deficient mice.

1.5 Calcium channels in primary aldosteronism

If the aldosterone production is partially uncoupled from its stimuli primary aldosteronism (PA) arises. PA is a frequent cause of secondary hypertension and is estimated to underlie about 6% of all hypertension cases affecting approx. 50 million people world wide[85]. Apart from hypertension, excess aldosterone production can cause hypokalemia and increased risk of cardiovascular disease[86]. Common causes of PA are diffuse hyperplasia of the adrenal gland (increase in the number of aldosterone synthase-positive cells in ZG), aldosterone producing (miro)nodules and aldosterone-producing adenomas (APAs)[87]. APAs and (micro)nodules exhibit increased expression of aldosterone synthase and are distinguished by size ((micro)nodules: $<$ 10 mm in diameter; APA: $\geq$ 10 mm in diameter).

Over the past decade, next-generation sequencing studies elucidated that PA is largely caused by genetic mutations. These mutations can occur sporadically as somatic mutations and in rare cases as hereditary germline mutations resulting in familial hyperaldosteronism (FH). Somatic and germline mutations were identified in ion channels, ion pumps and other genes in overlapping gene sets. For example, heterozygous gain-of function mutations in VGCC genes *CACNA1D*[52,88] (L-type) and *CACNA1H*[89] (T-type) have been shown to directly lead to elevated calcium influx.

Indirect increases in $[Ca^{2+}]_i$ by depolarizing ZG cells and activating VGCCs are associated, for example, with mutations in ion channels *CLCN2* (encodes chloride channel ClC-2)[90] and *KCNJ5* (encodes potassium channel Kir3.4)[91] as well as ion pump genes *ATP1A1*(encodes α_1- subunit of the Na^+/K^+-ATPase)[88,92] and *ATP2B3*[92] (encodes plasma membrane Ca^{2+}-ATPase).

Heterozygous mutations identified in the germline occur in genes *KCNJ5*[91], *CLCN2*[93,94], *CACNA1H*[62] and *CYP11B2* (aldosterone synthase)[95] and lead to FH.

Cases of mutations in *CACNA1H* are classified as the FH-IV subtype. The mutations M1549V[62] and M1549I[96] are located in the 6th transmembrane helix of the 3rd transmembrane domain an lead to early-onset PA in patients and in one case with M1549I additionally to a multiplex developmental disorder. It was demonstrated that the M1549V mutation resulted in a gain of channel function. The mutation caused a reduced inactivation and a shift of activation to more negative potentials (Fig. 9) leading to elevated calcium influx and aldosterone synthesis[62]. Additional mutations have been identified with slightly different or yet unknown biophysical properties (see Table 2).

Table 2. *Published CACNA1H variants associated with PA. Adapted from[75].*

Mutation	G/S*	Position	# of cases	Age at dx‡	Abnormalities	Electrophysiological phenotype
M1549V[62]	G	S6, DIII	8 (6m, 2f)	2m – 9y	No	Delayed inactivation, left-shifted activation
M1549I[96]	G	S6, DIII	1 (1m)	2m	No	Delayed inactivation, left-shifted activation
S196L[96]	G	S4, DI	2 (1m, 1f)	>30y	Nodule visible in CT	Delayed inactivation
V1951E[96]	G	C-terminus	1 (1f)	>50y	Left adrenal nodule	Faster recovery from inactivation
P2083L[96]	G	C-terminus	2 (2m)	>30y	Slight hyperplasia	Faster recovery from inactivation
R890H[97]	G	S4, DII	1 (2f)	>30y	No	Loss-of-Function; Smaller whole-cell currents in HEK293
I1430T[89]	S	S5, DIII	3 (1f, 2m)	>40y	2 APA, 1 not visible	Unknown, but increased aldosterone synthesis in HAC15 cells
P277S[98]	S	Extracell. between S5 and S6, DI	1	?	Unilateral hyperplasia or APA	Unknown
W482X[98]	S	Cytopl. between S6, DI and S1, DII	1	?	Unilateral hyperplasia or APA	Unknown
T615P[98]	S	Cytopl. between S6, DI and S1, DII	1	?	Unilateral hyperplasia or APA	Unknown
Q875R[98]	S	Extracell., after S3, DII	1	?	Unilateral hyperplasia or APA	Unknown
Q904X[98]	S	S4, DII	1	?	Unilateral hyperplasia or APA	Unknown
V1937M[99]	S	C terminus	1	43	0.6 cm left nodule	Unknown, but increased aldosterone synthesis in HAC15 cells

*: G: Germline; S: Somatic
‡: dx-diagnosis

Mutations in the *CACNA1D* gene (encodes L-type channel) $Ca_V1.3$ lead to *p*rimary *a*ldosteronism *s*eizures and *n*euromuscular *a*bnormalities PASNA)[52,88]. Furthermore, approximately 60% of micronodules observed in patients with PA lacking adenomas[100,101] and roughly 25% of micronodules found in seemingly normal adrenal glands, carry somatic *CACNA1D* mutations[102,103].

One of the identified *CACNA1D* mutations (I770M) shifts the voltage dependence of activation to more hyperpolarized potentials resulting in increased Ca^{2+} influx[52].

This results in elevated aldosterone synthesis within the adrenal gland and potentially also accounts for neurological irregularities. Therefore, the reduction of Ca^{2+} influx via $Ca_V1.3$ channels could potentially serve as a viable therapeutic strategy for mitigating symptoms in individuals affected by this mutation.

Most of the mutations in the ion channel or ion pump genes mentioned above result eventually in an increased calcium entry via VGCCs, emphasizing the importance of these channels for the physiological functions of the ZG.

2 Aims and objectives

The production of aldosterone in the ZG comprises complex mechanisms and is controlled by several stimuli. Many of these factors, such as the serum concentrations of potassium and Ang II, have been proposed to regulate this process by mediating oscillatory calcium influx into ZG cells. This rise in $[Ca^{2+}]_i$ is triggered by depolarization of the cell membrane leading to activation of VGGCs and also the release of calcium from intracellular stores (see Section 1.3).

Previous studies have suggested that these depolarizations require the T-type calcium channels, specifically $Ca_V3.2$ (see Section 1.4).

Even though $Ca_V3.2$ plays a crucial role in the electrical excitability of ZG cells, $Ca_V3.2$ knock-out mice did not display changes in systemic aldosterone or renin levels, nor changed responses to Ang II infusion, indicating additional calcium influx pathways. The exact molecular mechanisms responsible for the aldosterone synthesis in $Ca_V3.2$ knock-out mice remain presently undetermined.

Therefore, one aim of this work was to investigate the regulation of $[Ca^{2+}]_i$ in the ZG of $Ca_V3.2$-deficient mice. Moreover, the implications from these results on the physiological role of VGCCs in the ZG function and the pharmacology of the ZG are to be studied.

Additionally, mutations in human VGGCs such as $Ca_V3.2$ and $Ca_V1.3$ have been linked to primary aldosteronism . The gain-of function mutation M1459V in the $Ca_V3.2$ channel (gene *CACNA1H*) represents the most common mutation in the FH-IV subtype of familial hyperaldosteronism (see Section 1.5).

This work was additionally aimed to evaluate the impact of this mutation on calcium signaling by using the *Cacna1h*$^{M1560V/+}$ knock-in mice (homologous to the human M1549V mutation) as a model system.

Moreover, mutations in the *CACNA1D* gene (encodes L-type channel $Ca_V1.3$) also lead to primary aldosteronism and neurological abnormalities (see Section 1.5). The *Cacna1d*$^{I772M/+}$ mouse closely models the human phenotype showing elevated $[Ca^{2+}]_i$

and aldosterone levels. This work was aimed to study the potential of a pharmacological treatment with the specific L-type channel inhibitor isradipine to rescue the phenotype.

The following objectives were proposed in pursuit of the goals:

1. Investigating calcium oscillations in ZG cells of $Ca_V3.2$ knock-out mice and their dependency on extracellular stimuli (Ang II and extracellular K^+; see Section 4.1.1 and 4.1.2).
2. Elucidating the role of other VGCCs in mediating calcium signals in ZG cells of wild-type and $Ca_V3.2$ knock-out mice (see Section 4.1.3 and 4.1.7).
3. Investigating the contribution of additional calcium influx mechanisms (besides VGCCs) in a physiological setting in increasing $[Ca^{2+}]_i$ upon stimulation (see Section 4.1.8).
4. Characterisation of calcium oscillations in ZG cells of the *Cacna1h*$^{M1560V/+}$ mouse model (see Section 4.2).
5. Evaluating calcium levels in ZG cells of *Cacna1d*$^{I1560M/+}$ mice in the presence of specific L-type channel inhibitor isradipine (see Section 4.3.2).
6. Studying the behavioral phenotype and aldosterone levels of *Cacna1d*$^{I1560M/+}$ mice under isradipine treatment (see Section 4.3.3).

3 Methods, Procedures and Materials

3.1 Mice

3.1.1 The *Cacna1h*$^{M1560V/+}$ and *Cacna1h*$^{-/-}$ mouse model

The *Cacna1h*$^{M1560V/+}$ and *Cacna1h*$^{-/-}$ mice were generated as described previously[83]. Briefly, genome editing based on CRISPR/Cas9 was performed at the Yale Genome Editing Center to introduce the p.Met1560Val mutation on exon 25 of the *Cacna1h* gene into the mouse genome yielding *Cacna1h*$^{M1560V/+}$ mice (Cacna1h KI). Additionally, mice carrying an 8-bp deletion resulting in a frameshift and termination codon (p.His1570Glnfs*83, *Cacna1h*$^{+/-}$) were generated. *Cacna1h*$^{M1560V/+}$ and *Cacna1h*$^{+/-}$ mice backcrossed to the C57BL/6J strain. *Cacna1h*$^{+/-}$ mice were further bred to obtain homozygous knock-out (KO) mice (*Cacna1h*$^{-/-}$).

3.1.2 The *Cacna1d*$^{I772M/+}$ mouse model

CRISPR/Cas9-mediated genome editing in the *Cacna1d* gene (p.Ile772Met) was performed at the Yale Genome Editing Center as described previously[104] using fertilized eggs from C57BL/6J mice.

3.1.3 Breeding

Mice were bred at the Forschungseinrichtungen für Experimentelle Medizin (FEM; Charité - Universitätsmedizin Berlin). The breeding scheme implemented in this study aimed to maintain a controlled population of experimental animals.

Adult mice with at least 10 weeks of age were selected as breeding candidates to ensure they had reached sexual maturity. Breeding pairs were terminated after a maximum of four breeding events.

For *Cacna1h*$^{M1560V/+}$, and *Cacna1h*$^{+/+}$ (wild-type, WT) mice, heterozygous were bred with each other or with WT mice to generate both genotypes.

To generate *Cacna1h*$^{-/-}$ and WT mice, two different breeding strategies were employed based on the existing genotypes within the mouse colony. Either breeding pairs consisting of heterozygous knockout mice (carrying one wild-type allele and one knockout allele) of both sexes were used, or exclusively utilized homozygous knockout pairs alongside wild-type pairs were employed.

To obtain mice with the *Cacna1d*$^{I772M/+}$ (Cacna1d KI), initial attempts were made to crossbreed these mice with WT mice. However, successful pregnancies were not achieved when mating male *Cacna1d*$^{I772M/+}$ mice with female WT mice. On the other hand, when female *Cacna1d*$^{I772M/+}$ mice were bred with male WT mice, pregnancies occurred, but the resulting offspring were found deceased shortly after birth. Sperm extracted from *Cacna1d*$^{I772M/+}$ mice exhibited normal motility and was utilized for in vitro fertilization (IVF), which yielded viable offspring. In subsequent generations, traditional breeding methods still proved ineffective. Therefore IVF was employed for the production of all subsequent experimental animals.

3.1.4 Housing

Cacna1h$^{M1560V/+}$, *Cacna1h* KO, *Cacna1d*$^{I772M/+}$ and wild-type (WT) control mice were housed at the Forschungseinrichtungen für Experimentelle Medizin (FEM; Charité - Universitätsmedizin Berlin) under specific-pathogen free conditions in a 12h light/dark cycle with ad libitum access to food and water.

3.1.5 Ethical statements

All animal experiments in this project were approved by the supervisory authority (Landesamt für Gesundheit und Soziales (LaGeSo), G0210/17, G0095/20 and T0425/17). The animals were kept under standard mice housing conditions and treated according to the German and EU Animal Welfare regulations.

Mice were used for experiments between age 10 and 30 weeks (unless otherwise mentioned).

3.2 Calcium imaging in acute adrenal slices

Method

Calcium imaging is a technique to assess intracellular calcium concentrations. This method uses calcium-sensitive fluorescent dyes or genetically encoded sensors. The dyes generally comprise a Ca^{2+}-chelating motive and a fluophore. For staining of living cells, an acetoxymethyl (AM) ester is often attached, allowing the dye to cross the cell membrane[105]. After cleavage of the AM group by intracellular esterases, the now hydrophilic dye can not diffuse back through the cell membrane. In general, there are two categories of calcium indicators: non-ratiometric dyes, like Calbryte 520, and ratiometric dyes, such as Fura-2. Calbryte 520 has excitation and emission wavelengths at 490 nm and 515 nm, respectively (Fig. 13A)[106]. Upon binding Ca^{2+}, its fluorescence intensity is increased by >100 times. Quantitative assessment of $[Ca^{2+}]_i$ using non-ratiometric dyes can be achieved using fluorescence lifetime imaging[107]. Unfortunately, with the experimental setup available in this project, lifetime determination was not possible.

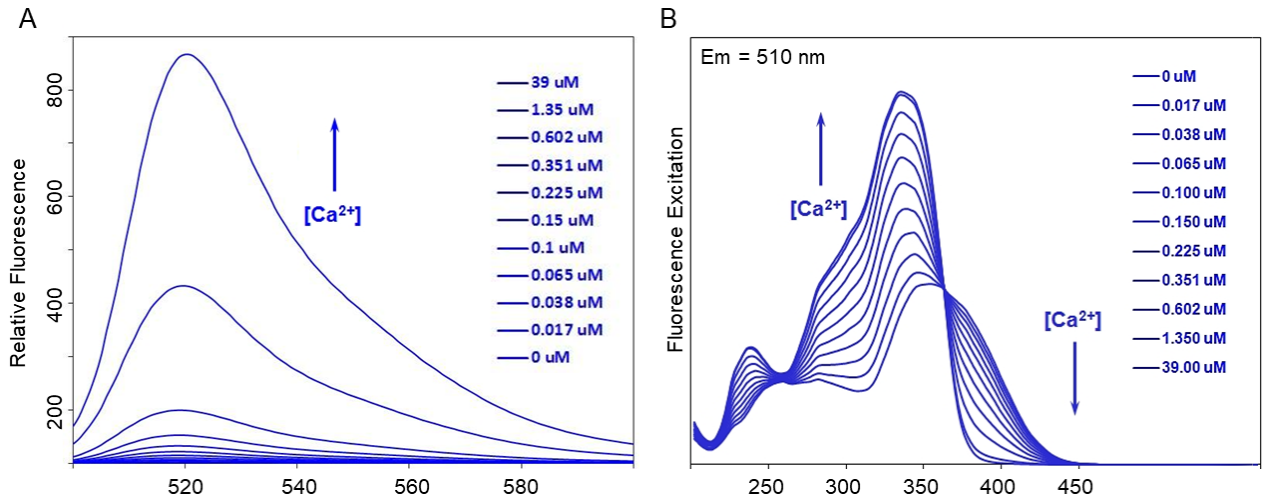

Figure 13. (A) *Fluorescence emission spectra of Calbryte 520 in solutions containing 0 to 39 µmol/l free Ca^{2+}.* ***(B)*** *Fluorescence excitation spectra of Fura-2 in solutions containing 0 to 39 µmol/l free Ca^{2+}. Adapted from[108,109]*

Instead, the fluorescence intensity was assessed. However, the use of non-ratiometric dyes only allowed the relative measurement of intracellular calcium concentrations as the intensity is not only dependent on $[Ca^{2+}]_i$ but also the unknown intracellular concentration of the dye. It is possible to get absolute $[Ca^{2+}]_i$ values by calibrating the relative signal in situ. However, this technique is prone to errors due to the long incubation times resulting

in a loss of cell viability and due to bleaching of the dye during to the long recording duration.

Absolute measurements can be more easily achieved by the use of ratiometric dyes. These undergo a shift in the emission or excitation spectra upon binding Ca^{2+}. The excitation peak of Fura-2, for example, shifts to shorter wavelengths with increases in Ca^{2+} concentration (Fig. 13B)[110]. The ratio of the intensity at 340 nm (Ca^{2+}-bound fluophore) and 380 nm excitation (Ca^{2+}-unbound fluophore) can be used in equation 1 to convert these values to intracellular calcium concentrations[110]. $[\mathrm{Ca}^{2+}]$ is the calcium concentration, R is the Fura-2 340/380 ratio, R_{min} and R_{max} are the 340/380 ratios in the absence of calcium or in the presence of a saturating concentration of calcium, respectively. S_{f2} is the fluorescence intensity at the 380 nm excitation wavelength when Fura-2 is not bound to calcium. S_{b2} is the fluorescence intensity at the 380 nm excitation wavelength when the dye is fully saturated with Ca^{2+}. S_{f2} and S_{b2} are calibration parameters specific to a particular set of experimental conditions, including the imaging system, equipment settings, and the Fura-2 dye preparation.

In order to asses $[Ca^{2+}]_i$ based on the ratio of fluorescence intensities at 340 nm and 380 nm it is necessary to perform a calibration to obtain R_{min} and R_{max}, S_{f2}, S_{b2}, K_d. The calibration should be performed under conditions used in the calcium imaging experiment to ensure accurate conversion of fluorescence ratios into calcium concentrations. However, it can be performed in a different cell preparation than the recording of interest.

$$[Ca^{2+}] = K_d * \frac{R - R_{min}}{R_{max} - R} * \frac{S_{f2}}{S_{b2}} \tag{1}$$

Procedure

For intracellular Ca^{2+} measurements in acute adrenal slices, similar to previously published procedures[81,83], mice were anesthetized using isoflurane (400 µL as open drop in a 2 l beaker) and euthanized by cervical dislocation (Fig. 14). The abdominal cavity was then opened using scissors. The adrenal glands were identified, rapidly extracted and transferred into ice-cold bicarbonate-buffered solution (BBS) (Table 3). During all following steps, BBS was continuously gassed with carbogen (95% O_2 + 5% CO_2) to guarantee adequate oxygen delivery to the cells. The surrounding fat tissue was removed and the glands were embedded in 4% low-melting agarose providing support and stability to the tissue sample. The agarose block containing the glands was glued to the mounting stage of a vibratome (7000 smz-2, Campden Instruments) and slices were cut at 120 µm thickness. Due to the small size of adrenal glands (each < 2 mm in diameter), embedding these

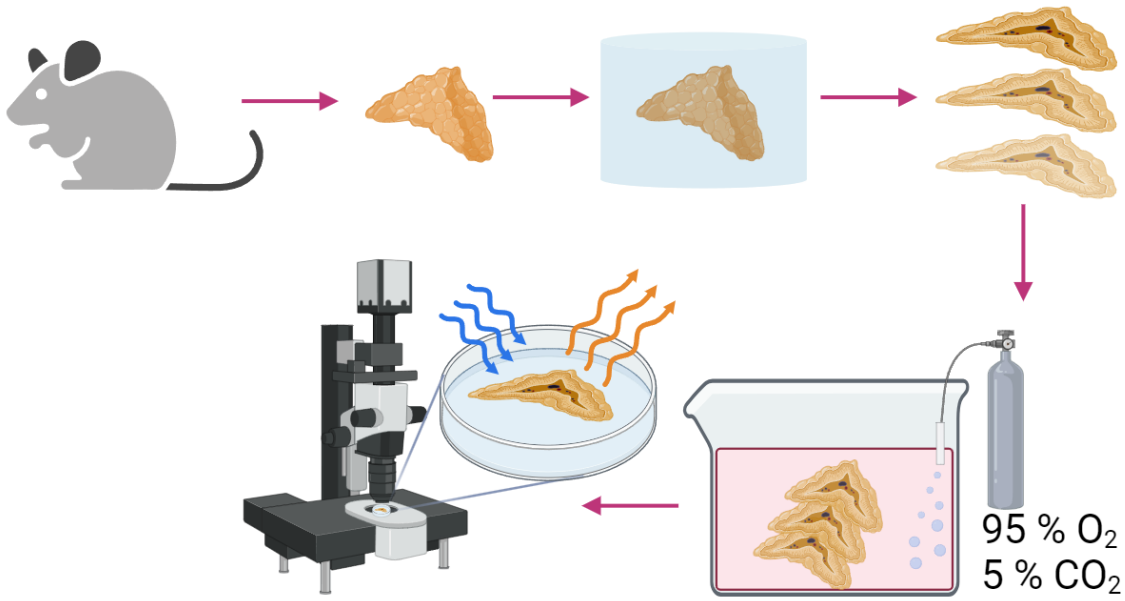

Figure 14. Scheme of the calcium imaging procedure. *Adrenal glands were extracted from mice and embedded in agarose to facilitate the preparation of thin sections (120 µm). Slices were incubated in gassed BBS and loaded with calcium fluorescent dye. Slices were placed in a recording chamber and continuously perfused with gassed solution from a reservoir. The fluorescence signal is recorded and a representative adrenal slice is depicted.*

organs in agarose helps in achieving uniform and consistent section thickness because the tissue is held firmly in place, which is usually not necessary in the case of larger tissue samples (e.g brain).

Adrenal glands in the agarose block and slices were maintained in ice-cold, gassed BBS during slicing. Slices were then transferred into BBS at 35 °C for 15 minutes for regeneration and subsequently stored for up to 6 h at RT in BBS supplemented with 2 mmol/l $CaCl_2$.

Slice staining was conducted in a cell culture insert within a single well of a 24-well plate at room temperature. The well was filled with 750 µL BBS (supplemented with 2 mmol/l $CaCl_2$) and continuously gassed with carbogen. The insert was filled with 250 µL containing initially either 64 µmol/l Fura-2 AM (final concentration: 16 µmol/l) and 0.16% Pluronic F-127 or 37 µmol/l Calbryte 520 AM (final concentration: 9.25 µmol/l) and 0.001% Pluronic dissolved in BBS (supplemented with 2 mmol/l $CaCl_2$). Slice incubation was performed in the staining solution for 1 h. Following Fura-2 AM staining, slices were transferred to fresh BBS (supplemented with 2 mmol/l $CaCl_2$ and without Fura-2) for 15 min de-esterification.

For recording, slices were placed in a recording chamber and continuously perfused with solution from a reservoir. The solution reservoir was gassed with carbogen and heated via an inline heating coil to a temperature of 30 ± 1 °C. BBS $2K^+$ and BBS $7K^+$ solutions (Table

3) were prepared and mixed in order to yield the potassium concentration of interest. Ang II (1 µmol/l) was added to yield final concentrations as indicated. Fura-2 was alternately excited at 340 and 385 nm using a FuraLED light source (Cairn Research) while Calbryte fluorescence was excited at 470 nm. Using an OptiMOS camera (QImaging) Images were taken every 100 ms with 10-ms exposure.

Table 3. *BBS (pH 7.4) in mmol/l*

Compound	BBS	BBS supplemented	BBS 2 K^+	BBS 7 K^+
NaCl	100	100	100	100
KCl	2	2	2	2
$NaHCO_3$	126	126	126	126
$CaCl_2$	0.1	2	2	2
$MgCl_2$	5	5	1	1
NaGluconate	–	–	5	–
KGluconate	–	–	–	5
D-glucose	10	10	10	10
HEPES	10	10	10	10

Calibration of Fura-2 signals To calibrate the 340/385 nm ratios to calcium concentrations adrenal slices stained with Fura-2 AM were incubated with solutions containing known extracellular calcium concentrations (Calcium Calibration Buffer Kit from Promocell). These solutions were further supplemented with 25 µmol/l ionomycin, an ionophore, allowing the influx of extracellular Ca^{2+} ions into the cell. Using this method the $[Ca^{2+}]_i$ can be controlled by the extracellular solutions. The selection of these solutions aimed to achieve final free calcium concentrations ranging from 0 to 39.8 µmol/l. Fluorescence ratios of 340/385 nm excitation were observed over time. Final values were determined once recordings remained within 5% of each other for either a) more than 30 minutes or b) for at least two observations (longer than 15 minutes) after a change in ratio values. The final ratio values were plotted against the corresponding calcium concentrations. A Hill equation was employed to fit the resulting curve, allowing for the determination of the K_d of Fura-2 within ZG cells. Ratios from other recordings could then be converted into absolute $[Ca^{2+}]_i$ according to equation 1 based on[110]. The results of the calibration can be found in section 4.2.1.

3.3 Primary cell culture of adrenal cortical cells

For electrophysiological recordings in dissociated adrenocortical cells, adrenal glands were extracted from mice following euthanizing by cervical dislocation under isoflurane anaesthesia (400 µL as open drop in a 2-l beaker). Glands were rapidly transferred into bath solution (Fig. 15, Table 4) on ice. After the removal of the surrounding fat tissue under a stereo-microscope, the glands were cut in half and the medulla manually removed. The glands were further cut into fragments (< 0.5 mm) and incubated in bath solution supplemented with collagenase type I (1 mg/ml), collagenase type IV (1 mg/ml), penicillin (50 U/ml) and streptomycin (50 mg/ml) for 20 min at 37℃ on a shaker set to 300 rpm. Subsequently, shear-based dissociation of the cells was performed in a 1 ml syringe attached to a cannula (20 G) and polyethylene tubing (30 cm length, 1.1 mm diameter). A flow rate of 700 µL/min of the cell suspension through the cannula and tubing was controlled by a syringe pump. The cell suspension was centrifuged for 5 min at 300 g and room temperature. The supernatant was removed and the cell pellet was resuspended in supplemented DMEM/F12 media (1 ml, Table 5). Coverslips (9 mm diameter) were cleaned by sonication (10 min) with Ultrasonol 7 (5% in H_2O) and were rinsed at least 5 times with water. Cleaned coverslips were stored in ethanol (70%) at 4℃ until further use. On the day of use, coverslips were coated with poly-L-lysine for a duration of 5 minutes, followed by rinsing with PBS and laminin (75µg/ml) coating for 45 minutes. Coverslips were rinsed with PBS and placed in a 24-well plate. 400 µl medium was added to each coverslip. Cells (200 µl) were seeded onto coverslips and incubated in a 5% CO_2 humidified atmosphere at 37℃ and used for whole-cell patch-clamp recordings the next day.

Table 4. *Bath solution (pH 7.4) for dissociating ZG cells*

Compound	mmol/l
NaCl	140
KCl	4
$CaCl_2$	2
$MgCl_2$	1
HEPES	10

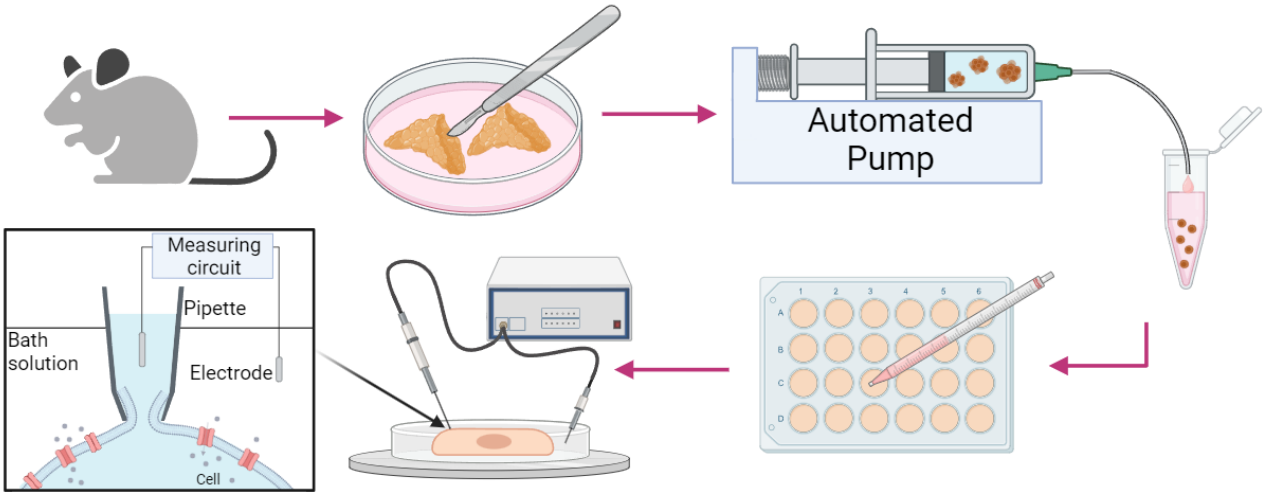

Figure 15. Scheme of the adrenal cortical cell dissociation and patch-clamp method. *Adrenal glands were extracted from mice and the surrounding fat tissue was removed. The glands were cut into fragments and incubated in bath solution supplemented with collagenase to ensure enzymatic dissociaton. Subsequently, shear-based dissociation of the cells was performed in a 1 ml syringe attached to a cannula and polyethylene tubing. The cell suspension was pushed through the cannula and tubing by an an automated syringe pump. After centrifugation of the cell suspension and removing of the supernatant, the cell pellet was resuspended in medium and seeded onto coverslips placed in a 24-well plate. Cells were incubated in a 5% CO_2 humidified atmosphere at 37℃ and subjected for whole-cell patch-clamp recordings the next day.*

Table 5. *Supplements for DMEM/F12 media for culturing of dissociated adrenal cortical cells*

Compound	
Ultroser G	2%
Penicillin	50 U/ml
Streptomycin	50 mg/ml
α-Tocopherol	1 µmol/l
Insulin Transferrin Selenium	1%
Ascorbic acid	100 µmol/l

3.4 Electrophysiological recordings

Method

Whole-cell patch-clamp recordings were conducted to record calcium currents in cells. In this method a glass micropipette electrode filled with an electrolyte solution is carefully

pressed against the cell membrane and slight negative pressure is generated in the pipette to create an electrically tight connection, the giga seal. Subsequently, the membrane patch beneath the pipette is ruptured through the application of short pulses of negative pressure. This establishes a whole-cell configuration and grants direct access to the cell's cytoplasm (Fig. 15). The pipette solution comes into contact with the cell's cytoplasm. A waiting time of approx. 1 min facilitates the equilibration of the cell cytoplasm with the pipette solution. This configuration allows for the control of the intracellular environment. The extracellular conditions are controlled by the bath solution surrounding the cell.

To measure calcium currents, a series of depolarizing voltage steps with specified durations and amplitudes is applied (Fig. 16). These steps start from a specific initial holding potential. Calcium channels open in response to the depolarizing changes in voltage, allowing calcium ions to flow into the cell, and this current is recorded.

K^+, Cl^-, and Na^+ currents are potential influencing factors and sources of contamination in Ca^{2+} current measurements. To reduce the impact of K^+ currents, tetraethylammonium (TEA, as TEA-Cl) and cesium ions (as CsCl), both of which block K^+ channels, were added to the extracellular and pipette solution, respectively (Table 6 and 7). The influence of Cl^- currents was considered negligible due to their slow activation kinetics and short time of recording, resulting in small mediated currents within the applied voltage range[111,112]. Moreover, the contribution of Na^+ currents was anticipated to be minimal, as demonstrated by previous findings indicating that they do not play a role in the oscillatory depolarizations of ZG cells[25].

Procedure

Recordings of calcium currents in dissociated adrenal cortical cells were carried out in HEPES-buffered extracellular solution (bath solution, Table 6). A coverslip was removed from a well of the 24-well plate, placed into the coverslip holder and fixed to the bottom of the holder using small drops of cyanoacrylate glue. A droplet of the bath solution was applied onto the coverslip to prevent the cells from drying out. After drying of the glue (5-10 seconds) the entire coverslip was washed with bath solution 3 times. The coverslip holder was placed into the microscope setup. All recordings were conducted at room temperature.

Calcium currents were recorded on a HEKA EPC 10 amplifier (HEKA Elektronik) using Patchmaster software. Borosilicate glass pipettes with resistances of 2–4 MΩ were pulled on a Sutter P-1000 puller (Harvard Apparatus), fire polished using a Narishige MF-890 microforge and filled with pipette solution (Table 7). At least 80% of the series resistance was compensated for.

Currents were recorded in response to two separate voltage clamp protocols[113] (Fig. 16): First from a holding potential of -80 mV, then from a holding potential of -40 mV. At -80 mV, voltage-gated calcium channels reside in the closed but activatable state leading to currents from all types of calcium channels (Fig. 16, left; Fig. 17).

With the second protocol (from -40 mV), the low-voltage activated T-type channels are already inactivated before the start of the recording. Only non-T-type calcium channels (including the L-type channels) remain available (Fig. 16, right). The subtraction of the current from the holding potential of -40 mV from the one from -80 mV revealed the T-type channel component.

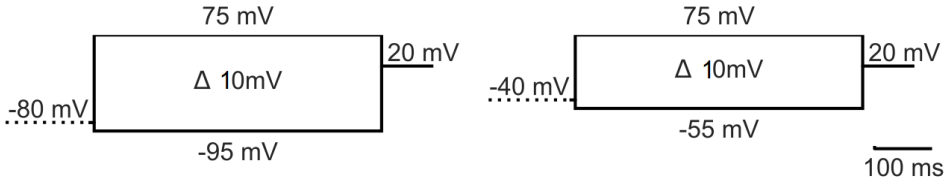

***Figure 16. Voltage clamp protocol in whole-cell patch-clamp experiments**. Voltage clamp protocols starting from a holding potential at - 80 mV with 10 mV voltage steps between -95 and +75 mV were applied to evoke T- and non T-type calcium currents (left). Starting from a holding potential at - 40mV with 10 mV voltage steps between -55 and +75 mV evoked only non-T-type calcium currents (right).*

The resulting maximum amplitude of a T- and L-type $[Ca^{2+}]_i$ current trace of a recorded cell was determined by fitting each current trace with the sum of two exponential decaying functions[52] (equation 2) and subsequently calculating the minimum point of that fitted curve (Fig. 18).

$$I(t) = a_1 \cdot e^{-\frac{t}{\tau_1}} + a_2 \cdot e^{-\frac{t}{\tau_2}} + c \tag{2}$$

I represents the current and t the time. The first and second exponential term represent the activation and inactivation of the Ca^{2+} channel, respectively. a_1 and a_2 are coefficients that scale the magnitude of the two exponential functions, with a_1 having positive values and a_2 having negative values. τ_1 and τ_2 (both having positive values) are the time constants associated with the first and second exponential functions. They represent the time constants of the activation and inactivation, respectively. c is a constant term that represents an offset value added to the function and determines the vertical shift of the curve.

In some cases the current remains almost constant over time. In these cases a biexponential fit is not appropriate and the fitting algorithm does not converge. Instead, the mean

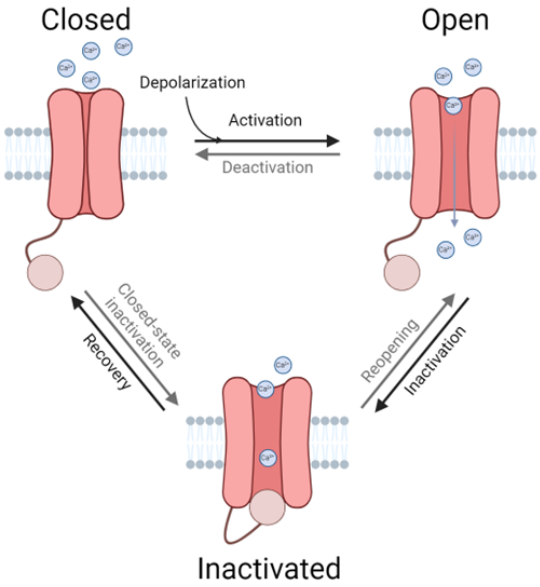

	Holding potential	
Calcium channel	**- 80 mV**	**- 40 mV**
T-Type (threshold of activation ~ - 60 mV)	Closed → Open	Inactivated
Non T-type (threshold of activation ~ - 40 mV)	Closed → Open	Closed → Open
	↓	↓
	T-Type and non T-Type Ca^{2+} currents	Non T-Type Ca^{2+} currents

Figure 17. Three-state model of VGCCs. *The transitions between the closed, open and inactivated states are shown (left). Depolarization from a holding potential of -80 mV activates both T- and non T-type calcium channels. Depolarization from a holding potential of -40 mV opens only non T-type calcium channels since T-type channels reside in an inactivated state (right).*

value was computed within the initial 0.1 seconds following the voltage step.

For each genotype and voltage clamp protocol, the values of the calculated maximum current amplitude (or the current mean) were plotted against the applied potential, and the resulting current-voltage relation datasets were subjected to fitting using equation 3[52]

$$I(V) = G \cdot (V - V_{rev}) \cdot \frac{1}{1 + e^{\frac{-(V - V_{0.5})}{k}}} \tag{3}$$

where I is the measured macroscopic current and V is the tested voltage. G (the maximum conductance), V_{rev} (the reversal potential), $V_{0.5}$ (the half-maximal activation) and k (the slope) are the fitting parameters determined by the fitting algorithm.

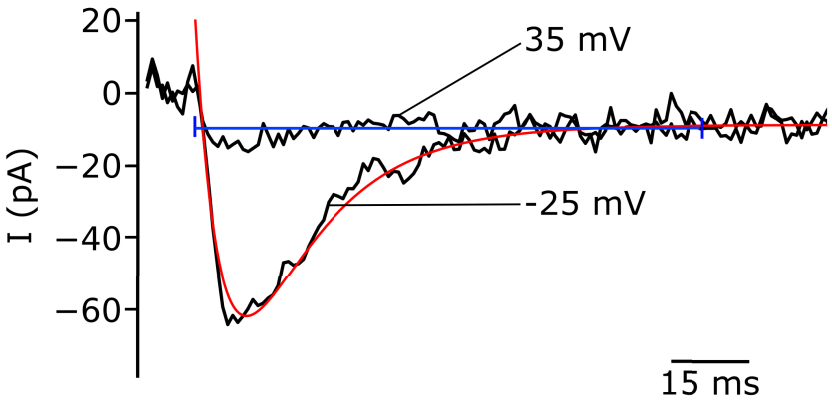

Figure 18. Representative current traces of a recorded cell. *The cell was held at -80 mV for 10 ms before applying voltage steps between -95 and 75 mV (Fig. 16). Only traces at -25 mV and 35 mV are displayed (black lines). The red line represents the fitted biexponential function. In cases, where the current remained almost constant (e.g. 35 mV), the fitting algorithm did not converge. In these cases the mean value was calculated within the first 100 ms following the voltage step (blue line).*

Table 6. *Extracellular solution (pH 7.4) for whole-cell patch-clamp experiments*

Compound	mmol/l
NaCl	100
KCl	4
$CaCl_2$	10
$MgCl_2$	1
TEACl	20
HEPES	10

Table 7. *Pipette solution (pH 7.4) for whole-cell patch-clamp experiments*

Compound	mmol/l
NaCl	10
EGTA	5
CsCl	140
$MgCl_2$	2
HEPES	10

3.5 RNA-sequencing

For RNA extraction from whole adrenal cortices, adrenal glands from 6 WT and 6 KO (3 male, 3 females each) were extracted after euthanizing by cervical dislocation under isoflurane anaesthesia (400 µL as open drop in a 2-l beaker). Glands were rapidly transferred into PBS on ice. The surrounding fat was removed, the glands were cut in half, manually separated from the medulla and placed in RNA-preserving solution (RNAlater, ThermoFisher). Total RNA was isolated using the RNeasy Mini Kit (Qiagen) with subsequent DNAse digestion according to the manufacturer's instructions. Purified RNA was then further processed and sequenced at the Core Unit Genomics of the Berlin Institute of Health at Charité – Universitätsmedizin Berlin as follows. Depletion of ribosomal RNA cDNA transcription was performed using the TruSeq Stranded Total RNA kit (Illumina). 150bp paired-end Sequencing was carried out on a NovaSeq 6000 device on a single lane of a SP flow cell (all from Illumina). Raw data was provided to us as FASTQ files. Results were analyzed by us on the background of Ensembl release 106 of the GRCm39 cDNA transcriptome. Transcriptome indexing was conducted using Salmon[114] (version 1.5.2). Initial quality control of the results was performed using MultiQC[115] (version 1.11). Further quality checks, filtering and trimming was performed using fastp[116] (version 0.12.4). Mapping of reads was also performed using Salmon. Upon inspection, one sample (male KO) had to be excluded from further analysis as ribosomal RNA made up more than 80 % of all reads (likely due to a failure of rRNA depletion).

Filtered gene data was further processed and analyzed using DESeq2[117] (version 1.38.3) in R (version 4.2.1). To identify differentially expressed genes (DEGs) the DESeq function was applied with the chosen threshold criteria of p-values < 0.05 (adjusted using the Benjamini–Hochberg correction) and a 2-fold change (log2 transformed fold change $\pm$ 1, after shrinkage using the apeglm method[118]).

Using the DESeq function resulted in normalized read counts (to account for differences in transcript length and total number of reads per samples) which were used for heatmap generation. If indicated, a Z-score normalization was performed on the normalized read counts across samples for each gene.

Functional enrichment analysis of the identified DEGs was assessed based on Gene Ontology[119] (GO) and KEGG pathway[120] over-representation using the ClusterProfiler[121] package (version 4.6.2) in R. A p-value less than 0.05 was considered as statistically significant.

3.6 Isradipine Treatment

Eight different groups were formed by randomly assigning half of the mice (WT: 11 female, 12 male; *Cacna1d*$^{I772M/+}$: 9 female, 9 male; age 13-14 weeks) into either a isradipine treatment or untreated control group. The randomization was carried out using a custom Python script and the Python library 'random'. The script was provided with a list of the animals IDs, their genotype and sex. A random subset of animal IDs were selected for each group and the size of this subset varied randomly between 4 and 5 for male and female *Cacna1d*$^{I772M/+}$ and 5 and 6 for female WT mice. Male WT mice were randomly assigned in to groups of six animals. The python library 'random' was provided with a 'seed' as a starting point to initialize randomization. This ensures that the randomization process will be reproducible. The resulting list containing the allocation to the treatment group was not available to personnel that conducted or analyzed the experiments. The experimenters were blinded to the administration of isradipine, by employing different personnel for the preparation and feeding of the yogurt (no isradipine) or isradipine-supplemented yogurt.

Mice were given either sweetened yogurt (330 mg, 9% glucose) without (control group) or supplemented with 12.5 mg isradipine per kg bodyweight (treated group) once daily. A slow-release formulation of isradipine (powder of Vascal uno 5 mg capsules, CHEP-LAPHARM Arzneimittel GmbH; 1mg isradipine in 33 mg powder formulation) was mixed with the sweetened yoghurt and weighed for dosing. The manufacturer confirmed that the capsules could be removed without compromising the slow-release function.

The slow-release formulation controls the release of the medication over an extended period by incorporating the active drug into a lipid-based matrix. When the slow-release formulation is ingested, it comes into contact with the fluids in the gastrointestinal tract. Over time, the matrix begins to swell allowing the active drug particles within the matrix to dissolve in the water and to be released[122].

After a week of treatment, three behavioral tests were conducted to assess activity, motor function, and ability to build nests. The open field, rotarod and nest construction test were conducted either 18 h, 4 h , or immediately after yogurt/isradipine feeding, respectively. Collection of blood samples was performed approx. 20 h after the last yogurt/isradipine dose.

Mice were either anesthetized using isoflurane via a vaporizer set to 5% at 1 l/min oxygen flow. Euthanasia was performed using terminal blood collection by cardiac puncture. The blood was collected into Vacutainer EDTA tubes (Becton Dickinson) and were centrifuged (10 min, 2000g, 4℃). The supernatant (plasma) was stored at -20℃ until further analysis.

3.7 Behavioral Phenotyping

3.7.1 Open field

Method

The open field test assesses general activity, exploratory and fear-related behavior in mice[123]. Generally, the open field is an square enclosure with surrounding walls preventing the mouse from escaping. The mouse is allowed to explore the arena for a short amount of time (usually 2-10 minutes). Mice that have fear tend to stay to the outside perimeter and spend less time in the center of the arena. Anxiety and fear causes mice to freeze and suppress locomotion.

Procedure

Mice were placed individually in the center of a square arena (50cm X 50cm, 50 cm height, Fig. 19). They were allowed to explore the open field for 6 minutes. The animal's activity was recorded using a video camera placed above the arena. The total distance moved (tracklength) was analyzed (Viewer 3.0.1, Biobserve).

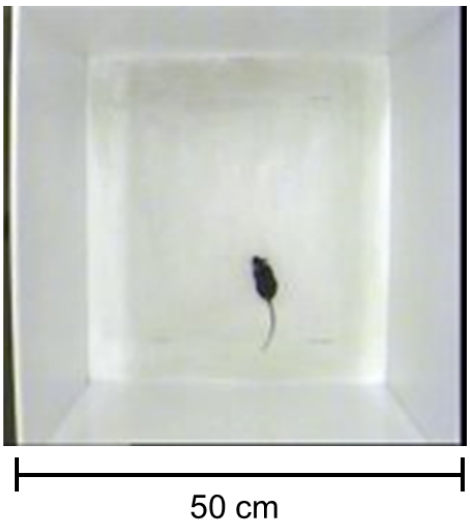

Figure 19. Experimental setup of the open field test. *The mouse is placed in the center of a square arena (50cm X 50cm, 50 cm height).*

3.7.2 Rotarod

Method

The rotarod test assesses balance and motor coordination in rodents[124]. During this test, the animals ability to remain on a horizontal, rotating beam is measured. The initial speed of the rod's rotation is set to 4 rpm and accelerates gradually to 40 rpm withhin the test duration of 5 minutes. During the test, the animals must walk continuously forward to avoid falling of the rod. The latency at which the animals fall of the rod is then recorded. An individual with impaired motor function will show reduced times spent on the rod.

Procedure

Quantification of motor function was performed using the rotarod test (RotaRod Advanced, TSE Systems GmbH, Germany, Fig. 20).The mice were placed on a rotating rod set to 4 rpm. Once they were able to safely walk on the rod, the timer was started and the rotational speed gradually increased to a maximum of 40 rpm within 5 minutes. The duration until the mice fell off was recorded. The experiment was conducted three times, with 15-minute intervals between each trial.

Figure 20. Experimental setup of the rotarod test. *Up to three mice can be place simultaneously in the setup. Adapted from[125].*

3.7.3 Nest Construction

Method

This test evaluates the ability of mice to build a nest when provided with clean nesting material[126]. For small rodents like mice, nest are vital as they facilitate heat conservation as well as for reproduction and shelter. The assessment of this natural behavior is based on the shape of the nest and the amount of used material.

Procedure

Immediately after feeding with yogurt/isradipine, mice were placed in seperate home-cages and were singly housed for the duration of the test. The cage included regular bedding, food and water ad libitum as well as a defined, previously weighed sheet of cellulose nesting material (5 x 5 cm square of pressed white cotton). After approximately 18 h, the structure of the built nest was assessed according to a scale from 0 to 5 and by weighing the remaining, unused nesting material (Table 8)[127].

Table 8. *Nests are assigned scores of 0 to 5 based on the shape of the nest an the amount of used nesting material.*

Score	Criteria
0	untouched cotton square
1	cotton square largely untouched (>90% intact)
2	cotton square is partially torn up (50-90% remaining intact)
3	cotton square is mostly shredded (< 50% remains intact; often without a identifiable nest site; < 90% is within a quarter of the cage floor area)
4	identifiable, but flat nest (> 90% of the material is torn up, gathered into a nest within a quarter of the cage floor area; walls are higher than mouse body height on less than 50% of its circumference)
5	(almost) perfect nest (> 90% of the cotton square is shredded, the nest is a crater with walls higher than mouse body height on more than 50% of its circumference)

3.8 Aldosterone ELISA

Method

Aldosterone levels in blood plasma were determined using a competitive solid phase enzyme-linked immunosorbent assay (ELISA). This technique detects an analyte (antigen, e.g. aldosterone) in a sample using antibodies directed against a unique antigenic site of the analyte[128]. The antibodies are immobilized to a solid phase e.g. the well of a 96-well plate (Fig. 21). The samples are added on to the antibody-coated wells and are incubated together with an enzyme-conjugate composed of horseradish-peroxidase and aldosterone. The enzyme-conjugate and the analyte from the samples compete against the binding sites of the antibodies. After removing all unbound substances by washing, a substrate solution is added. The horseradish-peroxidase from the conjugate reacts with the substrate producing a colorimetric signal. The intensity of the color is inversely proportional to the aldosterone levels in the sample. Absolute concentrations of the analyte in the sample can be determined by using concentration standards and construction of a standard curve.

Procedure

To obtain blood plasma samples, mice were anesthetized with isoflurane (via a vaporizer set to 3% at 1 l/min oxygen flow) and blood was collected by cardiac puncture into Vacutainer EDTA tubes (Becton Dickinson). Blood samples were centrifuged (10 min, 2000g, 4 ℃), and the supernatant (plasma) was stored at -20 ℃ until further analysis. Plasma aldosterone was determined by ELISA (aldosterone: RE52301, IBL International). Standard, control, and samples (100 µL) were added into appropriate wells coated with antibodies and incubated for 30 minutes at RT. The Enzyme Conjugate was added into each well, thoroughly mixed for 10 seconds and incubated for 60 minutes at RT. Using an automated plate washer the wells were rinsed three times with wash solution (100 µL per well). Subsequently, the substrate solution (100 µl) was added to each well and incubated for 30 minutes at RT. After termination of the enzymatic reaction by adding the stop solution (50 µl per well) the optical density of the solution in each well was measured at 450 nm.

3.9 Statistics

All P-values (except for the differential expression analysis) are results from a likelihood ratio test of linear mixed models and are indicated as follows: ns, $P \geq 0.05$; *, <0.05; **,

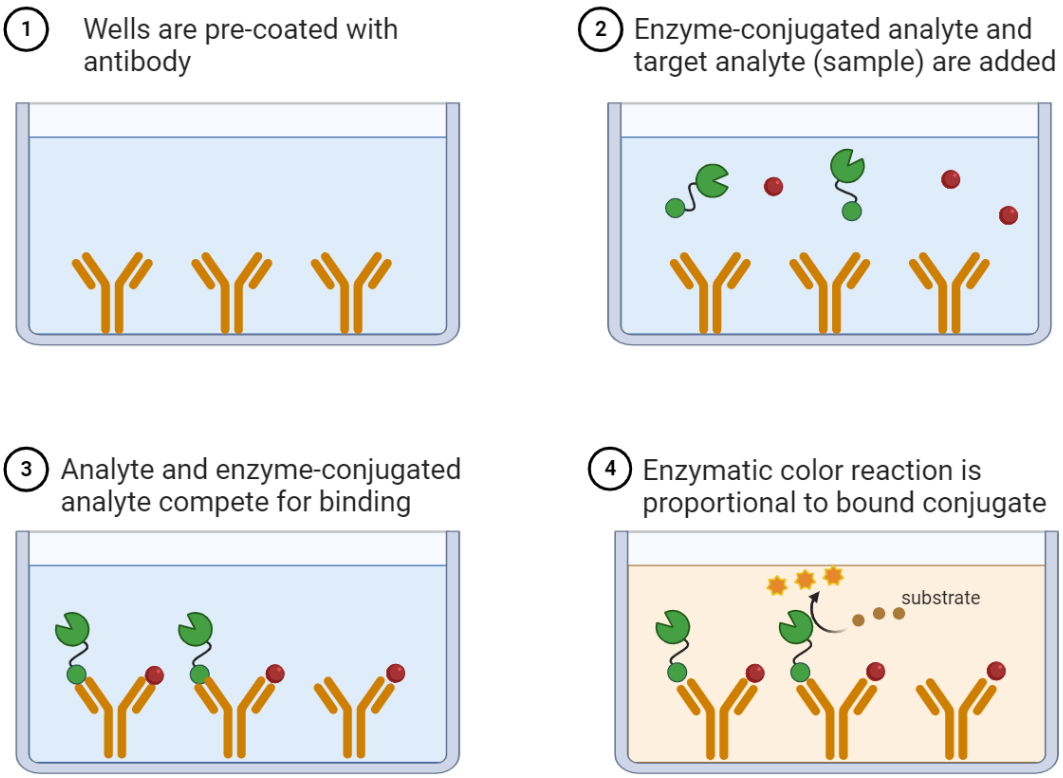

Figure 21. Schematic representation of the competitive ELISA principle. *Enzyme-conjugate and the target analyte (i.e. sample/aldosterone) compete for binding sites of the antibodies immobilized to the well. The enzymatic-conjugate catalyzes the enzymatic color reaction and the signal is proportional to the amout of bound conjugate.*

P<0.01; ***, P<0.001. Statistical mixed model analysis was performed in R (4.2.1) using the glmmTMB package (version 1.1.5). Normality of the data was assured visually using quartile-quartile plots and inspection of residuals after fitting. If data was not normally distributed, a diverse set of distributions was tested using DHARMa (version 0.4.6), and either the log-Tweedie or log-Gamma distribution was chosen for further analysis using glmmTMB. Individual recordings were treated as random effect.

For differential expression analysis, reads obtained by RNA sequencing were normalized and differentially analyzed using the DESeq2 package (version 1.38.3).

If not otherwise specified, all error bars and bands show 95% confidence interval (CI) of the mean value.

All box plots follow Tukey-style with the box showing 25^{th} (upper box limit), median (central horizontal line) and 75^{th} percentiles (lower box limit). Whiskers reach to the maximum and minimum values within a range of 1.5 inter-quartile range(distance between $25^{th}$and 75^{th} percentiles) and values outside of this range are shown as diamonds.

Figures

Figures 1, 2, 5, 6, 7, 14, 15, 17 and 21 were created using Biorender.com.

3.10 Chemicals and reagents

Table 9. *List of chemical, reagents and solvents*

Chemical, reagent or solvent	Molecular weight [g/mol]	CAS	Catalog number	Manufacturer (location, country)
(+)-α-Tocopherol, $C_{29}H_{50}O_2$	430.71	59-02-9	sc-214454	ChemCruz® Biotchemicals (Dallas, USA)
2-Mercaptoethanol, C_2H_6OS ≥99%, p.a.	78.13	60-24-2	4227.1	Carl Roth (Karlsruhe, Germany)
Agarose Low Melt, ROTI®Garose with lower melting and gelation temperatures	-	39346-81-1	6351.5	Carl Roth (Karlsruhe, Germany)
Aldosterone ELISA Kit	-	-	RE5230	IBL International (Hamburg, Germany)
Angiotensin II human, $C_{50}H_{71}N_{13}O_{12}$ powder ≥93% (HPLC)	1046.18	4474-91-3	A9525-1MG	Sigma-Aldrich (St. Louis, USA)
Calbryte™ 520 AM, ≥95%	1090.90	-	20650	AAT Bioquest (Pleasanton, USA)
Calcium Calibration Buffer Kit	-	-	C3008MP	Thermo Scientific (San Diego, USA)

Table 9. *List of chemical, reagents and solvents*

Chemical, reagent or solvent	**Molecular weight [g/mol]**	**CAS**	**Catalog number**	**Manufacturer (location, country)**
Calcium chloride dihydrate, $CaCl_2 \cdot 2\ H_2O$, $\geq$99%	147.01	10035-04-8	C3306-250G	Sigma-Aldrich (St. Louis, USA)
Collagenase Type II sterile filtered	-	-	BS.C2-28	Bio&Sell (Worthington, USA)
Collagenase Type IV sterile filtered	-	-	BS.C4-28	Bio&Sell (Worthington, USA)
CsCl				
D-(+)-Glucose, $C_6H_{12}O_6$ powder, BioReagent $\geq$99.5%	180.16	50-99-7	G7021-1KG	Sigma-Aldrich (St. Louis, USA)
DMEM/F-12 (1:1) Dulbecco's Modified Eagle Medium, F-12 Nutrient Mixture (Ham)	-	-	11320033	Gibco (Carlsbad, USA)
DMSO, $(CH_3)_2SO$ Dimethyl sulfoxide Hybri-Max™, sterile-filtered, BioReagent $\geq$99.7%	78.13	67-68-5	D2650-5X5ML	Sigma-Aldrich (St. Louis, USA)
EGTA, $C_{14}H_{24}N_2O_{10}$ $\geq$99%, p.a.	380.35	67-42-5	3054.2	Carl Roth (Karlsruhe, Germany)

Table 9. *List of chemical, reagents and solvents*

Chemical, reagent or solvent	**Molecular weight [g/mol]**	**CAS**	**Catalog number**	**Manufacturer (location, country)**
Ethanol, C_2H_6O ROTIPURAN® $\geq$99.8%, p.a.	46.07	64-17-5	9065.1	Carl Roth (Karlsruhe, Germany)
Ethanol, C_2H_6O $\geq$96%, vergällt	46.07	64-17-5	T171.5	Carl Roth (Karlsruhe, Germany)
Fura-2 AM UltraPure Grade $\geq$95%	1001.86	108964-32-5	21023	AAT Bioquest (Pleasanton, USA)
HEPES, $C_8H_{18}N_2O_4S$ *N*-2-Hydroxyethylpiperazine-*N'*-2-ethane sulphonic acid PUFFERAN®, Buffer Grade, $\geq$99.5 %	238.31	7365-45-9	HN78.2	Carl Roth (Karlsruhe, Germany)
Hydrochloric acid 37%, HCl AnalaR® NORMAPUR® Reag. Ph. Eur. analytical reagent	36.46	7647-01-0	20252.295P	VWR International LLC (Radnor, USA)
Ionomycin Ionophore	709.01	56092-81-0	sc-263405	Santa Cruz Biotechnology, Inc. (Dallas, USA)
Isofluran CP 1 ml/ml Isoflurane Anaesthetic gas	184.5	26675-46-7	1214	CP-Pharma (Burgdorf, Germany)
Isradipine	371.4	75695-93-1	Cay17536-5	Cayman Chemical (Ann Arbor, USA)

Table 9. *List of chemical, reagents and solvents*

Chemical, reagent or solvent	**Molecular weight [g/mol]**	**CAS**	**Catalog number**	**Manufacturer (location, country)**
ITS™+Premix Universal Culture Supplement (Insulin (5 µg/ mL), Transferrin (5 µg/ mL), and Selenious Acid (5ng/ mL))	-	-	354352	Corning (Bedford, USA)
Laminin, $\geq$90%	400000-900000	-	sc-29012	Santa Cruz Biotechnology, Inc. (Dallas, USA)
L-Ascorbic acid, $C_6H_8O_6$, Free acid, $\geq$98%	176.12	50-81-7	sc-202686	ChemCruz® Biochemicals (Dallas, USA)
Magnesium chloride hexahydrate, $MgCl_2 \cdot 6\ H_2O$, CELLPURE®, $\geq$99 %	203.30	7791-18-6	HN03.2	Carl Roth (Karlsruhe, Germany)
PBS (1x), phosphate buffered saline, ROTI®Cell, pH 7.4 ± 0.1, CELLPURE® ready-to-use, sterile, without Ca/Mg	-	-	9143.1	Carl Roth (Karlsruhe, Germany)

Table 9. *List of chemical, reagents and solvents*

Chemical, reagent or solvent	**Molecular weight [g/mol]**	**CAS**	**Catalog number**	**Manufacturer (location, country)**
Pen Strep (100x) Penicillin Streptomycin [+] 10.000 Units/ml Penicillin, [+] 10.000 µg/ml Streptomycin Prevention of Cell Culture Contamination	-	-	15140-122	Gibco (Grand Island, USA)
Pluronic®F-127, $(C_3H_6O \cdot C_2H_4O)_x$ Powder, BioReagent	ĩ12600	9003-11-6	P2443-250G	Sigma-Aldrich (St. Louis, USA)
Poly-L-Lysin, $(C_6H_{14}N_2O_2)_x$ 0.01% Lösung	-	25104-18-1	BS.L7250	Bio&Sell (Feucht, Germany)
Potassium chloride, KCl, Extra Pure, Specified Laboratory Reagents, Eur. Ph., >95%	74.55	7447-40-7	P/4240/60	Fisher Chemical (Loughborough, United Kingdom)
Potassium D-gluconate, $C_6H_{11}KO_7$ 99 %	234.25	299-27-4	B25135.0B	Thermo Scientific Chemicals (Heysham, United Kingdom)
RNase AWAY™ Surface Decontaminant Removes RNase & DNA Contamination	-	-	7005-11	Thermo Scientific (San Diego, USA)
RNeasy Mini Kit Total RNA isolation Kit	-	-	74106	Quiagen (Hilden, Germany)

Table 9. *List of chemical, reagents and solvents*

Chemical, reagent or solvent	**Molecular weight [g/mol]**	**CAS**	**Catalog number**	**Manufacturer (location, country)**
Sodium bicarbonate, $CHNaO_3$ $\geq$ 99.7%, ACS reagent	84.01	144-55-8	424270010	Thermo Scientific Chemicals (Heysham, United Kingdom)
Sodium chloride, NaCl p.a., ACS,ISO $\geq$99.5 %	58.44	7647-14-5	3957.2	Carl Roth (Karlsruhe, Germany)
Sodium gluconate, $C_6H_{11}NaO_7$, $\geq$99 %	218.14	527-07-1	S/4100/53	Fisher Chemical (Loughborough, United Kingdom)
TEACl				
Trypsin-EDTA (1X, 0.05%) Cell dissociation reagent	-	-	25300-054	Gibco (Carlsbad, USA)
TTA-P2	431	918430-49-6	T-155	Alomone labs (Jerusalem, Israel)
Ultroser™ G Serum substitute for animal cell culture	-	-	15950-017	Pall BioSepra (Cergy, France)
vascal® uno 5 mg Retardkapseln 100 Hard capsule, retard formulation Isradipine for treatment of mice	371.4	-	PZN 04640357	CHEPLAPHARM Arzneimittel GmbH (Greifswald, Germany)

4 Results

4.1 Calcium Signals in *Cacna1h* KO mice

The data in this section has additionally been published in[129]

4.1.1 ZG cells from $Ca_V3.2$ KO still exhibit intracellular calcium oscillations

To investigate $[Ca^{2+}]_i$ in ZG cells of WT and $Ca_V3.2$ KO mice, fresh slices from the adrenal gland were prepared and loaded with fluorescent calcium sensitive dyes (see Methods section 3.2). This technique retains ZG cells in a more physiological setting compared to cultured primary cells that were enzymatically or mechanically dissociated from tissue. The intensiometric calcium indicator Calbryte 520 AM was used to achieve a high temporal resolution while the ratiometric Fura-2 AM dye allowed for absolute measurements of the $[Ca^{2+}]_i$.

Stimulation of ZG cells from WT mice with Ang II (500 pM) and K^+ (4 mM) elicited pronounced $[Ca^{2+}]_i$ oscillations of intermediate frequency ($\sim$ 0.5 Hz) (Fig. 22A) similar to those observed in a previous study[81]. These Ca^{2+}oscillations consist of individual spikes (Ca^{2+}signals) which exhibited a homogeneous appearance regarding amplitude and frequency. Spikes were clustered in bursts that were separated by pauses without activity. These pauses represent the baseline. The $[Ca^{2+}]_i$ during the baseline remained at mostly constant levels.

As discussed in the introduction (see Section 1.4), it has been proposed that Ca^{2+}signals in the murine ZG are dependent on the function of $Ca_V3.2$.

However, ZG cells from mice lacking the $Ca_V3.2$ calcium channel also exhibited calcium signals in this project (Fig. 22B). Their appearance was very similar to those in WT slices. One of the most striking differences was that ZG cells from KO mice exhibited a significantly

elevated overall spiking activity (average number of spikes per seconds (Fig. 23A, data in Table A1) due to an increased spike frequency within bursts (Fig. 23B) as well shorter pauses between the bursts (Fig. 23C). The burst length was unchanged between the two genotypes (Fig. 23D).

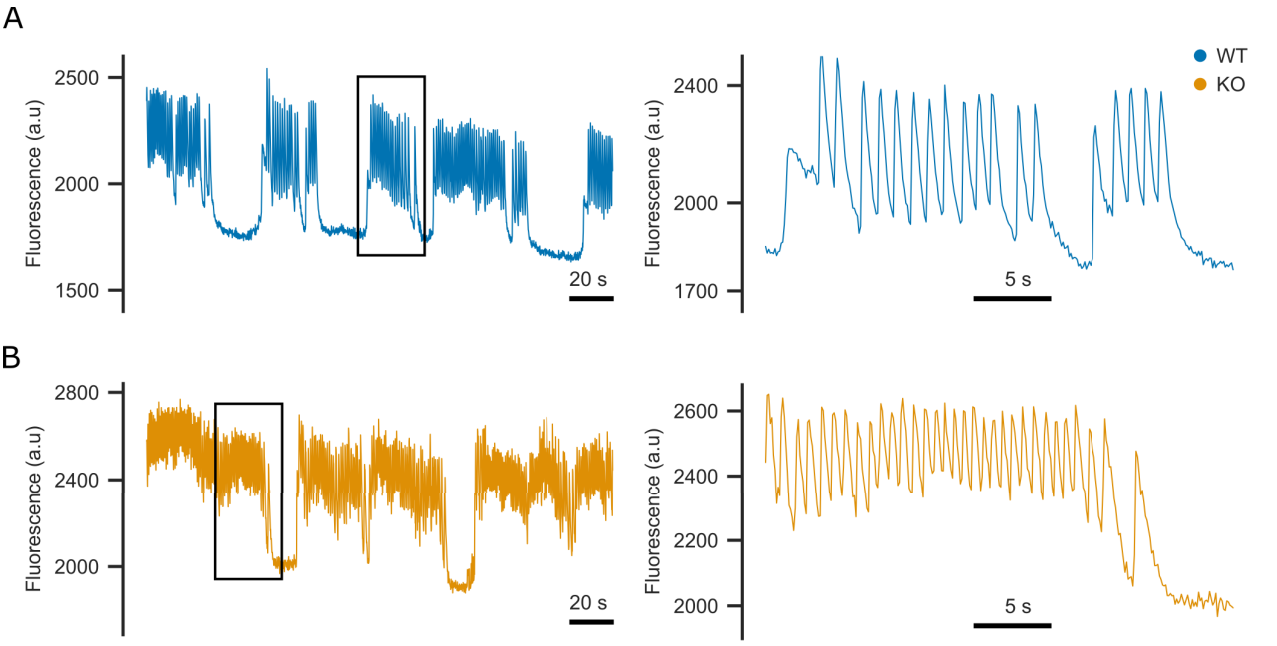

Figure 22. Calcium oscillations are preserved in mice lacking the Cacna1h gene. (A-B) *The fluorescence signals were captured over a 3.5-minute period from one representative ZG cell of a WT* ***(A)*** *and knockout* ***(B)*** *adrenal slice stained with Calbryte 520 AM. These cells were stimulated with 4 mmol/l K^+ and 500 pmol/l Ang II. On the right, a corresponding 30-second magnification (indicated by the black rectangle on the left) is shown.*

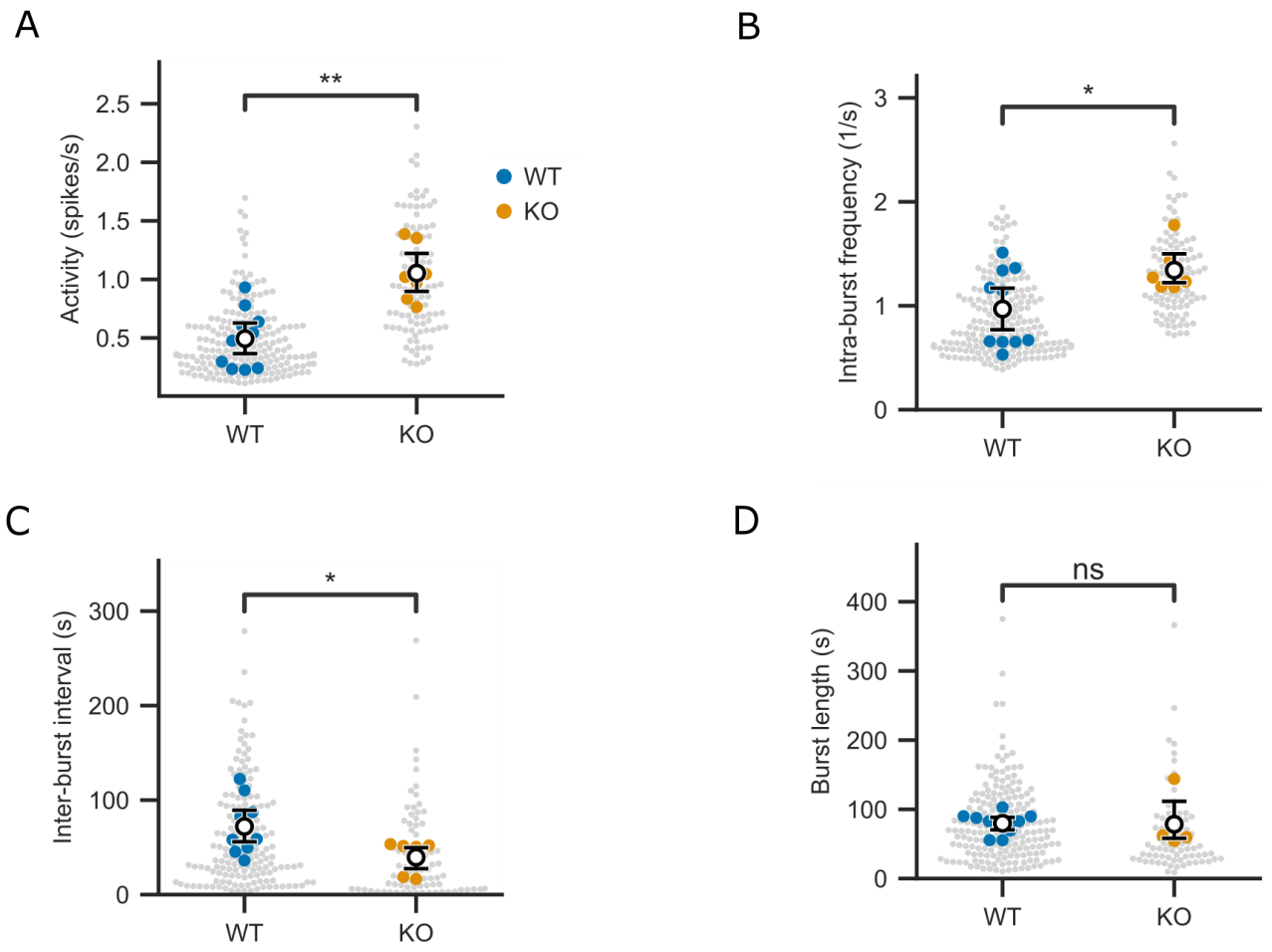

Figure 23. Activity and bursting parameters of WT and KO ZG cells. ***(A)*** *The calcium spike activity (average number of spikes per cell per second) recorded in ZG cells over 7.5 minutes is lower in WT than in KO mice. Adrenal slices were stained with Calbryte 520 AM.* ***(B)*** *The mean frequencies of calcium oscillations during a bursts (intra-burst frequency) were elevated in KO ZG cells compared to WT.* ***(C)*** *The average time not spent in calcium bursting (inter-burst interval) was decreased in KO cells.* ***(D)*** *The mean length of a burst was unchanged between genotypes. P values were assessed with a likelihood ratio test of linear mixed models (see section statistic 3.9). The mean of all mean values per slice in* ***A-D*** *are shown as white circles ± 95 % confidence intervals (CI, error bars). Mean values per slice and cell are shown as larger colored and smaller grey circles, respectively.*

4.1.2 The sensitivity to physiological stimuli is unchanged in ZG cells of $Ca_V3.2$ KO mice

To investigate whether the increase in activity in $Ca_V3.2$ KO cells represents a compensatory mechanism to reach mean $[Ca^{2+}]_i$ - which are required for aldosterone synthesis - similar to WT, ZG cells were loaded with the Fura-2 AM dye (see Methods section 3.2).

Mean $[Ca^{2+}]_i$ levels were measured in ZG cells stimulated with varying concentrations of potassium (Fig. 24A, data in Table A2) and Ang II (Fig. A24B, data in Table A3), the main physiologic stimuli of aldosterone synthesis.

Between genotypes, the mean $[Ca^{2+}]_i$ concentrations were similar over all tested concentrations. This indicates that the increase of activity and intra-burst frequency of calcium signals is sufficient to maintain the $[Ca^{2+}]_i$ and thus the physiological regulation of aldosterone synthesis.

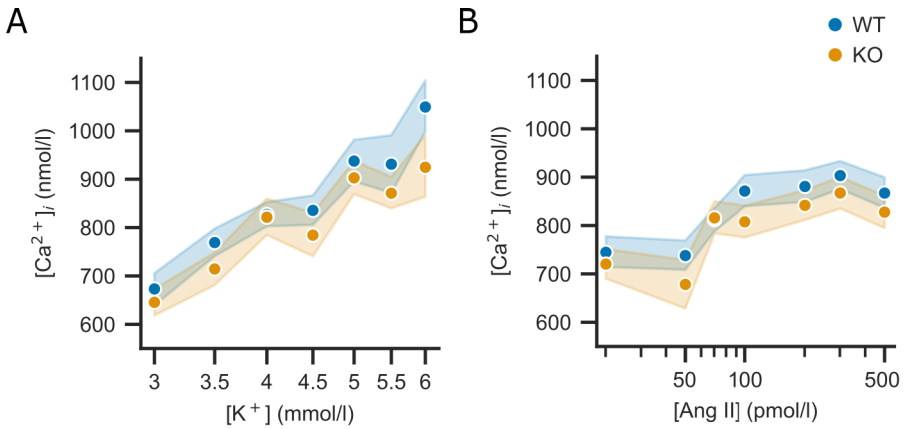

Figure 24. The average $[Ca^{2+}]_i$ was determined in ZG cells of slices stained with Fura-2 AM. *In **(A)**, the level of Ang II was maintained at 100 pmol/l, in **(B)**, the potassium concentration remained fixed at 4 mmol/l. Data are plotted as mean values of all cells (circles) ± 95% CI (shaded areas).*

4.1.3 Adrenal cortical cells from $Ca_V3.2$ KO mice exhibit only few differentially expressed genes

The loss of $Ca_V3.2$ in KO mice might result in the differential expression of compensatory genes. To identify up- or down regulated genes and to quantify the overall expression of VGCCs in WT, bulk RNA-sequencing was performed of adrenal cortices from 6 WT and 5 KO mice (see Methods section 3.5).

In WT, *Cacna1h* ($Ca_V3.2$), *Cacna1c* ($Ca_V1.2$) and *Cacna1d* ($Ca_V1.3$) exhibited the strongest expression among the VGCC pore-forming α_1-subunits (Figure 25A, data in Table A4-5).

For an overall analysis of differentially expressed genes (DEGs), a cutoff of at least a 2-fold change between KO and WT was chosen. With this analysis, 12 differentially expressed genes were identified (Figure 25B and C). Apart from a strong downregulation of *Cacna1h* mRNA in KO cells, most likely due to nonsense-mediated decay (NMD), the expression of other known VGCC genes was not significantly changed between genotypes (Figure 25B and C, data in Table A6).

The process of NMD entails the degradation of mRNAs containing translation termination codons situated in abnormal positions[130]. These mRNAs encode truncated proteins with no or undesired functions. NMD prevents the accumulation of these transcripts and mitigates the potential buildup of aberrant proteins.

A second analysis was performed without a specific threshold for the fold change between KO and WT samples, in order to not miss smaller changes in gene transcription involved in the aldosterone synthesis.

Conducting analyses without employing stringent cutoffs introduces the possibility of detecting more false positives. However, this approach was considered acceptable, given the focus on only a limited subset of genes associated with aldosterone synthesis.

This analysis was performed for known genes within the aldosterone synthesis pathway according to the KEGG database[120].

Predefined gene sets and pathways are genes grouped together based on their function and molecular interaction. A collection of such gene sets and pathways can be found in databases (e.g. GO[119], KEGG[120]).

While the use of a predefined gene sets may introduce a bias by potentially excluding unidentified or unannotated genes, these curated sets remain widely accepted for their efficiency and ability to provide meaningful insights into known pathways and functions.

In adrenal cortices from KO animals, a small but significant upregulation of *Agtr1a* (angiotensin II receptor) and *Star* (transports cholesterol into the mitochondria for conversion in aldosterone) as well as a downregulation of *Gna11* (encodes the Gq protein α-subunit, which activates the PLC-PIP_2-DAG-IP_3 cascade) were identified (Table A7).

To identifiy gene sets or pathways that significantly overlap with the set of observed DEGs an overrepresentation analysis was performed. Overrepresentation analyses for the set of DEGs did not yield any over- or under-represented sets or pathways withhin the KEGG or GO databases including the aldosterone synthesis in general.

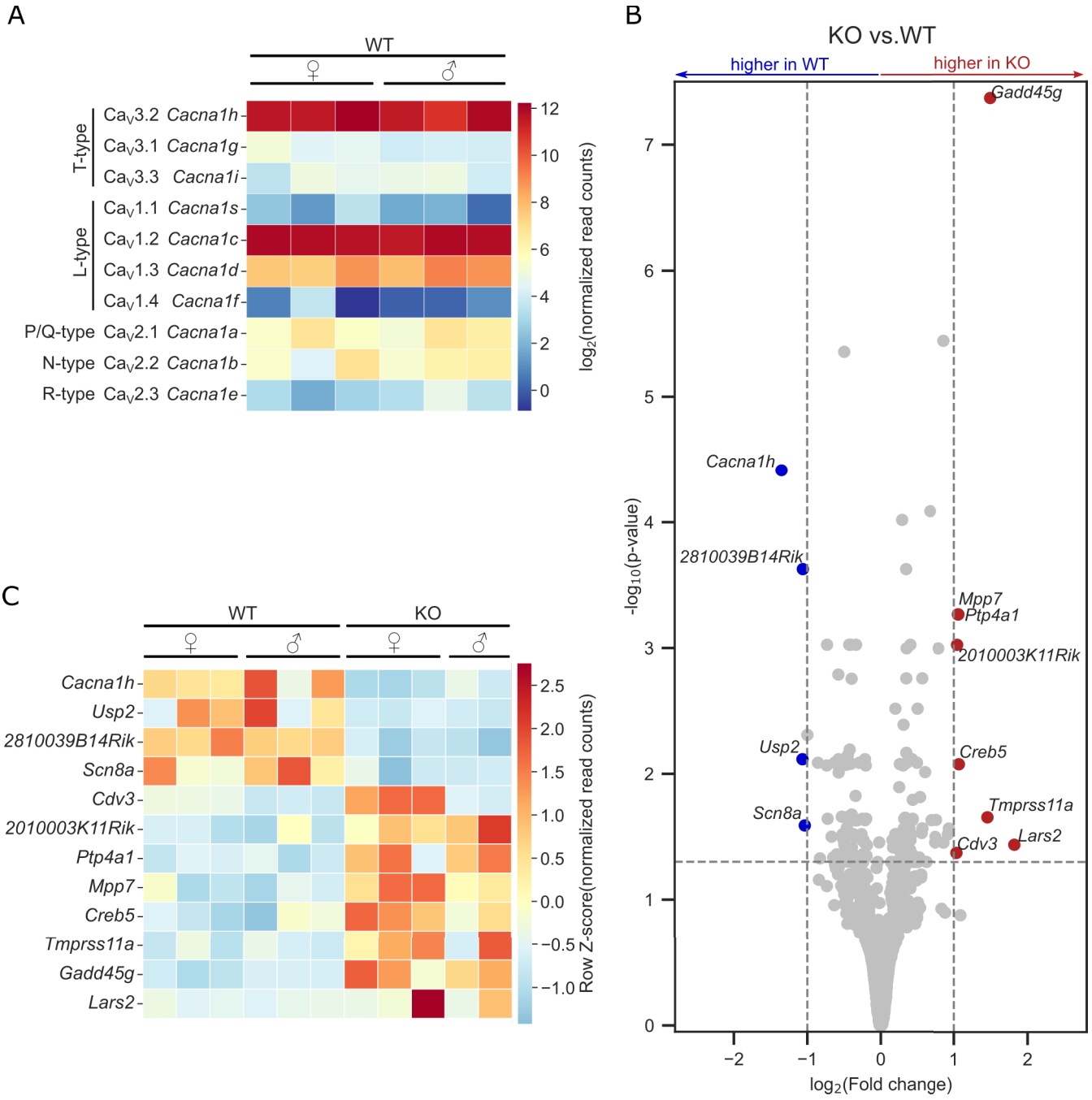

Figure 25. RNA-seq of adrenal cortical cells from WT and $Ca_V3.2$ KO mice reveals only few differentially expressed genes. ***(A)*** *Heat map illustrating the normalized log_2 transformed read counts of VGCC transcripts detected in WT samples (columns, $n_{animals}$, WT = 6).* ***(B)*** *Volcano plots with the log_2-fold change (LFC, cutoff = |1|) in gene expression in KO vs. WT samples ($n_{animals,WT}$ = 6, $n_{animals,KO}$ = 5) and the log_{10} transformed statistical significance (p-value, corrected for multiple testing, log_2 transformed cutoff=0.05). The 12 differentially expressed genes (DEGs) with more than 2-fold change are highlighted as up- (red) or down (blue) regulated.* ***(C)*** *Heatmap illustrating the row Z-score of the normalized read counts of significantly up- or down regulated genes sorted by their LFC.*

4.1.4 Adrenocortical cells lacking $Ca_V3.2$ exhibit L-type calcium currents

To study the calcium conductances present in WT and KO tissue, adrenal cortices were dissociated into a cell suspension (see Methods section 3.3) and whole-cell patch-clamp recordings were performed in these cells (see Methods section 3.4).

The ion concentrations for both the pipette and extracellular bath solution have been selected to replicate physiological conditions of the ionic strength (see Table 6 and 7), facilitating the recording of calcium currents.

The bath solution contains Na^+, Cl^-, K^+, and Mg^+ ions, mirroring the composition of the extracellular environment. To minimize the influence of K^+ channels, TEA-Cl, which blocks K^+ channels has been added to the bath solution.

The pipette solution follows a similar approach to mimic physiological conditions, except for the inclusion of Cs^+. Instead of KCl, CsCl is included to further reduce the influence of K^+ currents.

To enhance the amplitude of calcium currents and improve the signal-to-noise ratio, the extracellular Ca^{2+}concentration has been increased to 10 mmol/l compared to the typical physiological concentration of approx. 2 mmol/l.

EGTA has been introduced into the pipette solution to mitigate calcium-dependent inactivation of VGCCs.

To maintain a stable pH level of 7.4 in both the bath and pipette solutions, HEPES has been included.

Using two separate voltage protocols, calcium currents mediated by low voltage activated T-type calcium channels could be distinguished from currents mediated by non-T-type calcium channels[113] (see Section 3.4).

WT cells showed calcium currents mediated by both T- and non-T-type calcium channels (Fig. 26A-B, data in Table A8). However, all tested KO cells exhibited only non-T-type calcium currents but no T-type calcium currents (Fig. 26B, representative cell in Fig. 26C, data in Table A9). Additionally, the maximum amplitude and voltage-dependency of the non-T-type current was unchanged in KO compared to WT cells (Fig. 26A and B). This excludes large post-translational modifications mediated by non-T-type calcium channels to increase the calcium current and to compensate for the loss of $Ca_V3.2$.

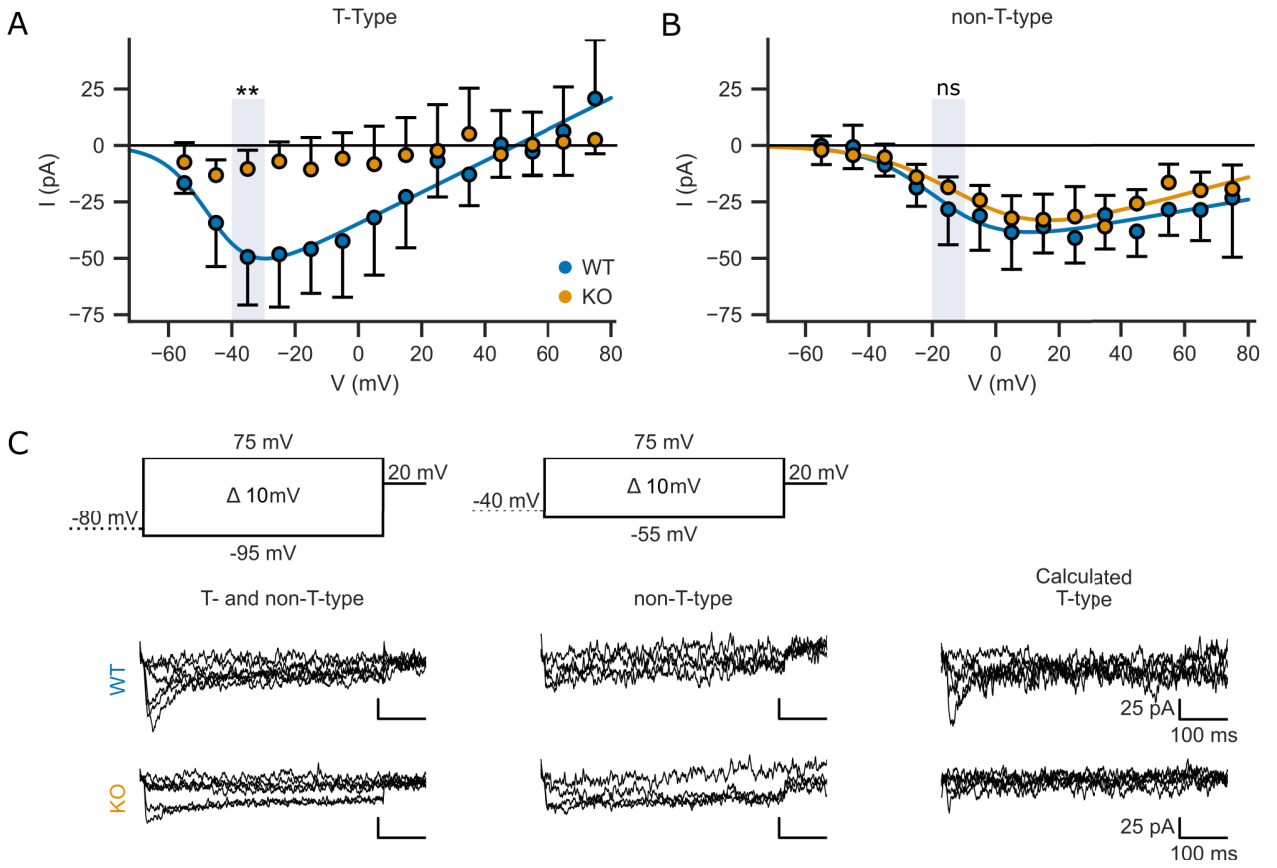

Figure 26. ZG cells from KO cells do not exhibit T-type currents. *Whole-cell patch-clamp recordings were conducted in isolated adrenocortical cells.* ***(A)*** *Voltage dependence of the T-type peak current amplitudes shown as I-V curves reveals larger amplitudes in WT compared to KO at -35 mV.* ***(B)*** *Voltage dependence of the non-T-type peak current amplitudes demonstrates similar amplitudes in both genotypes. Mean + or - 95% CI (only one half) are shown. Solid lines represent fits of the data by equation 3.* ***(C)*** *Exemplary recordings of calcium currents in isolated adrenocortical cells from both WT and KO mice were obtained using two different voltage clamp protocols. The first protocol from a holding potential of -80 mV involved voltage steps from -95 mV to +75 mV (upper, left). The second protocol started from -40 mV with voltage steps spanning from -55 mV to +75 mV (upper, middle). T-type current (right) was calculated by subtracting the current elicited from -40 mV (middle) from the current elicited from -80 mV (left).*

4.1.5 Calcium signals in ZG cells from $Ca_V3.2$ KO animals do not require other T-type Ca^{2+}channels

The absence of detectable T-type currents in whole-cell patch-clamp recordings already implied that $Ca_V3.2$ was the only T-type calcium channel present in adrenocortical cells.

In order to further confirm its role for calcium oscillations in ZG cells, adrenal slice preparations were subjected to the T-type calcium channel inhibitor TTA-P2[131]. The effect in both genotypes was again studied using calcium imaging. TTA-P2 was employed at a concentration of 15 µmol/l, slightly exceeding the concentration previously administered to ZG cells[82]. At this concentration, an almost complete inhibition of all T-type calcium channels is expected while the inhibiton of L-type channels is anticipated to be less than 10%[132].

In the presence of TTA-P2, ZG cells from KO mice exhibited unaltered oscillatory calcium fluctuations (Fig. 27A). This further implies the absence of other T-type channels. Treatment of WT slices resulted in a mixed response where some cells showed continued calcium spiking (Fig. 27B), while other became completely quiescent (Fig. 27C). In general, approximately 34% of the WT cells maintained their activity (Fig. 27D, data in Table A10-11) significantly decreasing the mean activity compared to untreated controls (Fig. 27E, data in Table A12). In contrast, the KO cells remained unaffected relative to controls (Fig. 27E, data in Table A13; Fig. 27F, absolute data in G).

Interestingly, WT cells that maintained their activity in the presence of TTA-P2 exhibited an increased intra-burst frequency (Fig. 28A, data in Table A14; absolute data in 28B and C, data in Table A15), reminiscent of but still below the level observed in KO cells.

These results confirm the important role of $Ca_V3.2$ in generating calcium spikes in WT mice. Moreover, it is evident that alternative calcium influx pathways must exist that can sustain calcium oscillations even in the absence of T-type calcium channels. These mechanisms are present in at least a subset of the WT cells and may contribute to the calcium oscillations observed in KO cells.

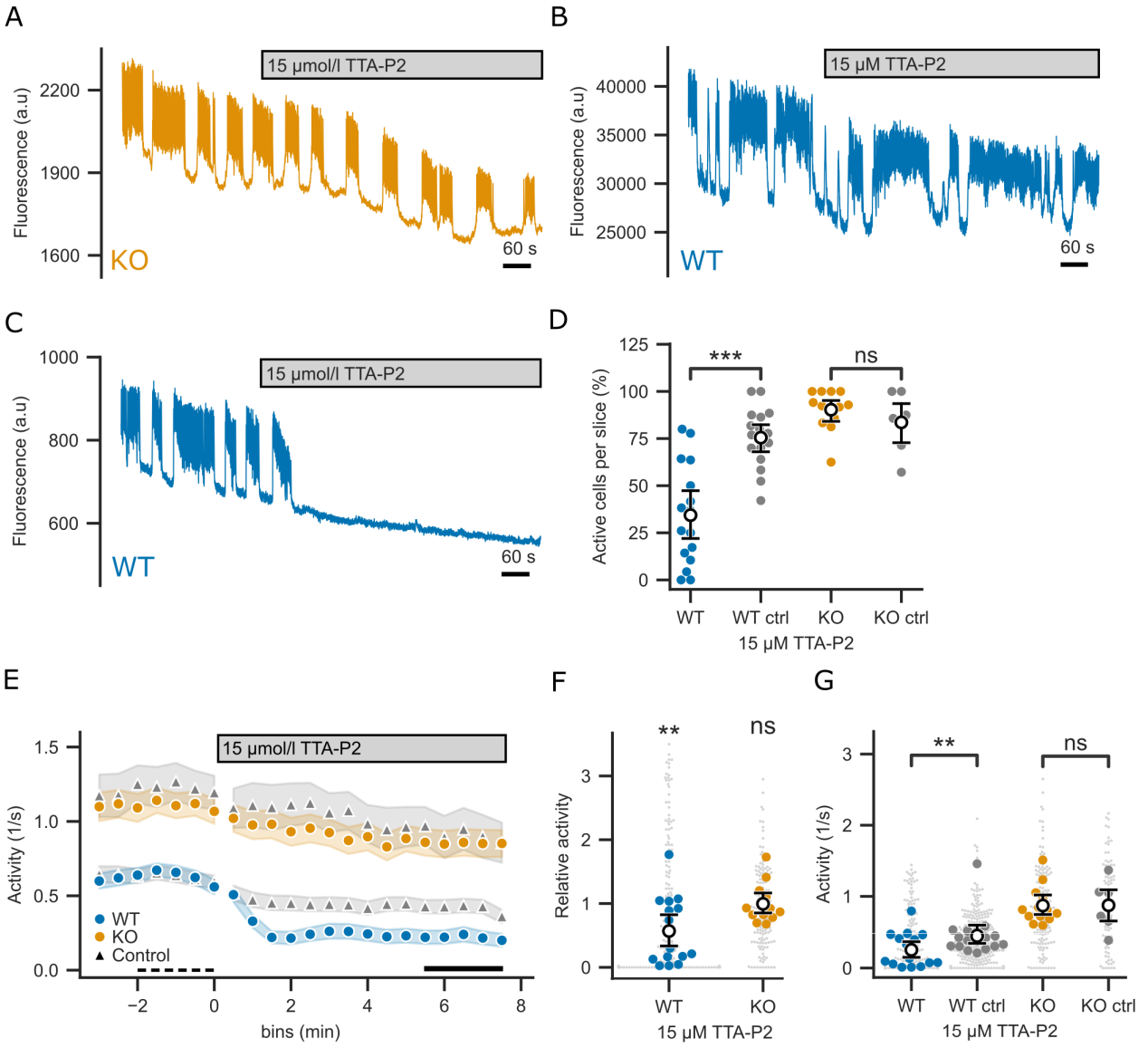

Figure 27. TTA-P2 does not affect calcium spiking in $Ca_V3.2$ KO ZG cells and only partially inhibits calcium oscillations in WT ZG cells of mice. (A-C) *Changes in Ca^{2+} spiking recorded in one representative KO **(A)** and two WT **(B-C)** ZG cells. Adrenal slices were stained with Calbryte 520 AM and recorded at 4 mmol/l K^+ and 500 pmol/l Ang II. Grey bars indicate TTA-P2 application. **(D)** Fraction of ZG cells in a slice that still exhibited calcium spike activity under 15 µmol/l TTA-P2 (determined in the time span from 5.5 to 7.5 minutes after addition of TTA-P2, indicated by the black line in (E) compared to the number of active cells before addition of TTA-P2 (from -2 to zero minutes, indicated by the black dashed line in (E)). This value was significantly decreased in WT slices but not KO slices compared to respective untreated controls. **(E)** In WT but not KO ZG cells calcium spike activity (in 0.5 minutes bins) was lowered by 15 µmol/l TTA-P2 (indicated by the grey bar, circles: mean) when compared to untreated controls (triangles: mean; shaded area: 95% CI). **(F)** Relative activity between 5.5 and 7.5 minutes after the start of the perfusion was significantly reduced by 15 µmol/l TTA-P2 in WT but not KO cells (absolute data in **G**). Individual values per slice and cell are shown as larger and smaller circles, respectively. Overall mean values over slices in D, F and G are shown as white circles ± 95% CI (error bars). Data in **(F)** were calculated relative to untreated control recordings. Values per genotype were tested against respective controls (likelihood ratio test of linear mixed models).*

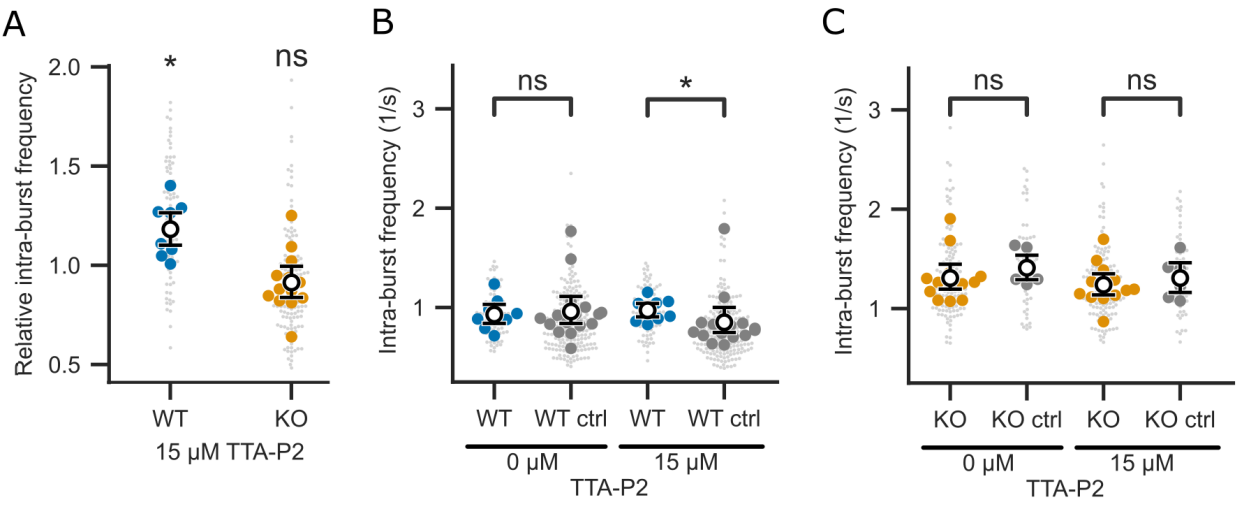

Figure 28. WT but not $Ca_V3.2$ KO cells showed a significantly changed intra-burst frequency upon perfusion with 15 µmol/l TTA-P2, when compared to corresponding controls. ***(A)*** *Only cells that remained active at 15 µmol/l TTA-P2 are shown (absolute data in* ***(B)*** *and* ***(C)****. Data are shown as overall mean per group (white circle) ± 95% CI (error bars). Individual values of cells and slices are shown as smaller and larger spots, respectively. Values per genotype were tested against respective controls (likelihood ratio test of linear mixed models).*

4.1.6 L-type calcium channels mediate calcium signals in the ZG of $Ca_V3.2$ KO mice

The expression data from WT mice obtained by RNA-sequencing showed that not only T-type channels were expressed by the adrenal cortex but also L- and, although to a lesser extent, N- and P/Q type calcium channels.

In order to assess the importance of L-type channels for calcium signaling in the ZG of WT and KO mice, adrenal slices were treated with the specific L-type channel inhibitor, isradipine, and calcium imaging was conducted.

Isradipine belongs to the dihydropyridine class of compounds, characterized by the presence of a dihydropyridine ring in its chemical structure, a common motive shared by calcium channel blockers. Unlike other dihydropyridines, Isradipine targets L-type channels $Ca_V1.3$ and $Ca_V1.2$ with an equal potency and is a clinically approved drug for the treatment of high blood pressure[133–135].

The concentration of isradipine was chosen to target L-type calcium channels with a high specificity[133,134,136,137]. A concentration of 0.05 µmol/l was used, which may not entirely suppress $Ca_V1.3$ activity (only around 70% inhibition) but should not have an impact on non-L-type calcium channels.

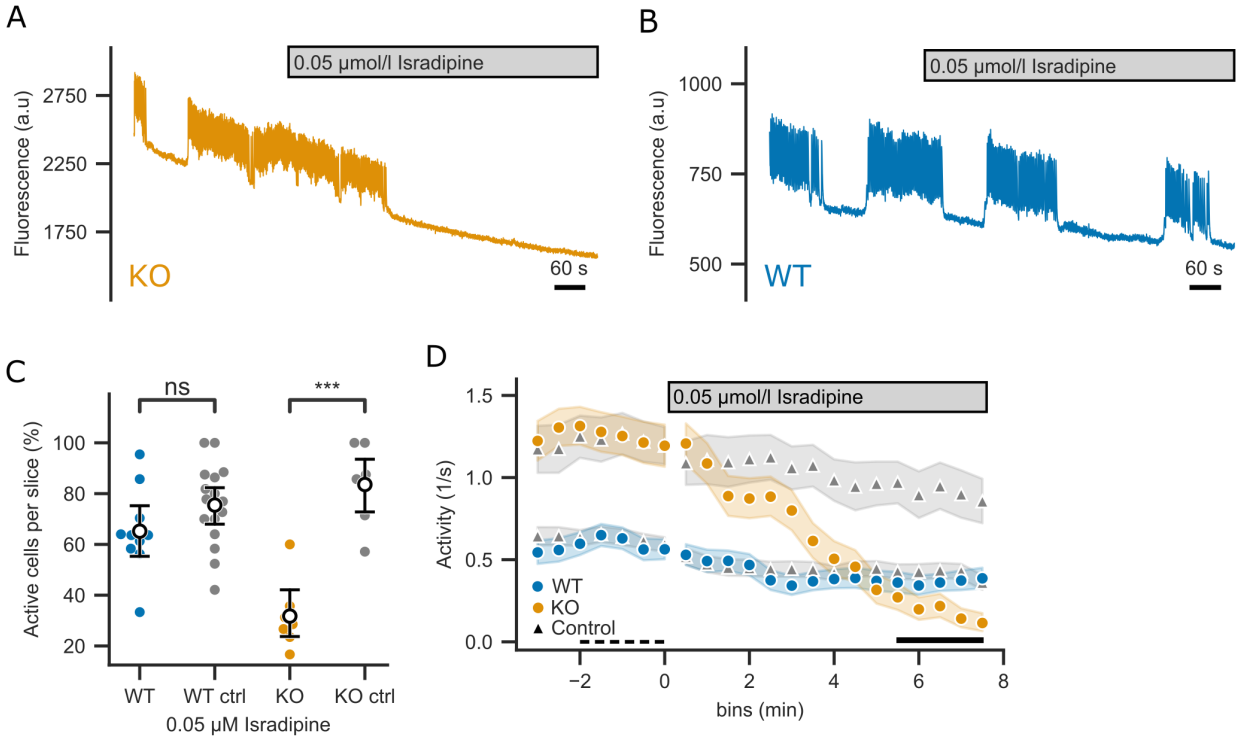

Figure 29. The L-type inhibitor isradipine inhibits calcium spikes in $Ca_V3.2$ KO but not WT cells. ***(A-B)*** *Changes in Ca^{2+} spiking recorded in one representative $Ca_V3.2$ KO* ***(A)*** *and WT* ***(B)*** *ZG cell from adrenal slices. Slices were stained with Calbryte 520 AM and recorded at 4 mmol/l K^+ and 500 pmol/l Ang II. Application of isradipine (0.05 µmol/l, indicated by the grey bars) inhibits calcium spikes in almost all KO but not WT cells.* ***(C)*** *Fraction of cells in a slice that are still active at 0.05 µmol/l isradipine (time span from 5.5 to 7.5 minutes after addition of isradipine, indicated by the black line in D) compared to cells at zero isradipine (from -2 to 0 minutes, indicated by the black dashed line in D) was significantly decreased in KO but not WT when compared to control.* ***(D)*** *Calcium spike activity (in 0.5 minutes bins) of ZG cells from KO but not WT adrenal slices, was lowered by 0.05 µmol/l isradipine (indicated by the grey bar, mean: circle; shaded area: 95% CI). Data in C are shown as overall mean per group (white circle) ± 95% CI (error bars). Individual values of cells and slices are shown as smaller and larger spots, respectively. Values per genotype were tested against respective controls (likelihood ratio test of linear mixed models).*

In $Ca_V3.2$ KO mice, the use of isradipine resulted in a substantial reduction in calcium spiking, characterized by a gradual onset of inhibition, while having nearly no impact on WT cells (Fig. 29A and B). At a concentration of 0.05 µmol/l isradipine may not entirely inhibit the activity of L-type channels. Consequently, a significant decrease in active cells to approximately 32% (Fig. 29C, data in Table 16-17) and the overall activity was observed between 5.5 to 7.5 minutes after the initiation of perfusion (Fig. 29D, data in Table A18).

In contrast, during the same time period, the majority of WT cells remained active and unaffected (Fig. 29C-D, data in Table A19; Fig. 30A, absolute data in B). Additionally, the

inhibition of L-type channels had no impact on the intra-burst frequency in neither WT nor KO cells that maintained their activity in the presence of isradipine (Fig. 30C and D, data in Table A 16-17, A20).

In summary, these findings suggest that L-type calcium channels play an essential role in maintaining calcium signals in mice that lack $Ca_V3.2$. However, no significant changes in calcium spiking in WT ZG cells were observed in the presence of L-type channels inhibitors alone.

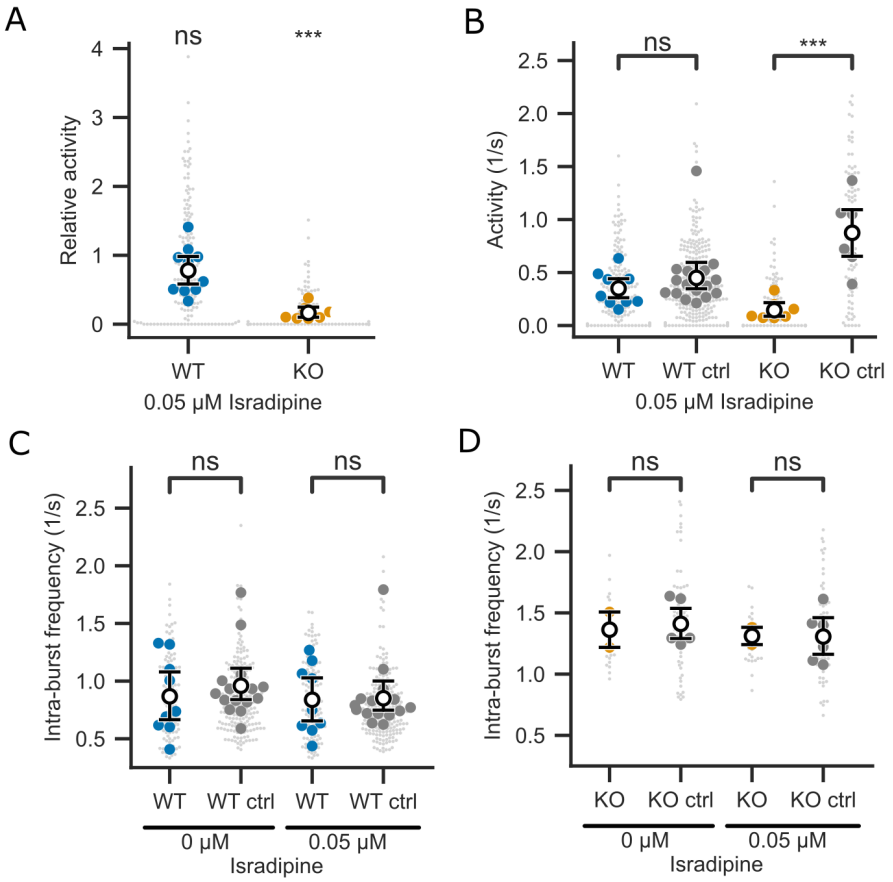

Figure 30. Isradipine lowered activity in $Ca_V3.2$ KO but not WT ZG cells while the intra-burst frequency remained unaffected in both genotypes. ***(A)*** *Calcium spike activity (relative to control) was significantly changed by isradipine in KO but not WT (absolute data in* ***(B)****.* ***(C-D)*** *intra-burst frequency was unchanged upon perfusion with 0.05 µmol/l isradipine in WT and KO cells compared to control. Only cells that remained active at 0.05 µmol/l isradipine were analyzed and shown in C and D. Data is shown as overall mean per group (white circle) ± 95% CI (error bars). Individual values of cells and slices are shown as smaller and larger spots, respectively. Values per genotype were tested against respective controls (likelihood ratio test of linear mixed models).*

4.1.7 Both L- and T-type calcium channels are necessary for the generation of Ang II induced calcium oscillations

The selective suppression of T-type calcium channels exclusively in WT cells and L-type calcium channels solely in KO cells indicated a crucial role of these two calcium channel types in generating calcium signals. It is, however, possible that other calcium channels are also involved in generating $[Ca^{2+}]_i$ oscillations. To further investigate this hypothesis, we simultaneously blocked T- and L-type calcium channels.

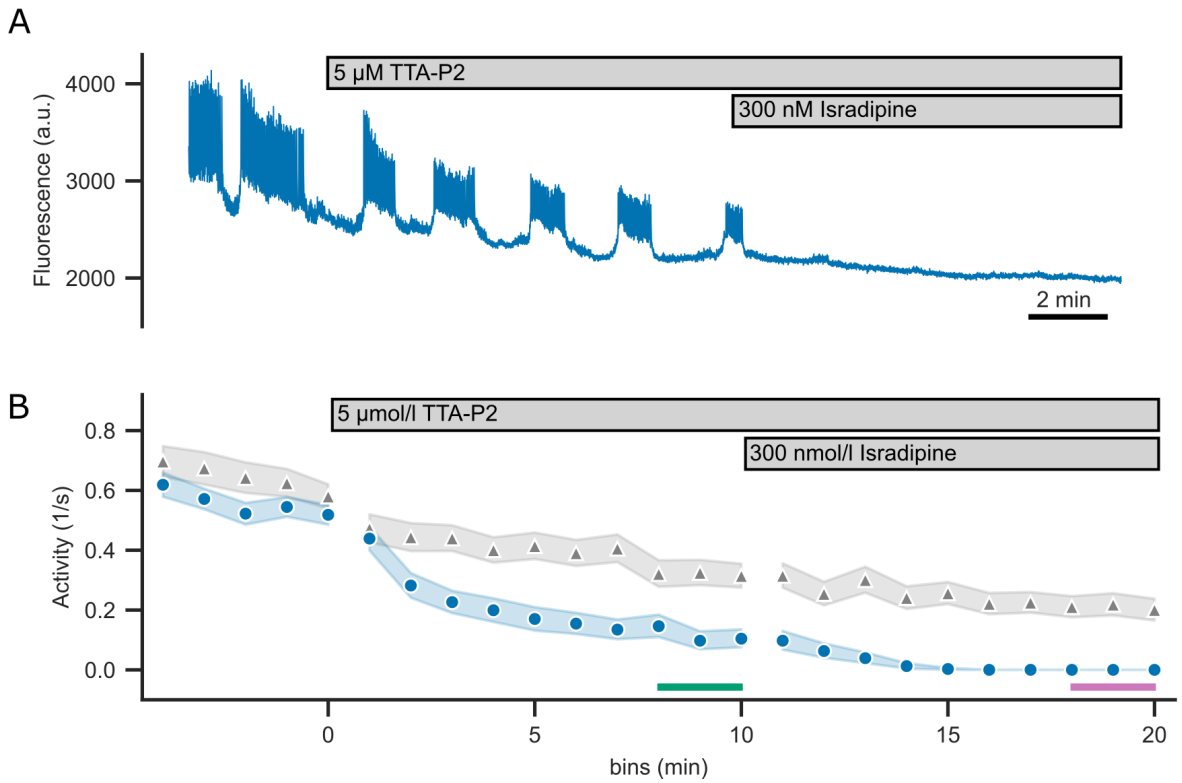

Figure 31. Inhibition of L- and T-type calcium channels simultaneously fully abolishes calcium signals. (A) *Changes in fluorescence intensity recorded from one representative WT ZG cell from an adrenal slice stained with Calbryte 520 AM and recorded at 4 mmol/l K^+ and 500 pmol/l Ang II. Application of both TTA-P2 (5 µmol/l) and isradipine (0.3 µmol/l) simultaneously abolishes calcium spikes.* ***(B)*** *Calcium spike activity (in 1-minute bins) of WT ZG cells was decreased by TTA-P2 (5 µmol/l) and isradipine (300 nmol/l) (mean: blue circle). Grey bars indicate the application of the inhibitors. Activity of control cells (no application of inhibitors) is shown as grey triangles (shaded areas represent 95% CI). The last two minutes of each condition comprising inhibitors of the recording (steady-state phase) are highlighted with color-coded lines (used in Fig. 32).*

The experimental protocol comprised two phases: first, a 10-minute period during which only the T-type calcium channel inhibitor TTA-P2 was perfused, followed by another 10 minutes during which TTA-P2 was supplemented with isradipine to additionally block L-type calcium channels (Fig. 31). To ensure a more specific inhibition of T- over L-type channels, we reduced the concentration of TTA-P2 to 5 µmol/l. Additionally, the concentration of isradipine was increased to 300 nmol/l to achieve complete inhibition of $Ca_V1.3$[133].

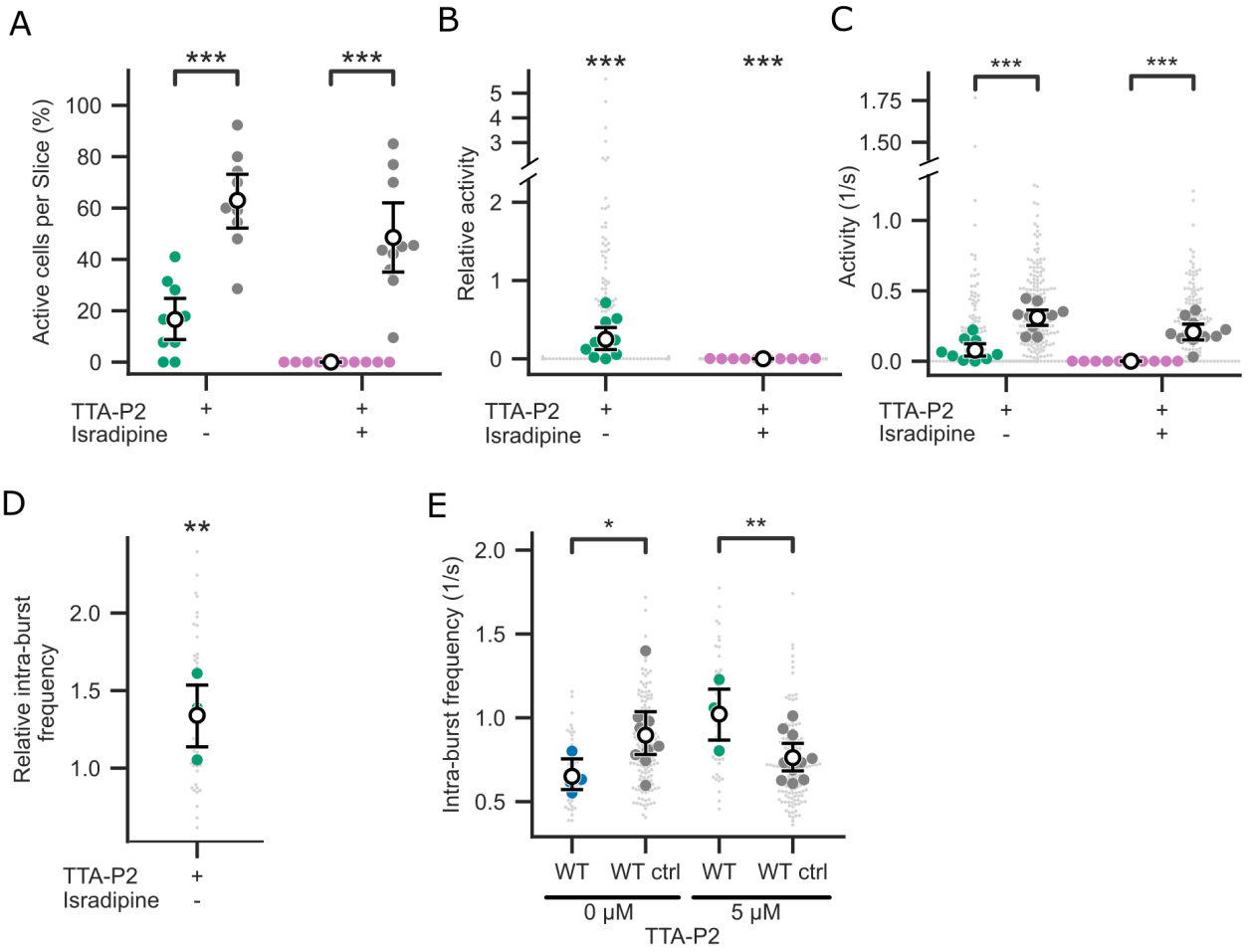

Figure 32. Application of both inhibitors reduced the number of active cells per slice. (A) *Fraction of cells in a WT adrenal slice that were active during the steady-state phases as indicated in Fig 31B compared to untreated controls (grey).* ***(B)*** *Calcium activity in ZG cells from WT adrenal slices during the steady-state phases as highlighted in Fig 31B (absolute data in* ***(C)****).* ***(D)*** *Intra-burst frequency of WT cells during the green steady-state phase as indicated in Fig 31B relative to controls (absolute data in* ***(E)****, only cells that are active during the green phase are shown). White circles show overall mean of slices per group. Colored circles in show mean values of slices (green or pink: WT; grey: WT control). For control, cells were perfused without calcium channel inhibitors. The color of the mean values correspond to the color-coded intervals in Fig. 31B. Values per genotype were tested against respective controls (likelihood ratio test of linear mixed models).*

Although there was a possibility of some non-specific inhibition of T-type channels, this was considered to be tolerable in this context due to the parallel incubation with TTA-P2.

In concordance with the findings observed at higher concentrations, the presence of TTA-P2 alone resulted in an incomplete reduction in activity (Fig. 31A and B, data in Table A21). Also, the number of active cells (Fig. 32A) as well as the activity (Fig. 32B, absolute data in C) was reduced (data in Table A22-23). The intra-burst frequency of cells with remaining activity during inhibition with TTA-P2 was increased (Fig. 32D, data in Table A24; absolute data in E, data in Table A25) similar to the observation presented previously in Fig. 28A-B.

However, when isradipine was added, all signals ceased, clearly indicating that the combination of both, T-type and L-type calcium channels is indispensable for calcium oscillations in the WT ZG and cannot be substituted by other calcium channels.

4.1.8 Only T- and L-type channels mediate Ang II-stimulated increases in calcium levels in murine ZG

Up until now, this study has been focused solely on examining oscillatory calcium fluctuations triggered by Ang II stimulation, However, it is possible that non-oscillatory increases in $[Ca^{2+}]_i$ may be mediated by alternative calcium sources such as intracellular stores or other calcium channels.

To test this hypothesis, the mean and baseline levels of the $[Ca^{2+}]_i$ were assessed over time. The baseline was defined as the $[Ca^{2+}]_i$ during pauses, i.e. segments lacking calcium spikes.

The experimental procedure consisted of four sequential phases. Initially, there was a 5-minute period during which a buffer solution devoid of Ang II and inhibitors was perfused.

Subsequently, there was a 10-minute stimulation with 100 pmol/l Ang II. Following this, inhibitors were introduced into the perfusion solution to effectively inhibit both T-type and L-type channels. For control recordings, cells were not exposed to inhibitors.

After a further 10 minutes, the concentration of Ang II was elevated to 500 pmol/l in both experimental groups.

In the absence of Ang II, ZG cells showed almost no Ca^{2+} spikes, and mean and baseline $[Ca^{2+}]_i$ were indistinguishable (Fig. 33A-B and 34A-B, data in Table A26-28). When the extracellular concentration of Ang II was increased to 100 pmol/l, cells exhibiting oscillatory activity became identifiable. This led to an elevation of the mean $[Ca^{2+}]_i$ above the baseline

values (Fig. 34A-B).

Subsequent perfusion with a combination of 5 µmol/l TTA-P2 and 300 nmol/l isradipine for 10 minutes inhibited $[Ca^{2+}]_i$ oscillations as observed previously. The mean (and, of course, baseline) $[Ca^{2+}]_i$ decreased to levels similar to those observed before the stimulation with Ang II (Fig. 34A and B).

Further increasing the concentration of Ang II to 500 pmol/l failed to elevate $[Ca^{2+}]_i$ as well as the time spent bursting when both T- and L-type calcium channels were still inhibited (Fig. 34C, data in Table A29).

These findings indicate that increases of $[Ca^{2+}]_i$ due to Ang II are solely attributed to the oscillatory entry of calcium through T-type ($Ca_V3.2$) and L-type ($Ca_V1.2$/$Ca_V1.3$) calcium channels. Other sources, such as alternative calcium channels or intracellular stores, do not seem to play a role in these increases.

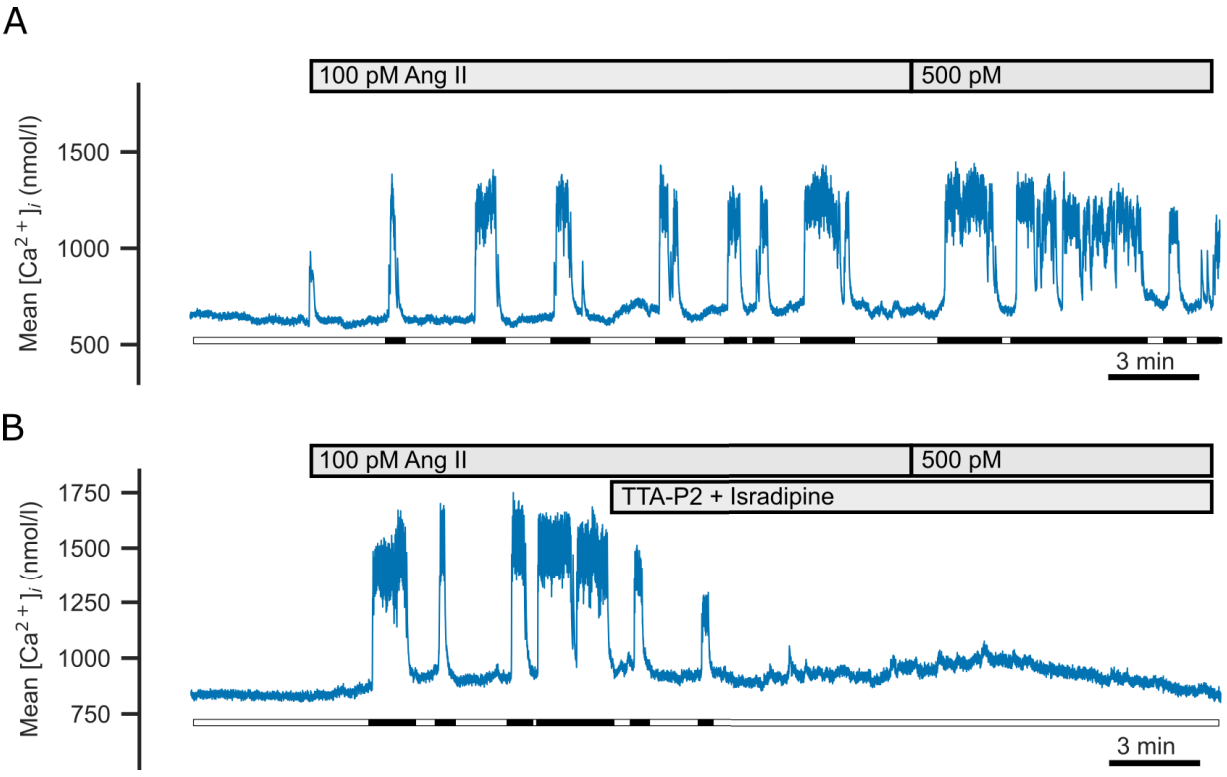

Figure 33. Ang II elicited calcium oscillations are mediated by T- and L-type channels. (A) *Representative trace of intracellular calcium concentrations of a ZG WT cell. Slices were stained with Fura-2-AM to asses the abolute $[Ca^{2+}]_i$and were recorded at varying concentrations of Ang II (indicated by the grey bars) without inhibitors (control).* ***(B)*** *Representative trace of intracellular calcium concentrations of a ZG WT cell. Adrenal slices were stained with Fura-2-AM-stained. The $[Ca^{2+}]_i$ was measured at varying concentrations of Ang II and with or without the presence of inhibitors TTA-P2 (5 µmol/l) and isradipine (300 nmol/l) as indicated by the grey bars. Empty and filled bars on the bottom of the trace in A and B indicate baseline and burst phases, respectively.*

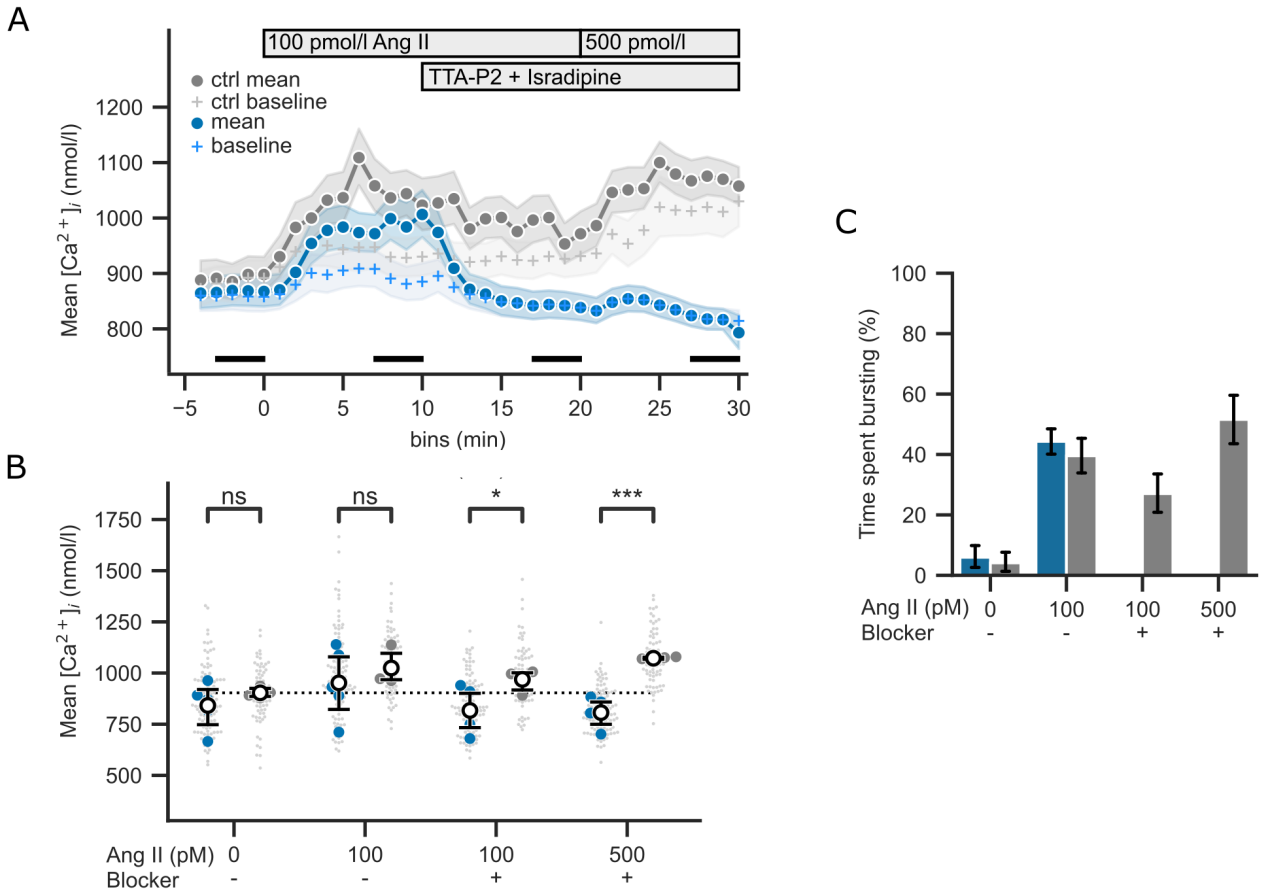

Figure 34. Only T- and L-type channels mediate Ang II-evoked increases in $[Ca^{2+}]_i$. (A) *Mean intracellular calcium concentrations (circles; ± 95% CI, shaded areas) at 4 mmol/l K^+ of ZG cells stained with Fura-2-AM. Ang II-evoked increase in $[Ca^{2+}]_i$ was abolished by 5 µmol/l TTA-P2 and 300 nmol/l isradipine. Further increase in Ang II concentration did not lead to an increase of $[Ca^{2+}]_i$ in the presence of inhibitors (blue; corresponding untreated control:grey). Mean $[Ca^{2+}]_i$ during baseline phases (no spkikes) are indicated by crosses (light blue: treated, light grey: untreated control). Application of Ang-II at varying concentrations and inhibitors is indicated by the grey bars.* ***(B)*** *Mean $[Ca^{2+}]_i$ of ZG cells stained with Fura-2-AM before and during perfusion with both inhibitors TTA-P2 (5 µmol/l) and isradipine (300 nmol/l) at different Ang II concentrations as highlighted by the black bars in A (grey: untreated controls). Mean values for each slice and cell are shown as larger and smaller circles, respectively. Overall means per group are shown as white circles ± 95% CI.* ***(C)*** *Time spent bursting of ZG cells before and during perfusion with both inhibitors at varying Ang II concentrations as highlighted by the black bars in A (blue: treated cells, grey: untreated controls, error bars: 95% CI).*

4.2 *Cacna1h* KI Mice exhibit elevated baseline and peak zona glomerulosa calcium levels.

The data in this section has additonally been published in[83]

Gain-of-function mutations in the *CACNA1H* gene underlie familial hyperaldosteronism type IV (FH-IV) and cause early-onset hypertension in humans[62]. The *Cacna1h*$^{M1560V/+}$ knockin (*Cacna1h* KI) mice serve as an animal model for the most prevalent mutation observed in FH-IV[83]. The KI mice exhibit a mild form of primary aldosteronism, characterized by elevated aldosterone-to-renin ratios compared to wildtype mice. Furthermore, the KI mice exhibit an 8 mmHg increase in systolic blood pressure and show heightened adrenal aldosterone synthase expression, which is associated with elevated intracellular calcium concentrations in ZG cells[138] (see Introduction section 1.5).

To investigate the impact of the M1560V mutation on calcium signaling at the cellular level, calcium imaging experiments were conducted using adrenal slices from *Cacna1h* KI mice (mice with the mutation) and wildtype mice. Non-ratiometric (Calbryte 520 AM) and ratiometric (Fura-2 AM) fluorescent calcium indicators were employed, with the latter allowing the measurement of absolute intracellular calcium concentrations (see Methods section 3.2). Using calcium imaging, individual calcium spikes and bursts of activity in both genotypes were observed.

Mean overall calcium concentrations were evaluated at different stimulus concentrations (3 and 5 mmol/l K^+), with each concentration tested in the absence and presence of 20 and 1000 pmol/l Ang II. Calcium levels were significantly higher in *Cacna1h* KI mice compared to WT mice at all tested concentrations of stimuli (Fig. 35A, data in Table A30). In contrast, the mean activity was not significantly increased in *Cacna1h* KI mice (Fig. 35B, data in Table A31).

At high Ang II levels (1000 pmol/l), the activity was even significantly reduced. This decrease in overall calcium activity in KI mice under high Ang II levels was attributed to lower frequencies of oscillations during bursts (Fig. 35C, data in Table A32), shorter burst durations (Fig. 35D, data in Table A33), and fewer bursts (Fig. 35E, data in Table A34), collectively leading to the observed decrease in activity.

Additionally, intracellular calcium concentrations during the baseline (segments without

spikes) and peak of a spike were examined separately. In the absence of Ang II, calcium spikes occurred infrequently, making statistical analysis of peak values challenging. However, baseline calcium levels were significantly elevated in KI mice at both 3 and 5 mmol/l K^+ (Fig. 36A and B, data in Table A35-36). Upon the addition of Ang II (20 and 1000 pmol/l), baseline and peak intracellular calcium levels were significantly increased in KI mice at both 3 and 5 mmol/l K^+.

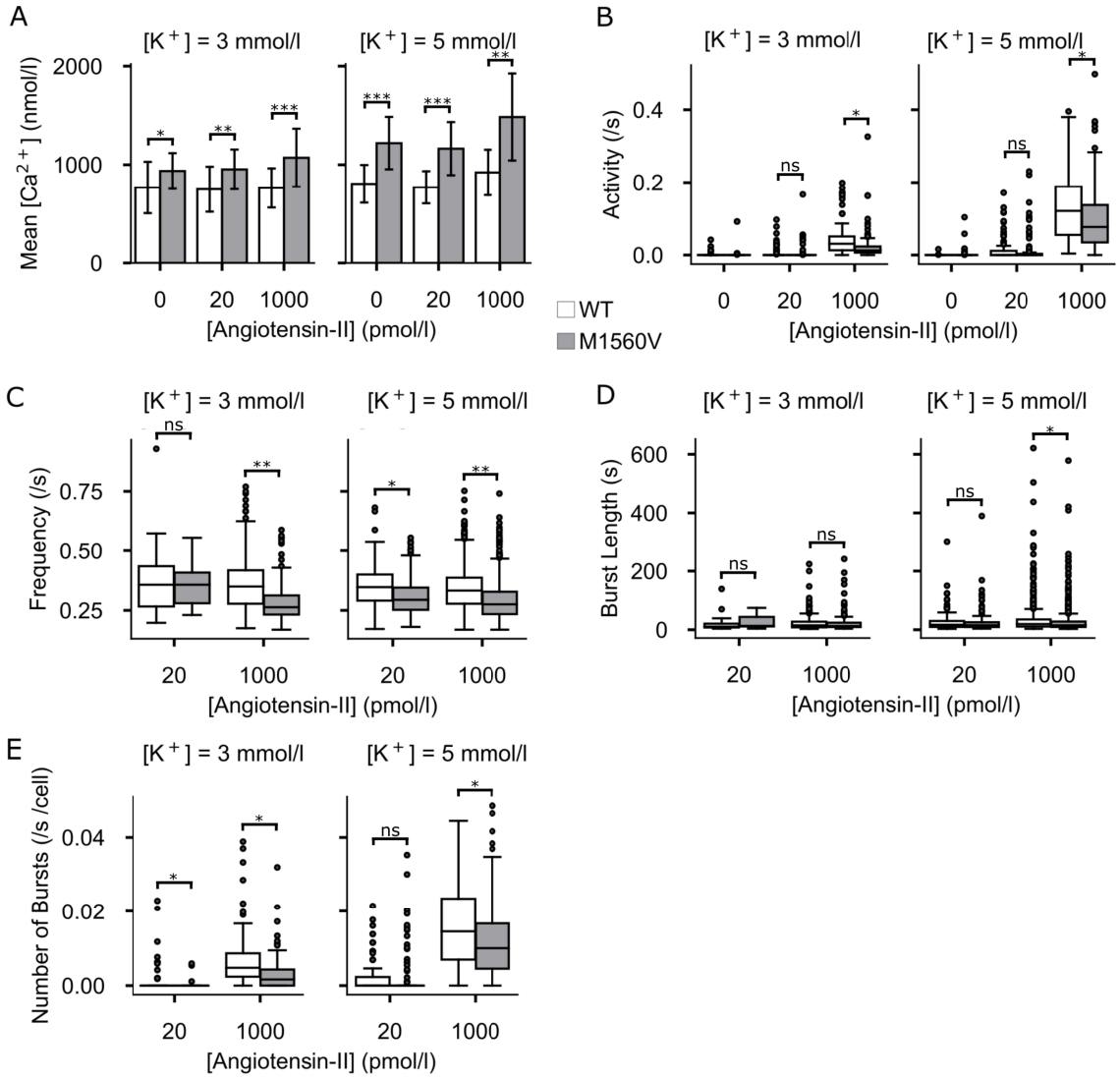

Figure 35. Cacna1h KI mice exhibit higher [Ca^{2+}]$_i$ than wild-type controls. (A) *Mean [Ca^{2+}]$_i$ of ZG cells from Fura-2-AM stained adrenal slices during perfusion with solutions containing the indicated K^+ and Ang II concentrations. Mean activity **(B)**, intra-burst frequency **(C)**, burst length **(D)** and number of bursts **(E)** of ZG cells from Fura-2-AM stained adrenal slices during the corresponding perfusion. Data in A and B are shown as bars (mean) ± SD. Box plots in C-E follow Tukey-style (see Methods section 3.9)*

.

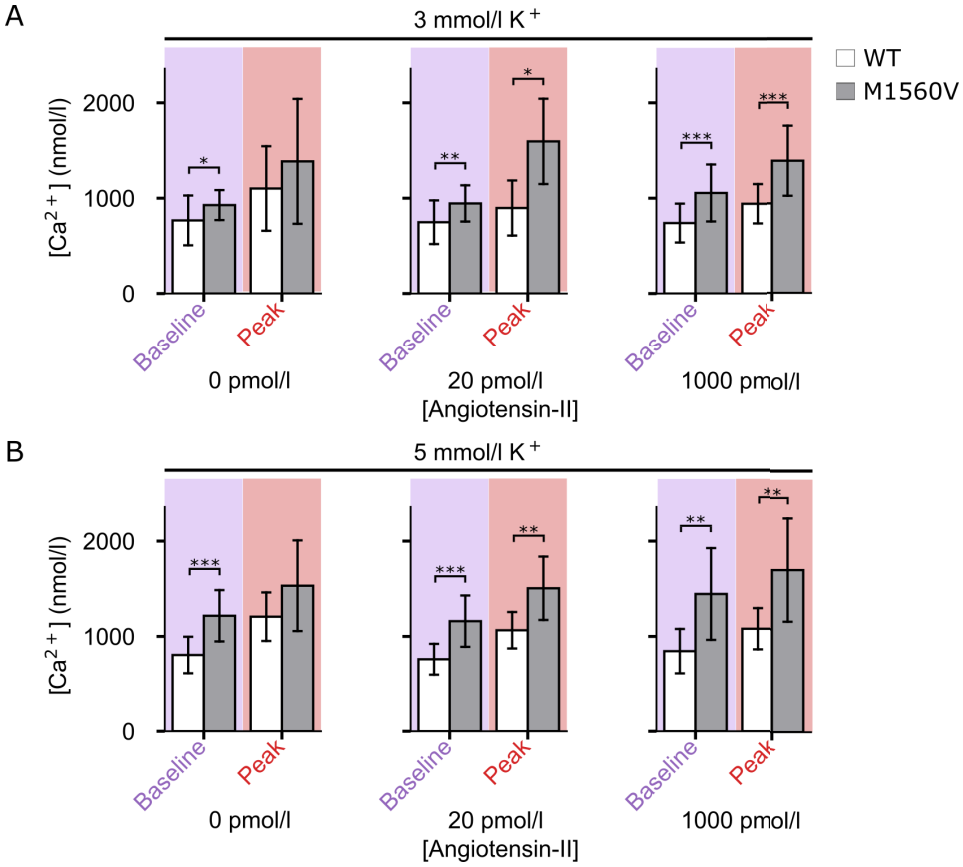

Figure 36. Baseline and peak calcium levels were significantly elevated in Cacna1h KI mice.(A-B) *Mean values for the baseline and peak $[Ca^{2+}]_i$ in ZG cells from adrenal slices stained with Fura-2-AM are shown for the indicated combinations of K^+ and Ang II concentrations. Data are shown as bars (mean) ± SD.*

Using Calbryte 520 AM for higher temporal resolution, average time courses of individual spikes were obtained, which then were normalized to the mean baseline and peak values obtained from Fura-2 AM recordings (Fig. 37A). The kinetics of the rise to peak and the fall to baseline calcium concentrations were obtained by fitting with exponential functions. The interval between the beginning and the peak of each spike was fit with an exponential function leading to the time constant of the activation. The interval between the peak and the end of each spike was fit with an exponential function resulting in the time constant of the deactivation. The time constants for the activation and inactivation were not significantly different between KI mice and WT mice (Fig. 37B and C, data in Table A37-38).

Based on this data, it appears that the M1560V mutation leads to alterations in calcium signalling in *Cacna1h* KI mice, resulting in increased mean overall calcium levels due to elevated baseline and peak calcium levels. However, the frequency of calcium spikes and the kinetics of calcium rise and fall during spikes do not seem to be affected by the mutation.

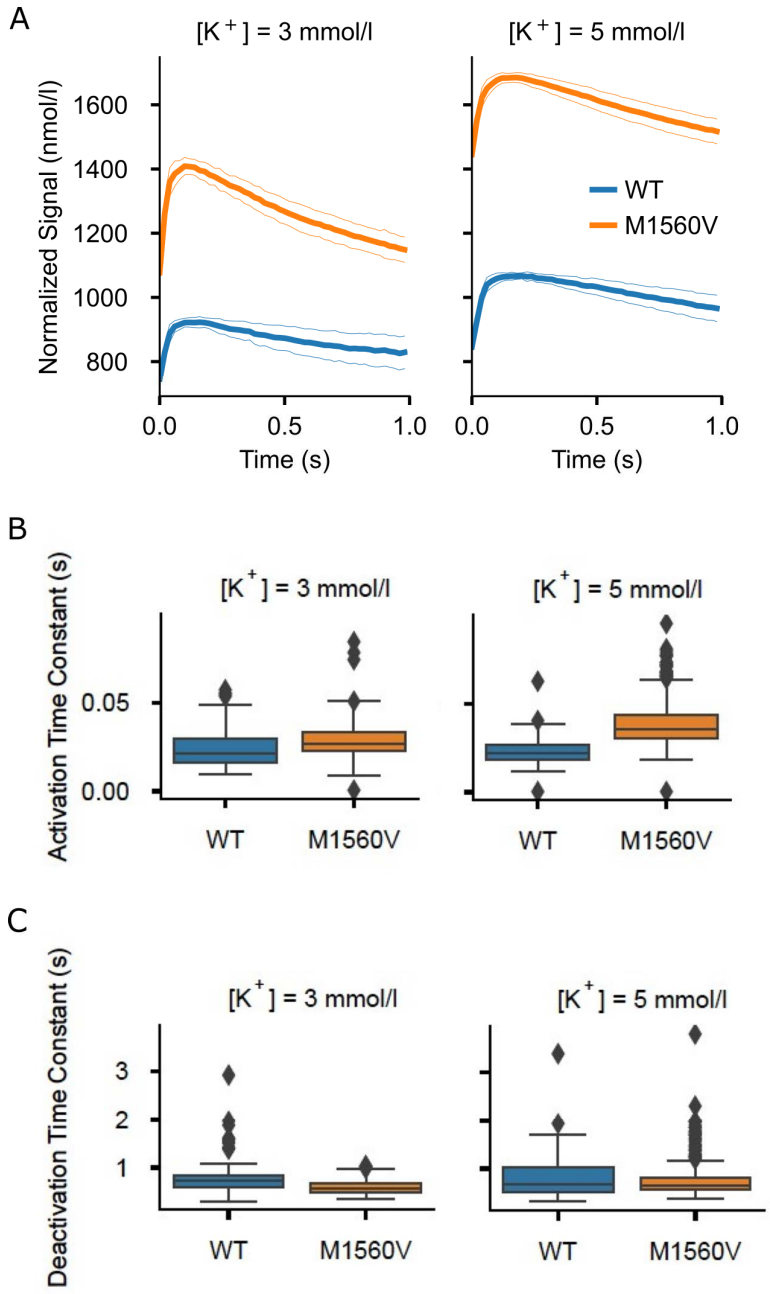

Figure 37. The kinetics of calcium spiking are unchanged between genotypes. ***(A)*** *Mean spikes were obtained at 3 (left) and 5 (right) mmol/l K^+ at 1 nmol/l Ang II (thick lines) from ZG cells stained with Calbryte 520 AM and recorded with a frame rate of 50 frames/s. The fluorescence intensity of all spikes was normalized to the baseline and peak values obtained by the Fura-2 AM recordings. The SD is indicated by the thin lines.* ***(B)*** *The interval between the beginning and the peak of each spike was fit with an exponential function resulting in the time constant of the activation.* ***(C)*** *The interval between the peak and the end of each spike was fit with an exponential function resulting in the time constant of the deactivation. The likelihood ratio test does not indicate statistically significant differences in values. Box plots follow the Tukey-style (see Methods 3.9).*

4.2.1 Calibration of Fura-2 in ZG cells of adrenal slices

In order to asses $[Ca^{2+}]_i$ based on the ratio of fluorescence intensities at 340 nm and 380 nm it is necessary to perform a calibration to obtain the dissociation constant K_d. The calibration was performed under conditions similar to those used in the calcium imaging experiment to ensure accurate conversion of fluorescence ratios into $[Ca^{2+}]_i$ (see Methods section 3.2).

340/385 nm ratios were measured at fixed Ca^{2+}concentrations and the data were fit with a Hill equation to obtain the K_d (Fig. 38A). Representative recordings of the 340/385 nm ratios are shown in (Fig. 38B). The calibration of Fura-2 in ZG cells revealed a high K_d of aprox. 2 µmol/l.

The discrepancy between the measured K_d value and the literature-reported value (224 nmol/l)[110] could be attributed to differences in factors such as pH and temperature[139,140]. Moreover, adrenal cells, being the site of steroidogenesis with cholesterol as the primary source of steroidogenic substrate, display elevated lipid concentrations[141]. Differences in lipid content may potentially have contributed to the observed variations in K_d values.

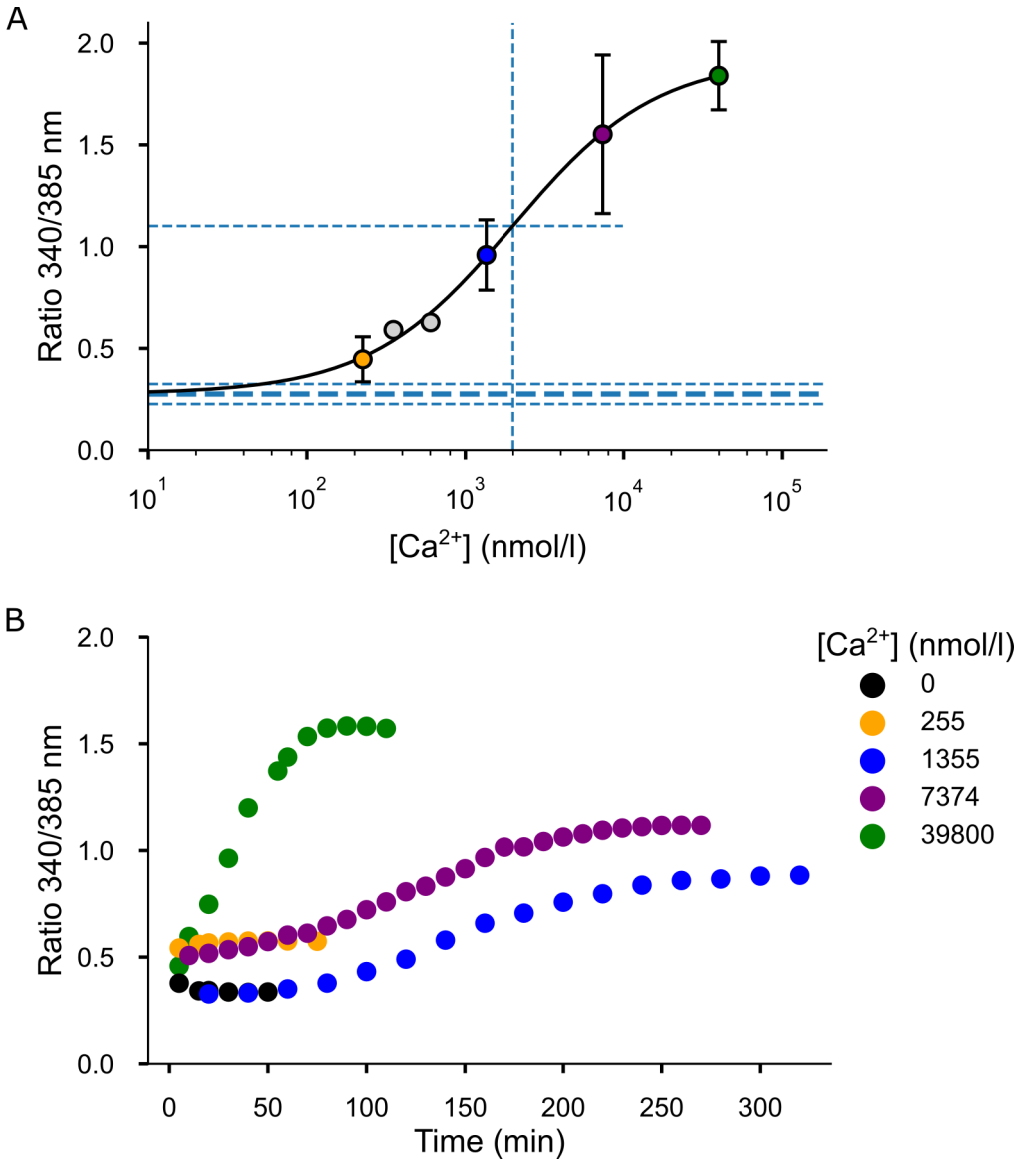

Figure 38. *A. Plot of the measured 340/385 nm ratios at fixed Ca^{2+} concentrations. $[Ca^{2+}]_i$ were controlled by using ionomycin and extracellular solutions with known Ca^{2+} concentrations. The mean of the ratio in the absence of calcium is shown as a thick blue horizontal dashed line with the standard deviation (SD) as thinner lines. For all other concentrations means are shown as circles ± SD (for sample sizes larger than 1). Data were fit using the Hill equation to yield a Kd (intersection of the black lines). B. Representative examples of the measured 340/385 nm ratios over time starting at the beginning of the incubation with ionomycin at variing Ca^{2+} concentrations of the extracellular solution. Colors correspond to Ca^{2+} concentrations in A.*

4.3 *Cacna1d* KI mice response to treatment with isradipine

The data presented in this section has also been published in[104]. The basal characterization of the *Cacna1d* KI mice will be incorporated in Marina Volkert's upcoming dissertation. Therefore, only a brief overview of these results, which will be discussed more extensively in her dissertation, is included in the following subsection 4.3.1.

My specific contributions consisted of conducting and analyzing calcium imaging experiments on ZG cells from *Cacna1d* KI mice with and without isradipine, isradipine treatments in *Cacna1d* KI mice and subsequently performing behavioral studies and blood and organ sample collection. The outcomes of these efforts are presented in section 4.3.2 and section 4.3.3 and are discussed in section 5.3 of this dissertation.

4.3.1 Characterization of the phenotype of *Cacna1d* KI mice

This subsection provides a short summary of the phenotype characterization covered in the dissertation of Marina Volkert and has also been published in[104].

De novo germline mutations in the *CACNA1D* gene are observed in a syndrome characterized by primary aldosteronism, seizures, and neurologic abnormalities (PASNA)[52,142,143].

To investigate whether one of these mutations is sufficient on its own to induce PASNA syndrome, a *Cacna1d* KI mouse model was generated. It was observed that these mice exhibit signs of the PASNA syndrome such as primary aldosteronism, increased susceptibility to seizures (when induced by ketamine and xylazine, a combination used as an anesthetic), and neurologic abnormalities including motor deficits and mild social impairment[104]. They demonstrated elevated aldosterone-renin-ratios when compared to WT. Additionally, *Cacna1d* KI mice exhibted elevated transcript levels of *Cyp11b2*, the gene encoding the aldosterone synthase, which catalyzes the last step in the aldosterone synthesis (see Fig. 8). Even during a high-salt diet, which should physiologically reduce the activity of the Renin-Angiotensin-Aldosterone-System, aldosterone levels remained elevated in these mice, confirming the presence of primary aldosteronism. On the molecular level, mean and baseline (phases without spikes) $[Ca^{2+}]_i$ in glomerulosa cells of *Cacna1d* KI mice were elevated, while the frequency of spiking and bursting parameters remained mostly unchanged.

To investigate the potential pharmacologic reversibility of both adrenal and neurologic phenotypes, the *Cacna1d* KI mouse model was subjected to the L-type calcium channel

inhibitor isradipine.

4.3.2 Isradipine lowers intracellular calcium levels in ZG cells of WT and *Cacna1d* KI mice.

Isradipine has demonstrated efficacy in significantly attenuating calcium spike activity in ZG cells lacking the T-type channel $Ca_V3.2$ (Fig. 29 and 31). These observations provided the motivation for exploring the potential of isradipine to lower the elevated $[Ca^{2+}]_i$ observed in *Cacna1d* KI ZG cells.

Isradipine was applied to adrenal slices at concentrations of 50 nmol/l, which can be reached in mouse plasma through subcutaneous delivery with osmotic minipumps. Additionally, a concentration of 300 nmol/l was employed, which, in a heterologous expression system, demonstrated inhibitory effects on nearly all $Ca_V1.3$ channels[133].

Cacna1d KI ZG cells responded with a decrease in the overall mean $[Ca^{2+}]_i$, while in WT, only a small and likely physiologically irrelevant decrease was observed (Fig. 39A, data in Table A39). Interestingly, $[Ca^{2+}]_i$ in KI cells was lowered to approximately the levels seen in untreated WT cells.

The baseline $[Ca^{2+}]_i$ was separated from the overall mean $[Ca^{2+}]_i$ and represents phases lacking calcium spike activity. Isradipine lowered baseline $[Ca^{2+}]_i$ in KI but not WT ZG cells (Fig. 39B, data in Table A39).This suggests that the mutated $Ca_V1.3$ channels may display an increased minimal open probability, resulting in elevated baseline influx of Ca^{2+}.

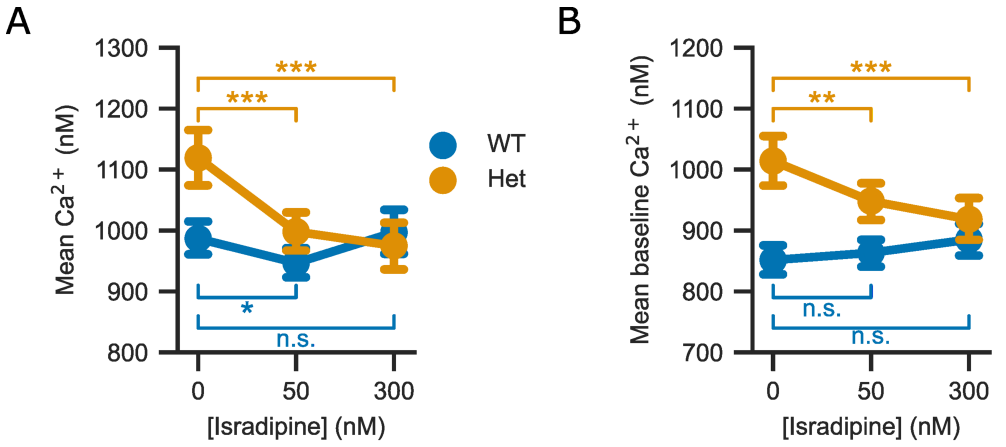

Figure 39. Isradipine reduces mean baseline and overall $[Ca^{2+}]_i$ in Cacna1d KI mice. ***(A)*** *Mean $[Ca^{2+}]_i$ of ZG cells stained with Fura-2-AM at varying concentrations of isradipine.* ***(B)*** *Mean $[Ca^{2+}]_i$ during baseline (phases without caclium spking) of ZG cells stained with Fura-2-AM at varying concentrations of isradipine. Cells were recorded at 4 mmol/l K^+ and 100 pmol/l Ang II. Data are represented as mean ± 95% CI*

4.3.3 *Cacna1d* KI mice respond to oral therapy with isradipine

Osmotic minipumps are often used to deliver drugs continuously and at controlled rates to unrestrained laboratory animals[144]. However, the implantation of these minipumps represents a distressing invasive procedure. Due to an already heightened mortality rate in *Cacna1d* KI mice[104], an oral administration of isradipine was chosen instead.

Isradipine is approved for hypertension therapy in humans and slow-release formulations exist. With these, dosage can be reduced to once daily[145].

Oral administration of slow-release isradipine (see methods Section 3.6) in mice may represent a viable therapeutic strategy for mice. Isradipine is contained within a matrix allowing for slow release once in contact with liquids. Drug uptake, inactivation and excretion can differ significantly between rodents and humans. A typical dosage in humans is 10 mg isradipine per day, resulting in a dosage around 0.15 mg/kg body weight/day.

In discussion with Prof. Jörg Striessnig (Institute of Pharmacology, University of Innsbruck), a much higher concentration (12.5 mg/kg body weight/day) was chosen based on previous reports[146]. This is likely required due to a lower oral availability and significantly higher clearance of dihydropyridines such as isradipine in rodents.

In this study, the required amount of slow-release isradipine in sweetened yogurt was administered once daily. The randomized allocation of mice into either the isradipine treatment group or the control group was carried out using a custom Python script.

Blinding procedures for the administration of yogurt (with or without isradipine) to the mice were implemented. This was achieved by having separate personnel handle the yogurt preparation and feeding. However, it was not feasible to blind the experimenters to the mice's genotypes because distinct physical characteristics among the mice made their genotypes apparent (see Methods section 3.6).

Both the treatment group and the placebo group (receiving sweetened yogurt only) showed rapid and voluntary ingestion of the yogurt. Mice that repeatedly did not consume the yogurt were excluded from further analysis. After a two-week treatment phase, the treatment was continued while behavioral tests were conducted to evaluate its impact on neurologic behavior. Rotarod testing was performed approximately 4 hours after yogurt or isradipine feeding, a time corresponding to the peak plasma levels in humans. In WT animals, there was no significant difference in rotarod performance between the therapy group and the placebo group (Fig. 40A,data in Table A40). In contrast, *Cacna1d* KI mice treated with is-

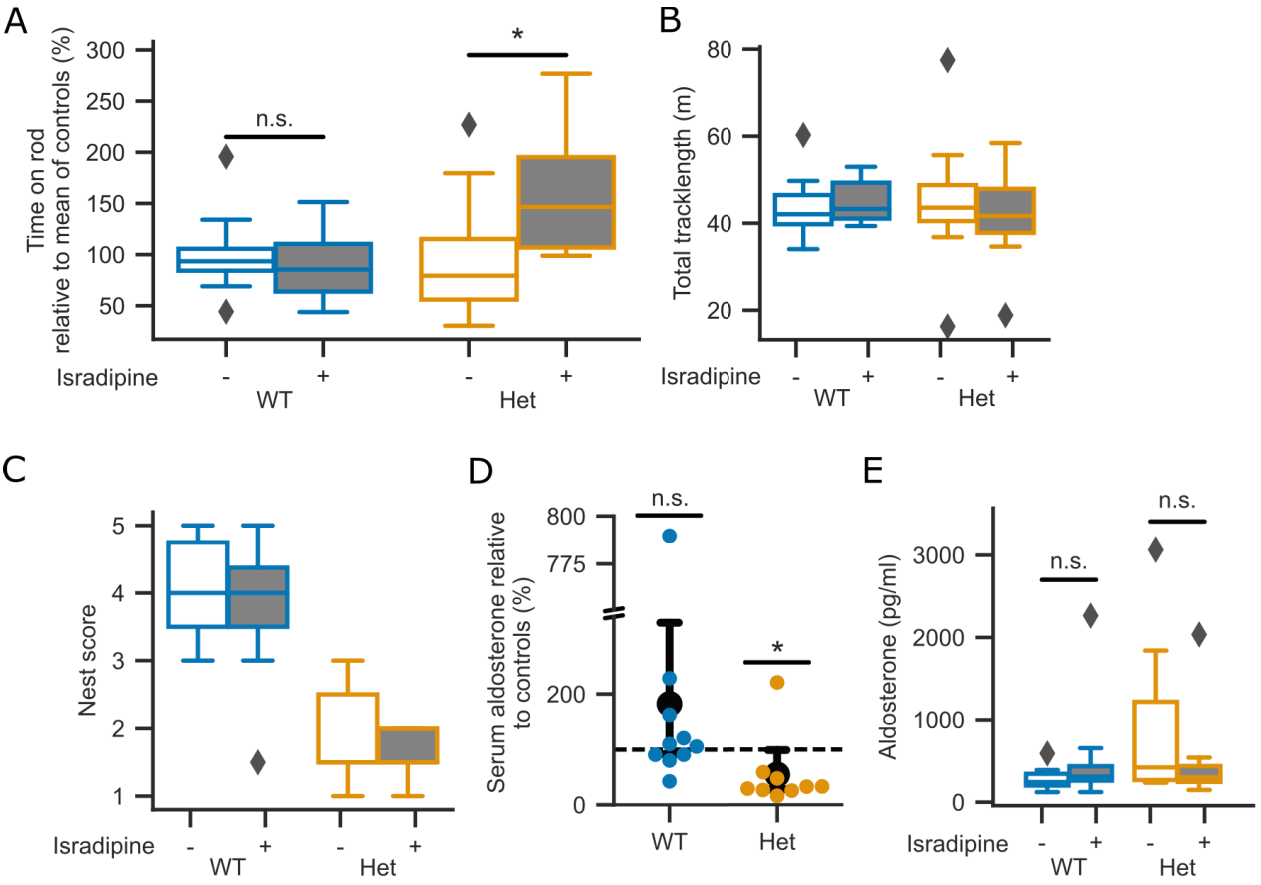

Figure 40. Isradipine treatment lead to an improved performance in the rotarod experiment in Cacna1d KI mice. (A) *The rotarod test was conducted 4 h after the last isradipine dose. Treated (+) Cacna1d KI mice (Het) show a significant improvement in performance to untreated controls (-). The performance of wild-type mice was not affected. The total track length assessed in the Open Field Test* ***(B)*** *and the nest-building performance* ***(C)*** *was not change by isradipne treatment in either genotype. These tests were conducted 18 hours after the last dose, a time when trough plasma levels are expected.* ***(D)*** *Assesment of aldosterone levels in blood serum samples collected 20 h after the last isradipine dose. Aldoseteron levels in treated Cacna1d KI mice were lower relative to untreated controls. Values were normalized to the mean of untreated mice of the corresponding genotype. Colored circles represent values of individual animals. Black circle and error bars indicate mean values per group and 95% CI.* ***(E)*** *Absolute data of D). Box plots follow the Tukey-style (see Methods 3.9)*

.

radipine spent, on average, 68% more time on the rod than Cacna1d KI mice that received the placebo, although their absolute performance did not reach WT levels.

No notable effect was observed in the tracklength assessed in the open field test, that was conducted 18 hours after the last dose, a time when trough plasma levels are expected[147] (Fig. 40B, data in Table A41). Similarly, there was no change in nest-building performance,

as the test covered both peak and trough plasma levels of isradipine (Fig. 40C, data in Table A42).

Aldosterone levels were assessed through terminal blood collection approximately 20 hours after the last dose. Treatment resulted in a reduction of serum aldosterone in KI mice relative to untreated controls, but not in WT mice (Fig. 40D, absolute data in E and Table A43).

Renin concentrations could not be evaluated due to the use of isoflurane[148] for anesthesia to prevent the induction of seizures.

Furthermore, isradipine levels were evaluated in terminal blood samples approximately 20 hours after the final dose. Unfortunately, no traces of isradipine were detected in the blood samples. This outcome is likely attributable to the administration of only a single dose within a 24-hour period, resulting in a considerable time gap between the last dose and the sample collection. Other studies have demonstrated that administering isradipine twice daily yields measurable levels of isradipine[149].

5 Discussion

5.1 Calcium signals in *Cacna1h* KO mice

The zona glomerulosa is a complex system that regulates the synthesis of aldosterone in response to various stimuli[71]. Previous studies have proposed that most of these factors, including serum potassium and Ang II, lead to oscillatory calcium influx into ZG cells by depolarizing the cell membrane[71] and also by releasing calcium from intracellular stores[150,151]. These depolarizations were previously reported to depend critically on the voltage-gated T-type calcium channel $Ca_V3.2$[25]. However, it is not the change in voltage itself, but rather the influx of calcium, that is essential for the physiological function of the ZG.

It is likely that these calcium oscillations in the ZG are caused by depolarizations as they exhibit similar frequencies and stimulus dependence (Fig. 10)[81–83]. Contrary to expectations if $Ca_V3.2$ were solely responsible for maintaining calcium signaling, knock-out mice did not exhibit reduced aldosterone levels (Fig. 12B)[83,84]. However, these studies focused on systemic effects in KO mice, and compensatory secondary mechanisms (e.g., activation of the RAAS or up-regulation of other calcium influx pathways in the ZG) may have mitigated the loss.

Therefore, this study aimed to investigate the mechanisms governing calcium influx in the ZG of mice lacking the $Ca_V3.2$ channel using acute slice preparations and isolated adrenocortical cells.

The loss of $Ca_V3.2$ in KO mice had minimal impact on calcium signaling (Fig. 22). Although there was a slight increase in spiking activity (Fig. 23), the average levels of $[Ca^{2+}]_i$ the ZG were similar to those in WT mice explaining why aldosterone levels remained unchanged (Fig. 24).

It was suggested that other T-type channels might compensate for the absence of $Ca_V3.2$ and play a role in aldosterone synthesis[84]. However, RNA-seq data (Fig. 25) did not indicate significant expression of T-type channels other than *Cacna1h* in the adrenal cortex of WT mice.

Furthermore, adrenocortical cells from KO mice lacked T-type currents (Fig. 26). Additionally, perfusion of adrenal slices from KO mice with the T-type inhibitor TTA-P2 did not cause alterations in calcium signaling (Fig. 27). This supports the notion that $Ca_V3.2$ is the only relevant T-type voltage-gated calcium channel in the ZG.

On the other hand, inhibition of L-type calcium channels with isradipine almost completely suppressed calcium oscillations in KO mice (Fig. 29), revealing the critical role of L-type calcium channels, particularly $Ca_V1.3$ and $Ca_V1.2$, the most prominently expressed L-type calcium channels in the murine and human adrenal cortex (Fig. 25A).

No indications of compensatory upregulation of L-type or any other calcium channels or transporters were found in KO mice (Fig. 25B-C).

Patch-clamp experiments showed similar voltage dependence and amplitudes between WT and KO excluding significant post-translational changes to voltage-gated calcium channels (Fig. 26).

In addition to the chronic loss of $Ca_V3.2$ observed in this knockout model, this study additionally demonstrates that physiological calcium signaling in the ZG is not exclusively reliant on $Ca_V3.2$. Acute inhibition of T-type voltage-gated calcium channels using the specific blocker TTA-P2 in WT mice only partially reduced activity by approximately 20% (Fig. 27D-G).

Complete inhibition of $[Ca^{2+}]_i$ oscillations could only be achieved by simultaneous blockade of L-type calcium channels with isradipine (Fig. 31). In contrast, acute inhibition of L-type channels alone did not impact calcium spiking (Fig. 29).

These findings suggest that the generation of oscillations in WT ZG cells primarily depends on $Ca_V3.2$.

Still, following acute inhibition of T-type calcium channels with TTA-P2, L-type channels can sustain some level of calcium signaling in WT cells (Fig. 27 and 31). Cells that maintain activity after $Ca_V3.2$ inhibition displayed higher intra-burst frequencies compared to before inhibition (Fig. 28C-D, 32D-E), indicating that a similar mechanism to that observed in KO cells is also present in a subset of WT cells.

According to murine single-nuclear RNA-seq data (unpublished data by Secener and Scholl), $Ca_V1.2$ expression is observed in all ZG cells, whereas transcripts for $Ca_V1.3$ were not detected in all ZG cells. The absence of $Ca_V1.3$ transcripts may be attributed to lower

expression levels and reduced sensitivity of single-nuclear sequencing. The reason why no L-type currents were observed in ZG cells in the study by Hu et al., even with stimulation using the L-type channel activator Bay K8644[25], remains confounding.

In contrast, the present study recorded L-type currents in all cells using whole-cell patch-clamp recordings, even without additional stimulation (Fig. 26B). While the discrepancy could be explained by differences in cell preparation methods (in-situ patch-clamp of ZG cells[25] versus dissociated adrenocortical cells in this study), the results from calcium imaging experiments and single-nuclear RNA-seq clearly support the relevance of L-type calcium channels in generating and maintaining calcium oscillations in the ZG of both genotypes in situ as well.

Prior research has already established the significance of L-type channels in the diseased ZG through studies identifying somatic gain-of-function mutations in $Ca_V1.3$ in individuals with primary aldosteronism[52,88]. Additionally, previous reports suggest that aldosterone synthesis in human ZG relies on both, T- and L-type calcium channels[63,152]. However, it remains uncertain whether human ZG cells display comparable voltage and intracellular calcium ($[Ca^{2+}]_i$) oscillations to those observed in mice. Species differences in ion channels appear to be primarily related to the composition of potassium channels, while the expression of calcium channels remains relatively similar.

The $[Ca^{2+}]_i$ oscillations in KO mice were observed to be faster than in WT mice (Fig. 23B), and this remains unexplained in this study. The mechanisms underlying the initiation and termination of oscillations beyond $Ca_V3.2$ and background potassium channels are not yet fully understood. The oscillatory cycle model involves various ion conductances to describe the membrane potential during a spike (see Fig. 11)[79].

At the beginning of the cycle (resting potential approx. -85 mV), depolarizing conductances trigger the opening of low voltage-activated $Ca_V3.2$ channels, leading to further depolarization of the membrane potential. This depolarization enables the activation of high voltage-activated channels (L-type channels). The influx of Ca^{2+} activates Ca^{2+}-dependent channels, which then restore the membrane potential to -85 mV, preparing for another oscillatory cycle.

This study confirms the notion that additional conductances are involved in the initial depolarization in WT mice since L-type channels require an even stronger depolarization to be activated than T-type channels. T- and L-type calcium channels are most likely unable to drive depolarization from a potassium-defined resting membrane potential on their

own. It has been demonstrated that the closure of TASK potassium channels mediates Ang II-dependent depolarization, but still other conductances must be involved the initial depolarization itself[25,80,153,154].

Moreover, the mechanisms of terminating individual spikes and bursts of calcium oscillations remain unclear. In the gain-of-function *Cacna1h* KI mouse model, slower spiking was observed (Fig. 35C)[83]. Considering that the knockout should generally lead to the opposite effect, a speculation arises that the frequency of calcium spiking may be inversely linked to $[Ca^{2+}]_i$. In the $Ca_V3.2$ KO model, this could contribute to maintaining physiological calcium levels (and thus aldosterone synthesis).

Further research is necessary to fully comprehend the functional significance of potassium channels and other conductances. Ideally, in situ electrophysiological studies should be combined with simultaneous calcium imaging to investigate these aspects further. Unfortunately, such experiments could not be conducted in the present study.

Additionally, this study demonstrated that Ang II primarily modulates $[Ca^{2+}]_i$ through alterations in the patterns of oscillations rather than by affecting baseline levels (Fig. 33 and 34). Simultaneous inhibition of T- and L-type calcium channels resulted in a complete cessation of Ang II-dependent $[Ca^{2+}]_i$ oscillations, as well as any changes in baseline $[Ca^{2+}]_i$. These findings indicate that other calcium influx pathways, aside from VGCCs, do not play a significant role in controlling aldosterone synthesis in response to Ang II.

The present study did not investigate whether the modulation of $[Ca^{2+}]_i$ by K^+ is similarly dependent on VGCCs. The observation that a response to physiological changes in K^+ only occurs in the presence of Ang II suggests this as a plausible assumption. However, it is essential to note that even after inhibiting T- and L-type calcium channels, baseline $[Ca^{2+}]_i$ remained high compared to most other cell types.

Further, unpublished observations (by Dinh and Stölting) suggest that extracellular calcium removal can further reduce baseline calcium levels, indicating the existence of other calcium conductances (Fig. 41). These are not essential for the actions of Ang II or potassium and are currently not fully understood.

In addition to uncovering the mechanisms of calcium signaling in the ZG and its role in aldosterone production, these findings have significant implications for future pharmacological interventions. Targeting T-type calcium channels has been proposed as a potential approach for treating primary aldosteronism or reducing aldosterone synthesis in

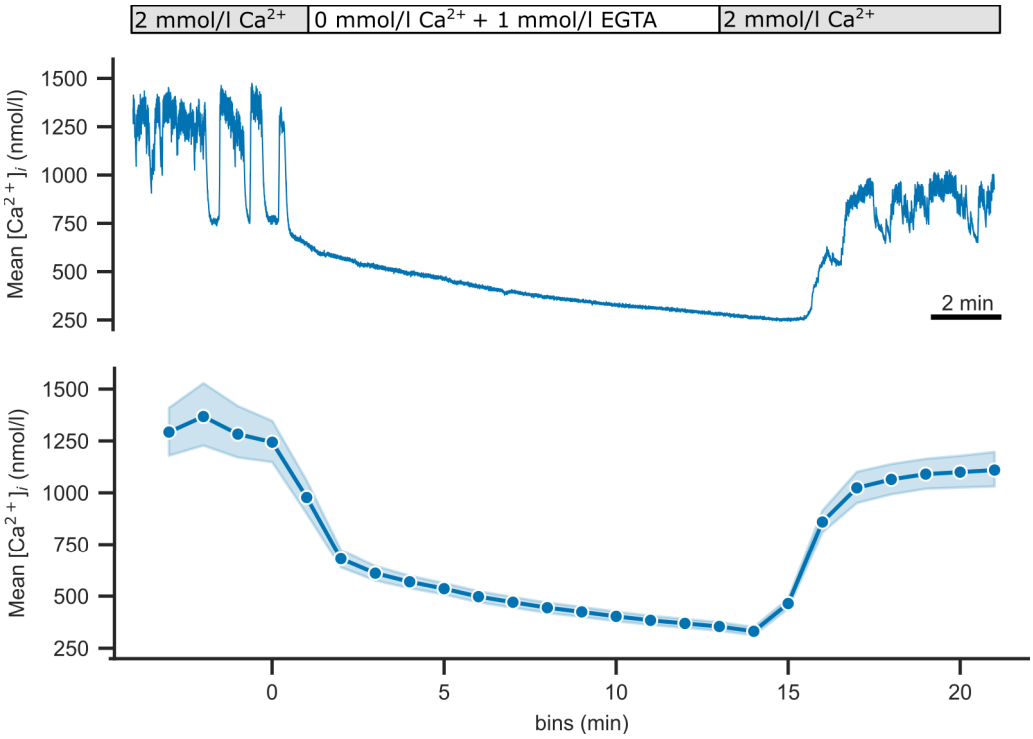

Figure 41. WT ZG cells show absence of signals and lowered mean as well as baseline $[Ca^{2+}]_i$ upon removal of extracellular Ca^{2+}. *Changes in mean $[Ca^{2+}]_i$ recorded from one representative WT ZG cell from an adrenal slice stained with Fura-2 AM (upper panel) and the average of all recorded cells (lower panel). Slices were initially perfused with BBS solutions (see Methods Table 3) containing 2 mmol/l Ca^{2+}. The perfusion solution was then changed to BBS without Ca^{2+} but supplemented with 1 mmol/l EGTA. Finally, the perfusion returned to the original conditions. Slices were stimulated with 4 mmol/l K^+ and 500 pmol/l Ang II during the whole recording. Data are plotted as mean values of all cells (circles) ± 95% CI (shaded areas). Application of the different extracellular Ca^{2+} concentrations is indicated by the grey bars.*

general[17]. However, the data from this present study suggest that long-term treatment with T-type channel inhibitors may be counteracted by calcium influx through L-type calcium channels. This could explain why mibefradil, a preferential T-type channel inhibitor, did not show sustained effects on aldosterone levels or blood pressure in vivo[155,156]. Nevertheless, selectively blocking $Ca_V3.2$ or $Ca_V1.3$ channels in cases of primary aldosteronism caused by gain-of-function mutations in these channels may still be a viable therapeutic strategy to mitigate pathological calcium influx into the ZG[52,83,88,104].

Interestingly, previous observations in the H295R cell line have shown that simultaneous blockade of both L- and T-type channels, using unspecific inhibitors like benidipine[157] or efonidipine[158], reduced aldosterone production. The potential extra-adrenal side effects of such broad channel inhibition, however, need to be evaluated, making this approach subject to further investigation.

5.2 *Cacna1h* KI Mice exhibit elevated baseline and peak zona glomerulosa calcium levels

Gain-of-function mutations in the *CACNA1H* gene are responsible for familial hyperaldosteronism type IV (FH IV) and early-onset hypertension in humans[62]. Mice that model FH IV by carrying a heterozygous gain-of-function mutation in the *Cacna1h* gene, exhibit elevated aldosterone:renin ratios, elevated blood pressure and increased adrenal aldosterone synthase expression[83].

Cacna1h KI adrenal slices showed increased baseline and peak intracellular calcium concentrations in the ZG compared to WT controls(Fig. 36).

Activation and inactivation of T-type calcium channels, including $Ca_V3.2$, is regulated by changes in membrane potential. As the voltage increases, the fraction of activated channels also increases in a sigmoidal manner, while the fraction of non-inactivated channels decreases in a similar fashion. The intersection of these curves creates a small voltage "window," which allows for a constitutive, non-inactivating current referred to as the "window current" (see Introduction Section 1.4 and Fig. 9). Previous studies have shown that $Ca_V3.2$ channels carrying the M1549V mutation (the human ortholog) exhibit activation curves shifted to more negative potentials, bringing them closer to the resting membrane potential of ZG cells[62]. This shift results in a larger "window current" compared to the WT channels. The increased constitutive current accounts for the higher intracellular baseline calcium levels observed in *Cacna1h* KI mice (Fig. 36).

Furthermore, the mutation also resulted in impaired channel inactivation, potentially leading to increased calcium influx at more depolarized potentials (i.e., during peaks). Interestingly, the spiking frequency was not elevated in *Cacna1h* KI mice (Fig. 35); in fact, it was lower than in controls under supra-physiological concentrations of stimuli.

These findings align with previous reports suggesting that $Ca_V3.2$ is not the initiating conductance in the depolarization phase (interspike interval) of the oscillatory cycle[25]. Studies have shown that during the initial depolarization phase, the $Ca_V3.2$ current remains relatively constant and small[25], which could account for the stably elevated baseline calcium levels observed in the mutant mice.

Furthermore, the observation that ZG cells lacking $Ca_V3.2$ are still capable of maintaining calcium spikes mediated by L-type channels strengthens this proposition (Fig. 22, 29 and 31). Given that L-type channels require a stronger depolarization for activation compared to T-type channels, it is likely that channels other than $Ca_V3.2$ are responsible for the initial

depolarization that triggers rapid calcium influx during the spikes.

Consequently, a gain-of-function mutation in *Clcn2*, leading to indirect elevation of intracellular calcium levels through glomerulosa cell depolarization, has been shown to cause increased calcium spiking frequencies[81,159]. However, under supraphysiological stimulation, lower spiking frequencies were observed, possibly due to two effects. Firstly, channels carrying the M1549V mutation exhibit slower recovery from inactivation, leading to delayed "availability" of the channel for the next spike[62]. Secondly, higher calcium levels in the presence of mutant channels may activate Ca^{2+}-dependent potassium channels, resulting in cell hyperpolarization and a delay in the occurrence of the next spike[160]. Conducting pharmacological investigations in the future could be essential for a more in-depth understanding of this effect.

In any event, the observed increase in baseline and peak calcium levels leads to an overall rise in mean $[Ca^{2+}]_i$ (Fig. 35 A), providing an explanation for the pathophysiology of FH-IV and suggesting the applicability of a targeted $Ca_V3.2$ channel inhibition in alleviating the pathological phenotype.

5.3 *Cacna1d* KI mice response to treatment with isradipine

The *Cacna1d* KI mice model human PASNA syndrome, displaying primary aldosteronism, heightened seizure susceptibility, and neurologic abnormalities, including motor deficits and mild social impairment[104]. ZG cells in *Cacna1d* KI mice demonstrated increased $[Ca^{2+}]_i$, while spiking and bursting parameters were mostly unchanged[104]. This study aimed to explore the potential reversibility of both adrenal and neurologic phenotypes using the calcium channel blocker isradipine.

In adrenal slices the overall mean and baseline $[Ca^{2+}]_i$ were reduced upon administration of isradipine (Fig. 39).

Treatment of *Cacna1d* KI mice with isradipine lead to a partial response of PASNA syndrome features. During the rotarod experiment 4 hours after isradipine administration, when peak plasma levels are expected, only KI mice exhibited improved performance (Fig. 40A). Furthermore, in *Cacna1d* KI mice, plasma aldosterone levels declined upon isradipine treatment (Fig. 40D).

No significant impact was observed in the open field test conducted 18 hours after the last dose (Fig. 40B), which corresponds to trough plasma levels. Similarly, nest-building

performance remained unchanged during the test (Fig. 40C), which covered both peak and trough plasma levels of isradipine.

Analysis of the baseline calcium concentrations outside of spiking events revealed that isradipine only affected *Cacna1d* KI mice but not WT (Fig. 39B). This suggests that the mutated $Ca_V1.3$ channels may demonstrate an elevated minimal open probability, resulting in an increased baseline influx of Ca^{2+}.

Furthermore, previous studies have demonstrated that this mutation results in a shift of channel activation and inactivation to more hyperpolarized potentials[52]. The calcium imaging data suggest that these shifts cause abnormal constitutive calcium influx closer to the ZG resting membrane potential in KI mice, which could be mitigated by isradipine. This may explain why isradipine reduced aldosterone levels in *Cacna1d* KI mice.

Considering that isradipine is an approved therapy for hypertension, calcium channel blocker treatment could be a viable option for patients with primary aldosteronism caused by *CACNA1D* mutations. Isradipine appears to be particularly suitable, compared to other dihydropyridines due to its known strong affinity towards the $Ca_V1.3$ subtype[135,144]. Different $Ca_V1.3$ mutations may exhibit varying responses to calcium channel inhibitors. This stimulates interest in exploring clinical outcomes in relation to the sensitivity of identified variants. Development of novel blockers with higher specificity for $Ca_V1.3$ could potentially lead to even more significant effects.

6 Summary and Outlook

Calcium is a crucial mediator in cellular signaling, influencing various essential cellular functions, including secretion, muscle contraction, and gene regulation. Dysregulated fluctuations in intracellular calcium levels can lead to severe cellular dysfunction.

In the adrenal gland's outermost layer, the ZG, calcium plays a vital role in modulating the synthesis of aldosterone, a hormone that regulates electrolyte and fluid balance, and consequently controlling blood pressure. The primary physiological stimuli of aldosterone production in the ZG are reductions in extracellular fluid volume and elevated serum potassium levels. The initiation of aldosterone synthesis in ZG cells by these stimuli is based on the depolarization of the ZG cells from their resting membrane potential. This depolarization, in turn, activates VGCCs, resulting in the influx of Ca^{2+}through these channels and the subsequent elevation of $[Ca^{2+}]_i$. The resultant increase in $[Ca^{2+}]_i$ regulates crucial events in the cascade of aldosterone production, including the expression of the aldosterone synthase, which catalyzes the last step in this cascade.

VGCCs occupy vital roles in an array of physiological processes across both excitable and non-excitable cells. These channels are ubiquitously distributed throughout various tissues in the body, encompassing the brain, kidneys, muscles, pancreas, and endocrine tissues, such as the ZG of the adrenal gland. Minor changes in VGCC activity, often attributable to mutations, result in an elevated risk for diverse diseases spanning cardiovascular disorders and neurological conditions such as epilepsy and autism.

In human ZG cells, T-type and L-type are the predominantly expressed channels among the VGCC family. Mutations in these channels are closely associated with PA, a condition estimated to impact approx. 50 million individuals globally.

PA is characterized by excessive aldosterone production, leading to hypertension, hypokalemia, and heightened susceptibility to cardiovascular diseases. Mutations in the *CACNA1H* gene (encoding $Ca_V3.2$) and *CACNA1D* (encoding $Ca_V1.3$) have been identified in PA patients and contribute directly to increased calcium influx and elevated aldosterone levels.

Previous studys have shown that ZG cells exhibit spontaneous depolarizations in their

membrane potential, with suggestions pointing to the involvement of T-type calcium channels, specifically $Ca_V3.2$, in generating these depolarizations. Furthermore, it has been observed that ZG cells display not only voltage oscillations but also oscillatory fluctuations in $[Ca^{2+}]_i$. It is plausible that these voltage oscillations underlie the observed calcium fluctuations, given their similarity in oscillatory frequency. However, it is most likely that the calcium fluctuations themselves, rather than the voltage variations, serve as direct regulators of aldosterone synthesis.

Despite the demonstrated significance of $Ca_V3.2$ in the electrical excitability of ZG cells, its precise role in aldosterone synthesis remains incompletely elucidated.

If $Ca_V3.2$ were solely responsible for calcium signaling, as implied by its role in generating voltage oscillations, one would anticipate a reduction in aldosterone levels in the absence of $Ca_V3.2$.

Interestingly, studies involving mice lacking $Ca_V3.2$ did not demonstrate alterations in systemic aldosterone levels, nor did they display modified responses to Ang II infusion. This observation suggests the existence of additional calcium influx pathways beyond $Ca_V3.2$.

Furthermore, the application of mibefradil, a preferential T-type channel inhibitor, failed to sustainably affect aldosterone levels or blood pressure *in vivo*. This indicates the potential involvement of non-T-type channels.

Additionally, the identification of mutations in the L-type channel $Ca_V1.3$ among patients with primary aldosteronism provides further substantiation for the participation of other VGCCs in the regulation of calcium signaling and aldosterone synthesis.

The objectives of this study were first, to investigate the regulation of $[Ca^{2+}]_i$ in the ZG of $Ca_V3.2$-deficient mice and second, to evaluate the impact of a $Ca_V3.2$ mutation identified in PA patients on calcium signaling, utilizing the *Cacna1h*$^{M1560V/+}$ knock-in mouse model. This mutation was identified in patients with PA.

Thirdly, this study sought to investigate the feasibility of a pharmacological intervention using the specific L-type channel inhibitor isradipine to ameliorate the phenotype in the *Cacna1d*$^{I772M/+}$ mouse model. This modes closely mirrors patients with PASNA syndrome.

In the first part of this research, employing the $Ca_V3.2$ knockout mouse model, an array of techniques including calcium imaging, RNA-sequencing, and whole-cell patch-clamp recordings lead to following key findings:

Calcium oscillations driven by Ang II and potassium persisted in KO mice and were instead mediated by L-type calcium channels.

Acute inhibition of T-type calcium channels did not abolish Ang II-mediated calcium influx in WT ZG cells. Instead, a subset of cells exhibited oscillatory calcium influx via L-type calcium channels.

Ang II augmented increases in $[Ca^{2+}]_i$ within ZG cells exclusively through the recruitment of T- and L-type calcium channels, without involvement of intracellular calcium stores.

These findings underscore the pivotal roles played by both T- and L-type calcium channels in the regulation of calcium influx in ZG cells under physiological conditions. Furthermore, these results suggest that T-type VGCCs are not obligatory for the maintenance of calcium oscillations in ZG cells, as L-type VGCCs can mediate the signals in their absence.

These observations bear significant implications for future pharmacological interventions. While inhibition of T-type calcium channels had been previously proposed as a promising strategy for mitigating hyperaldosteronism and suppressing aldosterone synthesis, the findings presented in this project suggest that long-term efficacy may be limited due to compensatory calcium influx via L-type calcium channels. This aligns with observations indicating that mibefradil, a preferential T-type channel inhibitor, failed to exert sustained effects on aldosterone levels or blood pressure in vivo.

Nevertheless, for primary aldosteronism patients exhibiting gain-of-function mutations in either $Ca_V3.2$ or $Ca_V1.3$, targeted inhibition of these VGCCs may still represent a viable therapeutic approach to alleviate pathological calcium influx within the ZG. This was investigated in the following parts of this project.

Therefore, the calcium signaling within *Cacna1h*$^{M1560V/+}$ knock-in mice, harboring a gain-of-function mutation in the $Ca_V3.2$ VGCC, a mutation identified in PA patients, was analyzed. These mice dislayed heightened baseline and peak intracellular calcium levels in ZG cells, suggesting the potential suitability of specific $Ca_V3.2$ channel blockade in ameliorating the pathological phenotype.

The final part of this project focused on investigating the inhibition of the L-type calcium channel $Ca_V1.3$ harboring a gain-of-function mutation identified in patients with PASNA syndrome and its efficacy to rescue the pathological phenotype. To this end, a mouse model mirroring this syndrome, by displaying the analogous gain-of-function mutation, was utilized. These mice showed increased calcium influx in ZG cells, elevated aldosterone levels, and neurolgical abnormalities, closely recapitulating the clinical phenotype observed in PASNA patients.

Employing the L-type specific inhibitor isradipine led to a reduction in $[Ca^{2+}]_i$ within ZG cella, along with lowered aldosterone levels and improved motor function.

These findings suggest that patients with PASNA syndrome due to *CACNA1D* mutations may benefit from treatment with L-type specific inhibitors.

However, the data from this project emphasize that, in patients exhibiting heightened aldosterone synthesis without an underlying gain-of-function mutation in a VGCC, a single-channel blockade, be it T-type or L-type, may not suffice to effectively lower aldosterone levels, as each of these channels sustains calcium activity in the absence of the other. Thus, a dual inhibition strategy, potentially employing non-specific inhibitors such as benidipine or efonidipine, may represent a suitable strategy and warrants further exploration. Nonetheless, the consideration of potential extra-adrenal side effects necessitates a thorough evaluation of this approach.

Bibliography

[1]R. Bagur and G. Hajnóczky: “Intracellular Ca2+ Sensing: Its Role in Calcium Homeostasis and Signaling”, Molecular Cell **66**, 780–788 (2017).

[2]D. E. Clapham: “Calcium Signaling”, Cell **131**, 1047–1058 (2007).

[3]M. Brini, D. Ottolini, T. Calì, and E. Carafoli: “Calcium in health and disease”, in *Metal ions in life sciences*, Vol. 13 (Springer London, 2013), pp. 81–137.

[4]R. J. P. Williams: “Calcium: the developing role of its chemistry in biological evolution”, in *Calcium as a cellular regulator*, edited by E. Carafoli and C. B. Klee (Oxford University Press, New York, 1999), pp. 3–27.

[5]M. Brini, T. Calì, D. Ottolini, and E. Carafoli: “Intracellular calcium homeostasis and signaling”, in *Metal ions in life sciences*, Vol. 12 (Springer London, 2013), pp. 119–168.

[6]E. R. Nightingale: “Phenomenological theory of ion solvation. Effective radii of hydrated ions”, Journal of Physical Chemistry **63**, 1381–1387 (1959).

[7]D. A. Williams, K. E. Fogarty, R. Y. Tsien, and F. S. Fay: “Calcium gradients in single smooth muscle cells revealed by the digital imaging microscope using Fura-2”, Nature **318**, 558–561 (1985).

[8]G. Guillon et al.: “Vasopressin stimulates steroid secretion in human adrenal glands: Comparison with angiotensin-II effect”, Endocrinology **136**, 1285–1295 (1995).

[9]C. Grienberger and A. Konnerth: “Imaging Calcium in Neurons”, Neuron **73**, 862–885 (2012).

[10]F. L. Bygrave and A. Benedetti: “What is the concentration of calcium ions in the endoplasmic reticulum?”, Cell Calcium **19**, 547–551 (1996).

[11]C. Fernandez-Sanz, S. De la Fuente, and S. S. Sheu: “Mitochondrial Ca2+ concentrations in live cells: quantification methods and discrepancies”, FEBS Letters **593**, 1528–1541 (2019).

[12]E. Strehler and M. Treiman: “Calcium Pumps of Plasma Membrane and Cell Interior”, Current Molecular Medicine **4**, 323–335 (2005).

[13]M. Egger and E. Niggli: “Regulatory function of Na-Ca exchange in the heart: Milestones and outlook”, Journal of Membrane Biology **168**, 107–130 (1999).

[14]D. Chin and A. R. Means: “Calmodulin: A prototypical calcium sensor”, Trends in Cell Biology **10**, 322–328 (2000).

[15]F. Rusnak and P. Mertz: “Calcineurin: Form and function”, Physiological Reviews **80**, 1483–1521 (2000).

[16]M. Uhlén et al.: “Tissue-based map of the human proteome”, Science **347**, 1260419 (2015).

[17]M. F. Rossier, E. A. Ertel, M. B. Vallotton, and A. M. Capponi: “Inhibitory Action of Mibefradil on Calcium Signaling and Aldosterone Synthesis in Bovine Adrenal Glomerulosa Cells 1”, Journal of Pharmacology and Experimental Therapeutics **287**, 824–831 (1998).

[18]J. C. Gomora, L. Xu, J. A. Enyeart, and J. J. Enyeart: “Effect of Mibefradil on Voltage-Dependent Gating and Kinetics of T-Type Ca2+ Channels in Cortisol-Secreting Cells”, Journal of Pharmacology and Experimental Therapeutics **292** (2000).

[19]S. N. Yang and P. O. Berggren: “The role of voltage-gated calcium channels in pancreatic β-cell physiology and pathophysiology”, Endocrine Reviews **27**, 621–676 (2006).

[20]D. B. Wheeler, A. Randall, and R. W. Tsien: “Roles of N-type and Q-type Ca2+ channels in supporting hippocampal synaptic transmission”, Science **264**, 107–111 (1994).

[21]G. W. Zamponi: “Regulation of voltage-gated calcium channels by synaptic proteins”, Advances in Experimental Medicine and Biology **740**, 759–775 (2012).

[22]S. W. Flavell and M. E. Greenberg: “Signaling mechanisms linking neuronal activity to gene expression and plasticity of the nervous system”, Annual Review of Neuroscience **31**, 563–590 (2008).

[23]D. G. Wheeler, R. D. Groth, H. Ma, C. F. Barrett, S. F. Owen, P. Safa, and R. W. Tsien: “CaV1 and CaV2 channels engage distinct modes of Ca2+ signaling to control CREB-dependent gene expression”, Cell **149**, 1112–1124 (2012).

[24]M. E. Mangoni, B. Couette, E. Bourinet, J. Platzer, D. Reimer, J. Striessnig, and J. Nargeot: “Functional role of L-type Cav1.3 Ca2+ channels in cardiac pacemaker activity”, Proceedings of the National Academy of Sciences of the United States of America **100**, 5543–5548 (2003).

[25]C. Hu, C. G. Rusin, Z. Tan, N. A. Guagliardo, and P. Q. Barrett: “Zona glomerulosa cells of the mouse adrenal cortex are intrinsic electrical oscillators”, The Journal of Clinical Investigation **122**, 2046–2053 (2012).

[26]A. C. Dolphin: “Voltage-gated calcium channels and their auxiliary subunits: physiology and pathophysiology and pharmacology”, Journal of Physiology **594**, 5369–5390 (2016).

[27]F. H. Yu, V. Yarov-Yarovoy, G. A. Gutman, and W. A. Catterall: “Overview of Molecular Relationships in the Voltage-Gated Ion Channel Superfamily”, Pharmacological Reviews **57**, 387–395 (2005).

[28]W. A. Catterall, E. Perez-Reyes, T. P. Snutch, and J. Striessnig: “International Union of Pharmacology. XLVIII. Nomenclature and structure-function relationships of voltage-gated calcium channels”, Pharmacological reviews **57**, 411–425 (2005).

[29]J. Yang, P. T. Elllnor, W. A. Sather, J. F. Zhang, and R. W. Tsien: “Molecular determinants of Ca2+ selectivity and ion permeation in L-type Ca2+ channels”, Nature **366**, 158–161 (1993).

[30]M. Noda et al.: “Primary structure of Electrophorus electricus sodium channel deduced from cDNA sequence”, Nature **312**, 121–127 (1984).

[31]B. A. Simms and G. W. Zamponi: “Neuronal voltage-gated calcium channels: Structure, function, and dysfunction”, Neuron **82**, 24–45 (2014).

[32]J. R. Tyson and T. P. Snutch: “Molecular nature of voltage-gated calcium channels: Structure and species comparison”, Wiley Interdisciplinary Reviews: Membrane Transport and Signaling **2**, 181–206 (2013).

[33]P. A. Anderson and R. M. Greenberg: “Phylogeny of ion channels: Clues to structure and function”, Comparative Biochemistry and Physiology - B Biochemistry and Molecular Biology **129**, 17–28 (2001).

[34]Y. Murata, H. Iwasaki, M. Sasaki, K. Inaba, and Y. Okamura: “Phosphoinositide phosphatase activity coupled to an intrinsic voltage sensor”, Nature **435**, 1239–1243 (2005).

[35]T. E. DeCoursey: “Voltage and pH sensing by the voltage-gated proton channel, HV1”, Journal of the Royal Society Interface **15**, `10.1098/rsif.2018.0108` (2018).

[36]S. R. Durell and H. R. Guy: “A putative prokaryote voltage-gated Ca2+ channel with only one 6TM motif per subunit”, Biochemical and Biophysical Research Communications **281**, 741–746 (2001).

[37]P. W. Fowler and M. S. Sansom: “The pore of voltage-gated potassium ion channels is strained when closed”, Nature Communications **4**, 1–8 (2013).

[38]M. Strong, K. G. Chandy, and G. A. Gutman: “Molecular evolution of voltage-sensitive ion channel genes: On the origins of electrical excitability”, Molecular Biology and Evolution **10**, 221–242 (1993).

[39]K. Ishibashi, M. Suzuki, and M. Imai: “Molecular cloning of a novel form (two-repeat) protein related to voltage-gated sodium and calcium channels”, Biochemical and Biophysical Research Communications **270**, 370–376 (2000).

[40]X. Cai and D. E. Clapham: “Ancestral Ca2+ signaling machinery in early animal and fungal evolution”, Molecular Biology and Evolution **29**, 91–100 (2012).

[41]B. J. Liebeskind, D. M. Hillis, and H. H. Zakon: “Evolution of sodium channels predates the origin of nervous systems in animals”, Proceedings of the National Academy of Sciences of the United States of America **108**, 9154–9159 (2011).

[42]E. Perez-Reyes: “Molecular physiology of low-voltage-activated T-type calcium channels”, Physiological Reviews **83**, 117–161 (2003).

[43]M. C. Nowycky, A. P. Fox, and R. W. Tsien: “Three types of neuronal calcium channel with different calcium agonist sensitivity”, Nature **316**, 440–443 (1985).

[44]B. P. Bean: “Classes of calcium channels in vertebrate cells”, Annual Review of Physiology **51**, 367–384 (1989).

[45]A. P. Fox, M. C. Nowycky, and R. W. Tsien: “Single-channel recordings of three types of calcium channels in chick sensory neurones.”, The Journal of Physiology **394**, 173–200 (1987).

[46]A. Randall and R. W. Tsien: “Pharmacological dissection of multiple types of Ca2+ channel currents in rat cerebellar granule neurons”, Journal of Neuroscience **15**, 2995–3012 (1995).

[47]B. Nilius, P. Hess, J. B. Lansman, and R. W. Tsien: “A novel type of cardiac calcium channel in ventricular cells”, Nature **316**, 443–446 (1985).

[48]E. Perez-Reyes, L. L. Cribbs, A. Daud, A. E. Lacerda, J. Barclays, M. P. Williamson, M. Fox, M. Rees, and J. H. Lee: “Molecular characterization of a neuronal low-voltage-activated T-type calcium channel”, Nature **391**, 896–900 (1998).

[49]J. Striessnig, M. Grabner, J. Mitterdorfer, S. Hering, M. J. Sinnegger, and H. Glossmann: “Structural basis of drug binding to L Ca2+ channels”, Trends in Pharmacological Sciences **19**, 108–115 (1998).

[50]R. C. Lambert, Y. Maulet, J. Mouton, R. Beattie, S. Volsen, M. De Waard, and A. Feltz: "T-type Ca2+ current properties are not modified by Ca2+ channel β subunit depletion in nodosus ganglion neurons", Journal of Neuroscience **17**, 6621–6628 (1997).

[51]D. Lipscombe, A. Andrade, and S. E. Allen: "Alternative splicing: Functional diversity among voltage-gated calcium channels and behavioral consequences", Biochimica et biophysica acta **1828**, 1522 (2013).

[52]U. I. Scholl et al.: "Somatic and germline CACNA1D calcium channel mutations in aldosterone-producing adenomas and primary aldosteronism", Nature Genetics **45**, 1050–1054 (2013).

[53]A. Pinggera and J. Striessnig: "Cav1.3 (CACNA1D) L-type Ca2+ channel dysfunction in CNS disorders", The Journal of Physiology **594**, 5839–5849 (2016).

[54]G. W. Zamponi: "Targeting voltage-gated calcium channels in neurological and psychiatric diseases", Nature Reviews Drug Discovery **15**, 19–34 (2016).

[55]T. M. Seccia, B. Caroccia, E. P. Gomez-Sanchez, C. E. Gomez-Sanchez, and G. P. Rossi: "The Biology of Normal Zona Glomerulosa and Aldosterone-Producing Adenoma: Pathological Implications", Endocrine Reviews **39**, 1029–1056 (2018).

[56]C. C. Jeff Huang and Y. Kang: "The transient cortical zone in the adrenal gland: The mystery of the adrenal x-zone", Journal of Endocrinology **241**, R51–R63 (2019).

[57]E. Howard-Miller: "A transitory zone in the adrenal cortex which shows age and sex relationships", American Journal of Anatomy **40**, 251–293 (1927).

[58]P. V. Holmes and A. D. Dickson: "X-zone degeneration in the adrenal glands of adult and immature female mice.", Journal of anatomy **108**, 159–68 (1971).

[59]P. Thomas: *Endocrine gland development and disease* (Academic Press, 2013).

[60]S. J. Spencer, S. Mesiano, J. Y. Lee, and R. B. Jaffe: "Proliferation and Apoptosis in the Human Adrenal Cortex during the Fetal and Perinatal Periods: Implications for Growth and Remodeling 1", The Journal of Clinical Endocrinology & Metabolism **84**, 1110–1115 (1999).

[61]M. D. Payet, T. Durroux, L. Bilodeau, G. Guillon, and N. Gallo-Payet: "Characterization of k+ and ca2+ ionic currents in glomerulosa cells from human adrenal glands", Endocrinology **134**, 2589–2598 (1994).

[62]U. I. Scholl et al.: "Recurrent gain of function mutation in calcium channel CACNA1H causes early-onset hypertension with primary aldosteronism", eLife **4**, 1–22 (2015).

[63]T. Yang, M. He, H. Zhang, P. Q. Barrett, and C. Hu: “L- And T-type calcium channels control aldosterone production from human adrenals”, Journal of Endocrinology **244**, 237–247 (2020).

[64]H. Matsunaga, N. Yamashita, Y. Maruyama, I. Kojima, and K. Kurokawa: “Evidence for two distinct voltage-gated calcium channel currents in bovine adrenal glomerulosa cells”, Biochemical and Biophysical Research Communications **149**, 1049–1054 (1987).

[65]D. P. Lotshaw: “Role of membrane depolarization and T-type Ca2+ channels in angiotensin II and K+ stimulated aldosterone secretion”, Molecular and Cellular Endocrinology **175**, 157–171 (2001).

[66]C. J. Cohen, R. T. McCarthy, P. Q. Barrett, and H. Rasmussen: “Ca channels in adrenal glomerulosa cells: K+ and angiotensin II increase T-type Ca channel current”, Proceedings of the National Academy of Sciences of the United States of America **85**, 2412–2416 (1988).

[67]A. D. Schrier, H. Wang, E. M. Talley, E. Perez-Reyes, and P. Q. Barrett: “α1H T-type Ca2+ channel is the predominant subtype expressed in bovine and rat zona glomerulosa”, American Journal of Physiology - Cell Physiology **280** (2001).

[68]N. G. Hattangady, L. O. Olala, W. B. Bollag, and W. E. Rainey: “Acute and chronic regulation of aldosterone production”, Molecular and Cellular Endocrinology **350**, 151–162 (2012).

[69]S. Shibata and T. Fujita: “The kidneys and aldosterone/mineralocorticoid receptor system in salt-sensitive hypertension”, Current Hypertension Reports **13**, 109–115 (2011).

[70]W. Thomas, V. McEneaney, and B. J. Harvey: “Aldosterone-induced signalling and cation transport in the distal nephron”, Steroids **73**, 979–984 (2008).

[71]A. SPAT: “Control of Aldosterone Secretion: A Model for Convergence in Cellular Signaling Pathways”, Physiological Reviews **84**, 489–539 (2004).

[72]X. Chen, E. M. Talley, N. Patel, A. Gomis, W. E. McIntire, B. Dong, F. Viana, J. C. Garrison, and D. A. Bayliss: “Inhibition of a background potassium channel by Gq protein α-subunits”, Proceedings of the National Academy of Sciences of the United States of America **103**, 3422–3427 (2006).

[73]D. P. Lotshaw: “Biophysical, pharmacological, and functional characteristics of cloned and native mammalian two-pore domain K+ channels”, Cell Biochemistry and Biophysics **47**, 209–256 (2007).

[74]T. Rohacs, A. Bago, F. Deak, L. Hunyady, and A. Spat: “Capacitative Ca2+ influx in adrenal glomerulosa cells: Possible role in angiotensin II response”, American Journal of Physiology - Cell Physiology **267** (1994).

[75]H. A. Dinh, G. Stölting, and U. I. Scholl: “CaV3.2 (CACNA1H) in Primary Aldosteronism”, in *Handbook of experimental pharmacology*, Vol. 279 (Springer, Berlin, Heidelberg, 2023), pp. 249–262.

[76]M. Häggström, M. Häggström, and D. Richfield: “Diagram of the pathways of human steroidogenesis”, WikiJournal of Medicine/Diagram of the pathways of human steroidogenesis **1** (2014).

[77]A. Spät, L. Fülöp, and G. Szanda: “The role of mitochondrial Ca2+ and NAD(P)H in the control of aldosterone secretion”, Cell Calcium **52**, 64–72 (2012).

[78]L. L. Cribbs et al.: “Member of the T-Type Ca 2+ Channel Gene Family”, Circulation Research, 103–109 (1998).

[79]P. Q. Barrett, N. A. Guagliardo, P. M. Klein, C. Hu, D. T. Breault, and M. P. Beenhakker: “Role of voltage-gated calcium channels in the regulation of aldosterone production from zona glomerulosa cells of the adrenal cortex”, Journal of Physiology **594**, 5851–5860 (2016).

[80]D. Penton et al.: “Task3 Potassium Channel Gene Invalidation Causes Low Renin and Salt-Sensitive Arterial Hypertension”, Endocrinology **153**, 4740–4748 (2012).

[81]J. Schewe, E. Seidel, S. Forslund, L. Marko, J. Peters, D. N. Muller, C. Fahlke, G. Stölting, and U. Scholl: “Elevated aldosterone and blood pressure in a mouse model of familial hyperaldosteronism with ClC-2 mutation”, Nature Communications 2019 10:1 **10**, 1–14 (2019).

[82]N. A. Guagliardo et al.: “Angiotensin II induces coordinated calcium bursts in aldosterone-producing adrenal rosettes”, Nature Communications **11**, 1–15 (2020).

[83]E. Seidel et al.: “Enhanced Ca2+ signaling, mild primary aldosteronism, and hypertension in a familial hyperaldosteronism mouse model (Cacna1hM1560V/+)”, Proceedings of the National Academy of Sciences of the United States of America **118**, `10.1073/pnas.2014876118` (2021).

[84]A. D. Thuesen, S. H. Finsen, L. L. Rasmussen, D. C. Andersen, B. L. Jensen, and P. B. Hansen: “Deficiency of T-type Ca2+ channels Cav3.1 and Cav3.2 has no effect on angiotensin II-induced hypertension but differential effect on plasma aldosterone in mice”, American Journal of Physiology - Renal Physiology **317**, F254–F263 (2019).

[85]S. Monticone et al.: “Prevalence and Clinical Manifestations of Primary Aldosteronism Encountered in Primary Care Practice”, Journal of the American College of Cardiology **69**, 1811–1820 (2017).

[86]S. Monticone, F. D’Ascenzo, C. Moretti, T. A. Williams, F. Veglio, F. Gaita, and P. Mulatero: “Cardiovascular events and target organ damage in primary aldosteronism compared with essential hypertension: a systematic review and meta-analysis”, The Lancet Diabetes and Endocrinology **6**, 41–50 (2018).

[87]T. A. Williams et al.: “International Histopathology Consensus for Unilateral Primary Aldosteronism”, Journal of Clinical Endocrinology and Metabolism **106**, 42–54 (2021).

[88]E. A. Azizan et al.: “Somatic mutations in ATP1A1 and CACNA1D underlie a common subtype of adrenal hypertension”, Nature Genetics **45**, 1055–1060 (2013).

[89]K. Nanba et al.: “Somatic CACNA1H Mutation As a Cause of Aldosterone-Producing Adenoma”, Hypertension, 645–649 (2020).

[90]R. K. Dutta, T. Arnesen, A. Heie, M. Walz, P. Alesina, P. Söderkvist, and O. Gimm: “A somatic mutation in CLCN2 identified in a sporadic aldosterone-producing adenoma”, European Journal of Endocrinology **181**, K37–K41 (2019).

[91]M. Choi et al.: “K+ channel mutations in adrenal aldosterone-producing adenomas and hereditary hypertension”, Science **331**, 768–772 (2011).

[92]F. Beuschlein et al.: “Somatic mutations in ATP1A1 and ATP2B3 lead to aldosterone-producing adenomas and secondary hypertension”, Nature Genetics **45**, 440–444 (2013).

[93]F. L. Fernandes-Rosa et al.: “A gain-of-function mutation in the CLCN2 chloride channel gene causes primary aldosteronism”, Nature Genetics **50**, 355–361 (2018).

[94]U. I. Scholl et al.: “CLCN2 chloride channel mutations in familial hyperaldosteronism type II”, Nature Genetics **50**, 349–354 (2018).

[95]R. P. Lifton, R. G. Dluhy, M. Powers, G. M. Rich, S. Cook, S. Ulick, and J. M. Lalouel: “A chimaeric llβ-hydroxylase/aldosterone synthase gene causes glucocorticoid-remediable aldosteronism and human hypertension”, Nature **355**, 262–265 (1992).

[96]G. Daniil et al.: “CACNA1H Mutations Are Associated With Different Forms of Primary Aldosteronism”, EBioMedicine **13**, 225–236 (2016).

[97]K. Wulczyn, E. Perez-Reyes, R. L. Nussbaum, and M. Park: “Primary aldosteronism associated with a germline variant in CACNA1H”, BMJ Case Reports **12**, e229031 (2019).

[98]C. H. Wu, K. Y. Peng, D. Y. Hwang, Y. H. Lin, V. C. Wu, and J. S. Chueh: "Novel mutations detection with next-generation sequencing and its association with clinical outcome in unilateral primary aldosteronism", Biomedicines **9**, 1167 (2021).

[99]C. S. Tseng, K. Y. Peng, S. M. Wang, Y. C. Tsai, K. H. Huang, W. C. Lin, Y. H. Hu, V. C. Wu, and J. S. Chueh: "A Novel Somatic Mutation of CACNA1H p.V1937M in Unilateral Primary Hyperaldosteronism", Frontiers in Endocrinology **13**, 816476 (2022).

[100]K. Omata et al.: "Cellular and genetic causes of idiopathic hyperaldosteronism", Hypertension **72**, 874–880 (2018).

[101]Y. Yamazaki et al.: "Histopathological classification of cross-sectional image-negative hyperaldosteronism", Journal of Clinical Endocrinology and Metabolism **102**, 1182–1192 (2017).

[102]K. Omata et al.: "Aldosterone-producing cell clusters frequently harbor somatic mutations and accumulate with age in normal adrenals", Journal of the Endocrine Society **1**, 787–799 (2017).

[103]K. Nishimoto et al.: "Aldosterone-stimulating somatic gene mutations are common in normal adrenal glands", Proceedings of the National Academy of Sciences of the United States of America **112**, E4591–E4599 (2015).

[104]G. Stölting et al.: "Isradipine therapy in Cacna1dIle772Met/+ mice ameliorates primary aldosteronism and neurologic abnormalities", JCI Insight, e162468 (2023).

[105]R. Y. Tsien: "Intracellular Measurements of Ion Activities", Annual Review of Biophysics and Bioengineering **12**, 91–116 (1983).

[106]J. Liao, D. Patel, Q. Zhao, R. Peng, H. Guo, and Z. Diwu: "A novel Ca2+ indicator for long-term tracking of intracellular calcium flux", BioTechniques **70**, `10.2144/btn-2020-0161` (2021).

[107]R. Sanders, H. C. Gerritsen, A. Draaijer, P. M. Houpt, and Y. K. Levine: "Fluorescence lifetime imaging of free calcium in single cells", Bioimaging **2**, 131–138 (1994).

[108]"Calbryte™ 520, potassium salt", Accessed 2023-09-10, https://www.aatbio.com/products/calbryte-520-potassium-salt.

[109]"Calcium Detection Probes & Assay Kits Fluo-8 ® • Cal-520 ® • Calbryte ™ 520", Accessed: 2023-10-21, https://www.biomol.com/datei (2018).

[110]G. Grynkiewicz, M. Poenie, and R. Y. Tsien: "A New Generation of Ca2+ Indicators with Greatly Improved Fluorescence Properties", Journal of Biological Chemistry **260**, 3440–3450 (1985).

[111]G. Stölting, M. Fischer, and C. Fahlke: “ClC-1 and ClC-2 form hetero-dimeric channels with novel protopore functions”, Pflugers Archiv European Journal of Physiology **466**, 2191–2204 (2014).

[112]G. Stölting, M. Fischer, and C. Fahlke: “CLC channel function and dysfunction in health and disease”, Frontiers in Physiology **5**, 111986 (2014).

[113]G. Stölting, R. C. De Oliveira, R. E. Guzman, E. Miranda-Laferte, R. Conrad, N. Jordan, S. Schmidt, J. Hendriks, T. Gensch, and P. Hidalgo: “Direct interaction of CaVβ with actin up-regulates l-type calcium currents in HL-1 cardiomyocytes”, Journal of Biological Chemistry **290**, 4561–4572 (2015).

[114]R. Patro, G. Duggal, M. I. Love, R. A. Irizarry, and C. Kingsford: “Salmon provides fast and bias-aware quantification of transcript expression”, Nature Methods **14**, 417–419 (2017).

[115]P. Ewels, M. Magnusson, S. Lundin, and M. Käller: “MultiQC: Summarize analysis results for multiple tools and samples in a single report”, Bioinformatics **32**, 3047–3048 (2016).

[116]S. Chen, Y. Zhou, Y. Chen, and J. Gu: “Fastp: An ultra-fast all-in-one FASTQ preprocessor”, in Bioinformatics, Vol. 34, 17 (Sept. 2018), pp. i884–i890.

[117]M. I. Love, W. Huber, and S. Anders: “Moderated estimation of fold change and dispersion for RNA-seq data with DESeq2”, Genome Biology **15**, 1–21 (2014).

[118]A. Zhu, J. G. Ibrahim, and M. I. Love: “Heavy-Tailed prior distributions for sequence count data: Removing the noise and preserving large differences”, Bioinformatics **35**, 2084–2092 (2019).

[119]M. Ashburner et al.: “The Gene Ontology Consortium. Gene ontology: tool for the unification of biology”, Nat. Genet. **25**, 25–29 (2011).

[120]M. Kanehisa and S. Goto: *KEGG: Kyoto Encyclopedia of Genes and Genomes*, Jan. 2000.

[121]T. Wu et al.: “clusterProfiler 4.0: A universal enrichment tool for interpreting omics data”, Innovation **2**, 100141 (2021).

[122]U. Schöffling: *Arzneiformenlehre: ein Lehrbuch der Galenik für Theorie und Praxis* (Dt. Apotheker Verl, 1998), p. 464.

[123]T. D. Gould, D. T. Dao, and C. E. Kovacsics: “Mood and Anxiety Related Phenotypes in Mice”, Neuromethods **42**, 1–20 (2009).

[124]S. P. Brooks: “Neurological Evaluation of Movement Disorders in Mice”, in (2011), pp. 65–86.

[125]TSE Systems: “RotaRod Advanced Modular RotaRod for Mice & Rats”, Accessed: 2023-06-28, https://www.tse-systems.com/ (2019).

[126]R. M. Deacon: “Assessing nest building in mice”, Nature Protocols **1**, 1117–1119 (2006).

[127]S. Schuster et al.: “No Title”, Molecular Psychiatry **20**, 1120–1131 (2015).

[128]D. J. Reen: “Enzyme-linked immunosorbent assay (ELISA).”, Methods in molecular biology (Clifton, N.J.) **32**, 461–466 (1994).

[129]H. A. Dinh, M. Volkert, A. K. Secener, U. I. Scholl, and G. Stölting: “T- and L-type calcium channels maintain calcium oscillations in the murine zona glomerulosa”, bioRxiv, 2023.06.09.544326 (2023).

[130]S. Lykke-Andersen and T. H. Jensen: *Nonsense-mediated mRNA decay: An intricate machinery that shapes transcriptomes*, Sept. 2015.

[131]W. D. Shipe et al.: “Design, synthesis, and evaluation of a novel 4-aminomethyl-4- fluoropiperidine as a T-type Ca2+ channel antagonist”, Journal of Medicinal Chemistry **51**, 3692–3695 (2008).

[132]W. J. Choe, R. B. Messinger, E. Leach, V. S. Eckle, A. Obradovic, R. Salajegheh, V. Jevtovic-Todorovic, and S. M. Todorovic: “TTA-P2 Is a Potent and Selective Blocker of T-Type Calcium Channels in Rat Sensory Neurons and a Novel Antinociceptive Agent”, Molecular Pharmacology **80**, 900 (2011).

[133]N. J. Ortner et al.: “Lower Affinity of Isradipine for L-Type Ca 2+ Channels during Substantia Nigra Dopamine Neuron-Like Activity: Implications for Neuroprotection in Parkinson’s Disease”, The Journal of Neuroscience **37**, 6761–6777 (2017).

[134]G. H. Hockerman, B. Z. Peterson, E. Sharp, T. N. Tanada, T. Scheuer, and W. A. Catterall: “Construction of a high-affinity receptor site for dihydropyridine agonists and antagonists by single amino acid substitutions in a non- L-type Ca2+ channel”, Proceedings of the National Academy of Sciences **94**, 14906–14911 (1997).

[135]M. J. Sinnegger-Brauns, I. G. Huber, A. Koschak, C. Wild, G. J. Obermair, U. Einzinger, J. C. Hoda, S. B. Sartori, and J. Striessnig: “Expression and 1,4-dihydropyridine-binding properties of brain L-type calcium channel isoforms”, Molecular Pharmacology **75**, 407–414 (2009).

[136]M. Lin, O. Aladejebi, and G. H. Hockerman: “Distinct properties of amlodipine and nicardipine block of the voltage-dependent Ca2+ channels Cav1.2 and Cav2.1 and the mutant channels Cav1.2/Dihydropyridine insensitive and Cav2.1/Dihydropyridine sensitive”, European Journal of Pharmacology **670**, 105–113 (2011).

[137]G. W. Zamponi: *Antagonist binding sites of voltage-dependent calcium channels*, 1998.

[138]C. D. Clyne, P. C. White, and W. E. Rainey: "Calcium regulates human CYP11B2 transcription", in Endocrine research, Vol. 22, 4 (1996), pp. 485–492.

[139]J. T. Gwynne and J. F. Strauss: "The role of lipoproteins in steroidogenesis and cholesterol metabolism in steroidogenic glands", Endocrine Reviews **3**, 299–329 (1982).

[140]D. Larsson, B. Larsson, T. Lundgren, and K. Sundell: "The effect of pH and temperature on the dissociation constant for fura-2 and their effects on [Ca2+](i) in enterocytes from a poikilothermic animal, Atlantic cod (Gadus morhua)", Analytical Biochemistry **273**, 60–65 (1999).

[141]F. A. Lattanzio and D. K. Bartschat: "The effect of pH on rate constants, ion selectivity and thermodynamic properties of fluorescent calcium and magnesium indicators", Biochemical and Biophysical Research Communications **177**, 184–191 (1991).

[142]N. J. Ortner, T. Kaserer, J. N. Copeland, and J. Striessnig: *De novo CACAN1D Ca2+ channelopathies: clinical phenotypes and molecular mechanism*, July 2020.

[143]A. Pinggera, A. Lieb, B. Benedetti, M. Lampert, S. Monteleone, K. R. Liedl, P. Tuluc, and J. Striessnig: "CACNA1D de novo mutations in autism spectrum disorders activate cav1.3 l-type calcium channels", Biological Psychiatry **77**, 816–822 (2015).

[144]E. Ilijic, J. N. Guzman, and D. J. Surmeier: "The L-type channel antagonist isradipine is neuroprotective in a mouse model of Parkinson's disease", Neurobiology of Disease **43**, 364–371 (2011).

[145]D. G. Holmes: "Isradipine: A slow-release formulation given once daily controls blood pressure for 24 h", American Journal of Hypertension **6**, 74S–76S (1993).

[146]F. L. Tse, J. M. Jaffe, A. E. Hassell, and H. F. Schran: "Bioavailability of isradipine in young and old rats: Effect of mode of administration", Journal of Pharmacy and Pharmacology **41**, 657–660 (1989).

[147]D. G. Holmes and K. Kutz: "Bioequivalence of a slow-release and a non-retard formulation of isradipine", American Journal of Hypertension **6**, 70S–73S (1993).

[148]J. L. Arroyo, E. Dawson, R. P. Reiner, E. Gonima, and F. Carrascosa: "Effect of Isoflurane and Halothane on the Endocrine System", in *Isoflurane* (Springer, Berlin, Heidelberg, 1986), pp. 317–322.

[149]N. J. Ortner et al.: "The human channel gating-modifying A749G CACNA1D (Cav1.3) variant induces a neurodevelopmental syndrome-like phenotype in mice", JCI Insight, e162100 (2023).

[150]J. A. Ely, C. Ambroz, A. J. Baukal, S. B. Christensen, T. Balla, and K. J. Catt: "Relationship between agonist- and thapsigargin-sensitive calcium pools in adrenal glomerulosa cells. Thapsigargin-induced Ca2+ mobilization and entry", Journal of Biological Chemistry **266**, 18635–18641 (1991).

[151]A. Spat, P. Enyedi, G. Hajnoczky, and L. Hunyady: "Generation and role of calcium signal in adrenal glomerulosa cells", Experimental Physiology **76**, 859–885 (1991).

[152]C. B. Xie et al.: "Regulation of aldosterone secretion by Ca v 1.3", Scientific Reports **6**, 10.1038/srep24697 (2016).

[153]D. Heitzmann et al.: "Invalidation of TASK1 potassium channels disrupts adrenal gland zonation and mineralocorticoid homeostasis", EMBO Journal **27**, 179–187 (2008).

[154]C. A. Gancayco, M. R. Gerding, D. T. Breault, M. P. Beenhakker, P. Q. Barrett, and N. A. Guagliardo: "Intrinsic Adrenal TWIK-Related Acid-Sensitive TASK Channel Dysfunction Produces Spontaneous Calcium Oscillations Sufficient to Drive AngII (Angiotensin II)-Unresponsive Hyperaldosteronism", Hypertension **79**, 2552–2564 (2022).

[155]R. Schmitt et al.: "Hemodynamic and humoral effects of the novel calcium antagonist Ro 40-5967 in patients with hypertension", Clinical Pharmacology & Therapeutics **52**, 314–323 (1992).

[156]I. Ragueneau, A. B. Sao, J. L. Démolis, B. Darné, C. Funck-Brentano, and P. Jaillon: "Comparison of sympathetic modulation induced by single oral doses of mibefradil, amlodipine, and nifedipine in healthy volunteers", Clinical Pharmacology and Therapeutics **69**, 122–129 (2001).

[157]O. Akizuki, A. Inayoshi, T. Kitayama, K. Yao, S. Shirakura, K. Sasaki, H. Kusaka, and M. Matsubara: "Blockade of T-type voltage-dependent Ca2+ channels by benidipine, a dihydropyridine calcium channel blocker, inhibits aldosterone production in human adrenocortical cell line NCI-H295R", European Journal of Pharmacology **584**, 424–434 (2008).

[158]K. Imagawa, S. Okayama, M. Takaoka, H. Kawata, N. Naya, T. Nakajima, M. Horii, S. Uemura, and Y. Saito: "Inhibitory effect of efonidipine on aldosterone synthesis and secretion in human adrenocarcinoma (H295R) cells", Journal of Cardiovascular Pharmacology **47**, 133–138 (2006).

[159]C. Göppner, I. J. Orozco, M. B. Hoegg-Beiler, A. H. Soria, C. A. Hübner, F. L. Fernandes-Rosa, S. Boulkroun, M. C. Zennaro, and T. J. Jentsch: "Pathogenesis of hypertension in a mouse model for human CLCN2 related hyperaldosteronism", Nature Communications **10**, 1–13 (2019).

[160]T. Yang, H.-L. Zhang, Q. Liang, Y. Shi, Y.-A. Mei, P. Q. Barrett, and C. Hu: "Small-Conductance Ca2+ -Activated Potassium Channels Negatively Regulate Aldosterone Secretion in Human Adrenocortical Cells", Hypertension **68**, 785–795 (2016).

Appendix

Cacna1h KO data

A1. *Calcium bursting parameters (Fig. 23)*

	WT			**KO**			
	Mean	CI (lower limit)	CI (upper limit)	Mean	CI (lower limit)	CI (upper limit)	p-value
Activity (1/s)	0.494	0.368	0.631	1.054	0.898	1.220	0.003, **
Intra-burst frequency (1/s)	0.969	0.777	1.173	1.343	1.223	1.500	0.013, *
Inter-burst interval (s)	73.823	58.706	89.901	39.596	27.559	49.615	0.013, *
Burst length (s)	80.718	72.233	88.582	69.630	51.174	96.538	0.242, ns
n(animals)	7 (7+0)[#]			5 (3+2)[#]			
n(slices)	11			7			
n(cells)	208			103			

[#]: male+female

A2. *Mean calcium concentration at 100 pmol/l Ang II and indicated K+ concentrations in nmol/l (Fig. 24A).*

	WT						**KO**						
K^+ (mmol/l)	Animals (male + female)	Slices	Cells	Mean	95% CI (lower limit)	95% CI (upper limit)	Animals (male + female)	Slices	Cells	Mean	95% CI (lower limit)	95% CI (upper limit)	p-value
3.0	3 (0+3)	4	57	673.109	640.176	705.589	7 (1+6)	11	162	645.48	680.019	748.391	0.571, ns
3.5	4 (2+2)	6	97	769.015	741.215	796.764	5 (3+2)	9	85	714.374	782.856	858.993	0.367, ns
4.0	4 (3+1)	6	89	826.939	802.065	852.085	6 (1+5)	12	102	821.389	740.414	829.582	0.848, ns
4.5	4 (1+3)	6	120	835.522	805.055	866.717	5 (1+4)	6	73	784.304	868.558	936.949	0.521, ns
5.0	4 (2+2)	6	81	937.409	893.847	982.227	5 (1+4)	6	91	902.708	839.545	903.299	0.374, ns
5.5	3 (1+2)	6	52	930.973	871.769	990.086	5 (3+2)	9	99	870.952	863.787	991.088	0.556, ns
6.0	3 (2+1)	6	88	1049.245	997.559	1103.995	3 (1+2)	5	59	924.61	680.019	748.391	0.316, ns

A3. *Mean calcium concentration at 4 mmol/l K+ and indicated Ang II concentrations in nmol/l (Fig 24B).*

	WT						**KO**						
Ang II (pmol/l)	Animals (male + female)	Slices	Cells	Mean	95% CI (lower limit)	95% CI (upper limit)	Animals (male + female)	Slices	Cells	Mean	95% CI (lower limit)	95% CI (upper limit)	p-value
20	8 (5+3)	7	116	744.666	714.61	778.21	8 (3+5)	9	96	720.323	689.729	750.844	0.259, ns
50	7 (3+4)	10	127	737.938	708.891	768.572	5 (3+2)	5	53	678.321	629.572	728.491	0.766, ns
70	7 (5+2)	13	173	812.12	787.717	836.24	7 (4+3)	12	94	815.891	783.031	850.125	0.749, ns
100	5 (4+1)	12	85	871.254	839.655	904.306	8 (3+5)	16	119	807.653	774.643	841.156	0.363, ns
200	9 (5+4)	6	131	880.731	848.105	913.548	11 (3+8)	16	172	841.667	810.604	872.044	0.296, ns
300	8 (4+4)	14	103	903.257	874.88	932.768	9 (3+6)	13	140	867.233	835.629	900.215	0.175, ns
500	7 (5+2)	8	155	867.103	836.186	898.888	10 (6+4)	14	159	821.247	789.112	855.352	0.496, ns

A4. *Normalized log_2-transformed read counts of voltage-gated calcium channel transcripts detected in WT and KO samples (Fig. 25A)*

	WT							**KO**					
	S1	**S2**	**S3**	**S4**	**S5**	**S6**	**mean**	**S7**	**S8**	**S9**	**S10**	**S11**	**mean**
Cacna1a	5.43	6.85	5.52	5.14	6.85	6.37	6.03	5.12	4.97	6.59	5.43	5.38	5.50
Cacna1b	5.45	4.33	6.94	5.30	6.23	6.31	5.76	6.32	5.88	6.15	5.63	6.15	6.03
Cacna1c	12.02	11.83	11.73	11.54	11.96	11.87	11.83	11.79	12.05	11.87	11.94	12.04	11.94
Cacna1d	7.66	7.46	8.84	7.91	9.18	8.81	8.31	8.81	8.46	8.79	8.35	8.08	8.50
Cacna1e	3.14	1.76	2.89	3.32	4.75	3.45	3.22	3.73	2.50	3.11	2.75	4.40	3.30
Cacna1f	0.76	3.59	-0.87	0.00	0.12	1.03	0.77	2.43	1.27	0.00	1.04	-0.03	0.94
Cacna1g	5.15	4.44	4.59	3.94	4.12	4.07	4.38	6.41	4.33	3.85	4.30	3.72	4.52
Cacna1h	11.62	11.53	12.23	11.48	10.86	11.95	11.61	10.84	9.84	10.43	9.64	10.08	10.16
Cacna1i	3.50	4.96	4.61	4.80	4.87	3.95	4.45	5.30	5.71	4.14	4.22	3.58	4.59
Cacna2d1	12.84	12.40	12.79	12.59	13.19	12.85	12.78	13.22	13.08	13.24	13.05	13.16	13.15
Cacna2d2	5.89	5.75	6.53	5.50	6.33	5.51	5.92	5.79	6.89	6.01	5.73	5.80	6.04
Cacnb1	6.22	6.35	6.75	6.13	6.20	6.43	6.35	6.15	5.62	6.71	6.17	6.18	6.17
Cacnb2	10.55	10.71	10.48	10.65	10.48	10.41	10.55	10.18	10.37	9.99	10.35	10.54	10.28
Cacnb3	8.03	7.79	7.98	7.97	7.68	7.70	7.86	7.97	7.69	7.72	7.47	7.61	7.69
Cacnb4	1.87	2.29	5.99	3.60	3.75	5.30	3.80	4.69	2.75	3.26	3.36	2.63	3.34

A5. *The log_2 transformed fold-change and P-values of voltage-gated calcium channel transcripts compared in KO vs. WT samples (Fig. 25A)*

	Log_2 fold-change	**P-value**	**P_{adj}-value**
Cacna1a	-0.014	0.164	1.000
Cacna1b	0.002	0.876	1.000
Cacna1c	0.037	0.268	1.000
Cacna1d	0.003	0.818	1.000
Cacna1e	-0.00007	0.991	1.000
Cacna1f	-0.0007	0.835	1.000
Cacna1g	0.006	0.492	1.000
Cacna1h	-1.348	0.000	*** 0.000
Cacna1i	0.005	0.593	1.000
Cacna2d1	0.239	0.005	0.079
Cacna2d2	0.006	0.644	1.000
Cacnb1	-0.012	0.420	1.000
Cacnb2	-0.139	0.018	0.263
Cacnb3	-0.045	0.159	1.000
Cacnb4	-0.008	0.166	1.000

A6. *The 12 differentially expressed genes (DEGs) in KO vs. WT samples with log_2-fold change (LFC, cutoff = 1) and statistical significance (p-value, corrected for multiple testing) (Fig. 25B-C).*

	log_2 fold change	**p-value**
Cacna1h	-1.348	$3.9x10^{-05}$
Usp2	-1.064	$7.7x10^{-03}$
2810039B14Rik	-1.058	$2.4x10^{-04}$
Scn8a	-1.032	0.026
Cdv3	1.035	0.042
2010003K11Rik	1.044	$9.4x10^{-04}$
Ptp4a1	1.055	$5.4x10^{-04}$
Mpp7	1.061	$5.4x10^{-04}$
Creb5	1.068	$8.4x10^{-03}$
Tmprss11a	1.455	0.022
Gadd45g	1.493	$4.3x10^{-08}$
Lars2	1.82	0.036

A7. *Genes of the aldosterone synthesis and secretion pathway (KEGG mmu04925) with log_2-fold change (LFC) in gene expression KO vs. WT samples and the statistical significance (p-value, corrected for multiple testing)*

Symbol	LFC	p-value	Symbol	LFC	p-value	Symbol	LFC	p-value
Cacna1h	-1,348	$3{,}9 \times 10^{-05}$	***Atp1b1***	0,023	0,812	***Cyp21a1***	-0,004	0,971
Star	0,347	0,007	***Atp1b2***	-0,013	0,816	***Atp2b4***	0,005	0,973
Creb5	1,068	0,008	***Prkacb***	0,033	0,820	***Cyp11a1***	-0,008	0,974
Gna11	-0,198	0,023	***Itpr2***	0,027	0,828	***Creb3l3***	0,001	0,975
Agtr1a	0,431	0,048	***Calml4***	-0,016	0,835	***Cacna1d***	0,003	0,976
Creb1	0,193	0,067	***Itpr3***	-0,016	0,843	***Calm2***	-0,006	0,981
Scarb1	0,309	0,118	***Adcy6***	0,019	0,847	***Prkd3***	-0,008	0,982
Dagla	-0,356	0,157	***Atf4***	0,020	0,855	***Atp2b2***	0,002	0,983
Orai1	-0,170	0,237	***Calm3***	-0,026	0,857	***Atp1a2***	-0,004	0,984
Kcnj5	-0,054	0,252	***Itpr1***	0,024	0,860	***Atp1a3***	0,002	0,985
Plcb3	-0,143	0,259	***Adcy3***	-0,016	0,864	***Adcy4***	-0,003	0,985
Camk1	-0,111	0,268	***Agtr1b***	-0,021	0,866	***Atp1a4***	-0,001	0,988
Nr4a2	-0,012	0,297	***Kcnk9***	-0,007	0,870	***Atf1***	-0,003	0,989
Camk2d	0,080	0,403	***Gnaq***	0,025	0,870	***Prkd2***	-0,002	0,989
Prkce	0,079	0,419	***Gnas***	0,024	0,885	***Adcy7***	0,002	0,989
Atf6b	-0,077	0,479	***Mc2r***	-0,010	0,887	***Camk2a***	-0,001	0,992
Hsd3b6	-0,016	0,501	***Cacna1g***	0,006	0,887	***Agt***	0,001	0,993
Kcnk3	0,068	0,509	***Nr4a1***	-0,003	0,888	***Hsd3b2***	0,001	0,993
Camk4	0,016	0,527	***Atf2***	-0,020	0,902	***Creb3l4***	-0,012	#
Prkaca	-0,060	0,565	***Hsd3b1***	0,011	0,912	***Prkcg***	-0,009	#
Atp1a1	0,066	0,590	***Plcb4***	0,013	0,916	***Cacna1s***	-0,007	#
Atp2b1	0,043	0,613	***Cacna1i***	0,005	0,920	***Pomc***	-0,006	#
Lipe	0,022	0,682	***Ldlr***	0,012	0,923	***Cacna1f***	-0,001	#
Pde2a	-0,019	0,695	***Plcb1***	0,017	0,923	***Atp1b4***	-0,001	#
Plcb2	-0,019	0,703	***Adcy2***	0,008	0,926	***Camk1g***	0,000	#
Daglb	-0,046	0,718	***Prkca***	-0,009	0,926	***Calml3***	0,000	#
Adcy8	0,010	0,720	***Atp1b3***	0,016	0,932	***Hsd3b3***	0,001	#
Prkd1	-0,042	0,731	***Creb3l1***	0,006	0,934	***Hsd3b8***	‡	
Adcy9	-0,042	0,737	***Npr1***	-0,013	0,938	***Hsd3b9***	‡	
Adcy5	0,028	0,769	***Adcy1***	0,006	0,940	***Hsd3b4***	‡	
Cacna1c	0,037	0,771	***Creb3l2***	0,014	0,941	***Hsd3b5***	‡	
Prkcb	-0,023	0,796	***Camk2b***	-0,004	0,955	***Nppa***	‡	
Calm1	0,035	0,799	***Creb3***	0,010	0,962	***Calm5***	‡	
Atp2b3	-0,026	0,806	***Camk2g***	-0,006	0,969	***Calm4***	‡	

#: Low mean normalized count

‡: No read counts detected across all samples

A8. *Patch Clamp recordings in WT (Fig. 26A-B)*

	WT T-type			Non-T-type		
U (mV)	I (pA)	95% CI (lower limit)	95% CI (upper limit)	I (pA)	95% CI (lower limit)	95% CI (upper limit)
-95	‡			‡		
-85	‡			‡		
-75	‡			‡		
-65	‡			‡		
-55	-16.666	-21.208	-12.938	-0.167	-4.473	4.009
-45	-34.305	-53.887	-15.06	-0.68	-10.106	8.533
-35	-49.403	-70.534	-29.438	-8.657	-13.413	-3.429
-25	-48.19	-71.216	-25.164	-18.712	-26.757	-11.479
-15	-45.912	-65.153	-25.571	-28.287	-44.046	-14.777
-5	-42.355	-66.828	-23.587	-31.179	-45.936	-17.708
5	-31.97	-56.364	-11.757	-38.536	-54.818	-23.023
15	-22.767	-44.874	-6.406	-35.955	-47.483	-25.199
25	-6.787	-22.684	4.987	-41.008	-52.033	-29.202
35	-12.857	-26.476	0.463	-30.859	-41.409	-22.117
45	0.47	-14.112	15.473	-38.188	-49.185	-26.974
55	-2.768	-13.404	5.003	-28.53	-39.947	-19.614
65	6.34	-13.252	25.932	-28.676	-42.26	-15.092
75	20.756	-2.993	46.881	-23.328	-49.651	-3.028
n(animals)		3 (1+2)				
n(cells)		7				

‡: No peak current detected

A9. *Patch Clamp recordings in KO and statistical comparison to WT (Fig. 26A-B)*

	KO T-type			Non-T-type				
U (mV)	I (pA)	95% CI (lower limit)	95% CI (upper limit)	I (pA)	95% CI (lower limit)	95% CI (upper limit)	p-value (T-type)	p-value (Non-T-type)
-95	‡			‡				
-85	‡			‡				
-75	‡			‡				
-65	‡			‡				
-55	-7.379	-17.447	1.281	-2.133	-8.399	4.204	#	#
-45	-13.143	-22.237	-6.423	-4.302	-6.249	-2.275	#	#
-35	-10.398	-19.51	-2.136	-5.222	-10.641	0.436	p= 0.003, **	#
-25	-7.04	-15.232	1.471	-14.054	-21.388	-8.532	#	#
-15	-10.625	-26.618	3.761	-18.532	-23.827	-13.969	#	p=0.676, ns
-5	-5.797	-19.106	5.655	-24.256	-31.091	-17.892	#	#
5	-8.314	-24.82	8.286	-32.279	-43.212	-22.469	#	#
15	-4.256	-16.812	12.339	-32.894	-44.991	-21.546	#	#
25	-2.355	-17.474	18.09	-31.502	-46.041	-18.553	#	#
35	5.098	-12.989	25.352	-36.032	-45.875	-27.46	#	#
45	-3.948	-10.338	1.431	-25.785	-34.461	-19.547	#	#
55	0.256	-13.134	14.761	-16.499	-25.486	-8.458	#	#
65	1.585	-5.67	8.69	-19.975	-27.238	-12.051	#	#
75	2.52	-3.674	9.088	-19.361	-28.721	-8.995	#	#
n(animals)		4 (3+1)						
n(cells)		9						

#: Not tested

‡: No peak current detected

A10. *Statistical information of absolute calcium bursting parameters at 15 µmol/l TTA-P2 in WT slices and number of recorded animals, slices and cells (Fig 27D, G; Fig. 28B, C).*

	WT			**WT control**			
	Mean	CI (lower limit)	CI (upper limit)	Mean	CI (lower limit)	CI (upper limit)	p-value
Activity (1/s)	0.256	0.153	0.370	0.449	0.348	0.597	0.003, **
Intra-burst frequency (1/s)	0.972	0.906	1.041	0.851	0.747	1.003	0.047, *
Active cells per slice (%)	34.371	22.233	47.316	75.494	68.198	82.513	2.513x10-6, **
n(animals) (male+female)	10 (10+0)			15 (9+6)			
n(slices)	16			17			
n(cells)	291			288			

A11. *Statistical information of absolute calcium bursting parameters at 15 µmol/l TTA-P2 in KO slices and number of recorded animals, slices, and cells (Fig 27D, G; Fig. 28B, C).*

	KO			**KO control**			
	Mean	CI (lower limit)	CI (upper limit)	Mean	CI (lower limit)	CI (upper limit)	p-value
Activity (1/s)	0.871	0.745	1.018	0.875	0.662	1.096	0.958, ns
Intra-burst frequency (1/s)	1.239	1.136	1.351	1.307	1.162	1.459	0.446, ns
Active cells per slice (%)	90.288	84.286	95.110	83.588	73.129	93.793	0.230, ns
n(animals) (male+female)	7 (4+3)	7 (3+4)					
n(slices)	13	7					
n(cells)	162	83					

A12. *Calcium spike activity during perfusion with 15 µmol/l TTA-P2 in 1/s in WT and WT control (no blocker, Fig. 27)E*

	WT			**WT control**		
bin (min)	Activity	95% CI (lower limit)	95% CI (upper limit)	Activity	95% CI (lower limit)	95% CI (upper limit)
-3	0.599	0.548	0.652	0.643	0.588	0.7
-2.5	0.62	0.566	0.673	0.643	0.59	0.699
-2	0.639	0.59	0.689	0.632	0.583	0.681
-1.5	0.672	0.626	0.719	0.655	0.608	0.704
-1	0.657	0.612	0.704	0.638	0.588	0.686
-0.5	0.623	0.575	0.671	0.612	0.566	0.658
0	0.56	0.51	0.611	0.592	0.547	0.636
0.5	0.507	0.457	0.557	0.518	0.468	0.568
1	0.329	0.286	0.375	0.473	0.423	0.524
1.5	0.22	0.18	0.262	0.452	0.404	0.504
2	0.215	0.174	0.258	0.45	0.4	0.501
2.5	0.241	0.196	0.286	0.441	0.396	0.489
3	0.261	0.211	0.311	0.443	0.396	0.492
3.5	0.26	0.212	0.311	0.439	0.393	0.487
4	0.243	0.197	0.292	0.417	0.372	0.464
4.5	0.225	0.18	0.271	0.444	0.397	0.491
5	0.231	0.186	0.28	0.446	0.402	0.491
5.5	0.221	0.176	0.267	0.427	0.382	0.473
6	0.221	0.178	0.268	0.426	0.38	0.473
6.5	0.24	0.192	0.29	0.434	0.388	0.481
7	0.216	0.173	0.262	0.428	0.381	0.476
7.5	0.201	0.158	0.245	0.361	0.316	0.408

A13. *Calcium spike activity during perfusion with 15 µmol/l TTA-P2 in 1/s in KO and KO control (no blocker, Fig. 27E)*

	KO			**KO control**		
bin (min)	Activity	95% CI (lower limit)	95% CI (upper limit)	Activity	95% CI (lower limit)	95% CI (upper limit)
-3	1.099	1	1.197	1.173	1.025	1.313
-2.5	1.118	1.024	1.213	1.175	1.027	1.32
-2	1.091	0.997	1.188	1.25	1.121	1.378
-1.5	1.141	1.056	1.226	1.231	1.096	1.366
-1	1.106	1.02	1.193	1.267	1.142	1.393
-0.5	1.12	1.039	1.203	1.218	1.096	1.339
0	1.068	0.983	1.155	1.194	1.081	1.304
0.5	1.021	0.929	1.113	1.088	0.956	1.218
1	0.976	0.88	1.074	1.108	0.96	1.255
1.5	0.981	0.887	1.077	1.094	0.943	1.245
2	0.931	0.836	1.028	1.112	0.965	1.259
2.5	0.954	0.857	1.051	1.123	0.986	1.256
3	0.924	0.833	1.015	1.058	0.923	1.191
3.5	0.872	0.781	0.965	1.073	0.943	1.198
4	0.897	0.803	0.993	0.984	0.855	1.107
4.5	0.829	0.737	0.922	0.945	0.798	1.09
5	0.885	0.797	0.973	0.963	0.831	1.098
5.5	0.859	0.768	0.949	0.969	0.843	1.098
6	0.848	0.755	0.942	0.894	0.753	1.036
6.5	0.858	0.769	0.95	0.948	0.809	1.09
7	0.851	0.759	0.946	0.898	0.756	1.042
7.5	0.852	0.76	0.944	0.855	0.725	0.992

A14. *Statistical information of calcium bursting parameters relative to control at 15 µmol/l TTA P2 (Fig. 27F, Fig. 28A).*

	WT			**KO**		
	Mean	CI (lower limit)	CI (upper limit)	Mean	CI (lower limit)	CI (upper limit)
Activity	0.569	0.341	0.823	0.995	0.851	1.164
Intra-burst frequency (1/s)	1.182	1.101	1.265	0.913	0.837	0.995

A15. *Statistical information of absolute intra-burst frequency (1/s) at 0 µmol/l TTA-P2 in remaining active WT, KO and corresponding control slices (Fig. 28B-C).*

	WT			**WT control**			
	Mean	CI (lower limit)	CI (upper limit)	Mean	CI (lower limit)	CI (upper limit)	p-value
Intra-burst frequency (1/s)	0.929	0.840	1.029	0.960	0.841	1.114	0.9769, ns
	KO			**KO control**			
Intra-burst frequency (1/s)	1.307	1.196	1.444	1.410	1.291	1.533	0.2702, ns

A16. *Statistical information of absolute calcium bursting parameters at 0.05 µmol/l isradipine in WT slices (Fig. 29C, 30B-D).*

	WT			**WT control**			
	Mean	95% CI (lower limit)	95% CI (upper limit)	Mean	95% CI (lower limit)	95% CI (upper limit)	p-value
Activity (1/s)	0.350	0.264	0.444	0.449	0.348	0.597	0.255, ns
Intra-burst frequency (1/s)	0.838	0.656	1.023	0.851	0.747	1.003	0.749, ns
Active cells per slice (%)	65.202	55.317	75.238	75.494	68.198	82.513	0.1011, ns
n(animals)	9			15			
n(slices)	10			17			
n(cells)	178			288			

A17. *Statistical information of absolute calcium bursting parameters at 0.05 µmol/l isradipine in WT slices (Fig. 29C, 30B-D).*

	KO			**KO control**			
	Mean	95% CI (lower limit)	95% CI (upper limit)	Mean	95% CI (lower limit)	95% CI (upper limit)	p-value
Activity (1/s)	0.144	0.088	0.217	0.875	0.662	1.096	3.107×10^{-6}, ***
Intra-burst frequency (1/s)	1.312	1.241	1.382	1.307	1.162	1.459	0.879, ns
Active cells per slice (%)	31.771	23.758	42.109	83.588	73.129	93.793	3.326×10^{-6},***
n(animals)	6			7			
n(slices)	7			7			
n(cells)	107			83			

A18. *Calcium spike activity in KO during perfusion with 0.05 µmol/l isradipine in 1/s (Fig. 29D)*

	KO			**KO control**		
bin (min)	Activity	95% CI (lower limit)	95% CI (upper limit)	Activity	95% CI (lower limit)	95% CI (upper limit)
-3	1.223	1.105	1.346	1.173	1.025	1.313
-2.5	1.304	1.195	1.418	1.175	1.027	1.32
-2	1.314	1.197	1.431	1.25	1.121	1.378
-1.5	1.278	1.157	1.4	1.231	1.096	1.366
-1	1.253	1.137	1.371	1.267	1.142	1.393
-0.5	1.213	1.087	1.34	1.218	1.096	1.339
0	1.194	1.067	1.321	1.194	1.081	1.304
0.5	1.207	1.085	1.33	1.088	0.956	1.218
1	1.086	0.962	1.209	1.108	0.96	1.255
1.5	0.887	0.767	1.009	1.094	0.943	1.245
2	0.872	0.749	0.999	1.112	0.965	1.259
2.5	0.884	0.766	1.005	1.123	0.986	1.256
3	0.799	0.678	0.925	1.058	0.923	1.191
3.5	0.614	0.509	0.72	1.073	0.943	1.198
4	0.505	0.402	0.613	0.984	0.855	1.107
4.5	0.457	0.362	0.559	0.945	0.798	1.09
5	0.316	0.231	0.408	0.963	0.831	1.098
5.5	0.271	0.191	0.356	0.969	0.843	1.098
6	0.198	0.131	0.27	0.894	0.753	1.036
6.5	0.218	0.147	0.292	0.948	0.809	1.09
7	0.141	0.087	0.203	0.898	0.756	1.042
7.5	0.115	0.064	0.175	0.855	0.725	0.992

A19. *Calcium spike activity in WT during perfusion with 0.05 µmol/l isradipine in 1/s (Fig. 29D)*

	WT			**WT control**		
bin (min)	Activity	95% CI (lower limit)	95% CI (upper limit)	Activity	95% CI (lower limit)	95% CI (upper limit)
-3	0.544	0.474	0.617	0.643	0.588	0.7
-2.5	0.559	0.487	0.632	0.643	0.59	0.699
-2	0.597	0.527	0.669	0.632	0.583	0.681
-1.5	0.649	0.582	0.719	0.655	0.608	0.704
-1	0.63	0.564	0.698	0.638	0.588	0.686
-0.5	0.562	0.496	0.631	0.612	0.566	0.658
0	0.563	0.503	0.625	0.592	0.547	0.636
0.5	0.53	0.467	0.596	0.518	0.468	0.568
1	0.492	0.424	0.563	0.473	0.423	0.524
1.5	0.493	0.433	0.556	0.452	0.404	0.504
2	0.468	0.405	0.536	0.45	0.4	0.501
2.5	0.375	0.315	0.437	0.441	0.396	0.489
3	0.342	0.284	0.402	0.443	0.396	0.492
3.5	0.368	0.311	0.428	0.439	0.393	0.487
4	0.382	0.323	0.443	0.417	0.372	0.464
4.5	0.388	0.327	0.451	0.444	0.397	0.491
5	0.371	0.31	0.433	0.446	0.402	0.491
5.5	0.361	0.298	0.424	0.427	0.382	0.473
6	0.343	0.285	0.404	0.426	0.38	0.473
6.5	0.361	0.308	0.415	0.434	0.388	0.481
7	0.373	0.314	0.435	0.428	0.381	0.476
7.5	0.387	0.324	0.452	0.361	0.316	0.408

A20. *Statistical information of absolute intra-burst frequency (1/s) at 0 µmol/l isradipine in remaining active WT, KO and corresponding control slices (Fig. 30C-D).*

	WT			**WT control**			
	Mean	95% CI (lower limit)	95% CI (upper limit)	Mean	95% CI (lower limit)	95% CI (upper limit)	p-value
Intra-burst frequency (1/s)	0.868	0.670	1.078	0.960	0.841	1.114	0.2939, ns
	KO			**KO control**			
Intra-burst frequency (1/s)	1.363	1.218	1.507	1.410	1.291	1.533	0.4994, ns

A21. *Calcium spike activity during perfusion with 5 µmol/l TTA-P2 and 300 nmol/l isradipine in 1/s (Fig. 31B).*

	WT			**WT control**		
Bins (min)	Activity	95% CI (lower limit)	95% CI (upper limit)	Activity	95% CI (lower limit)	95% CI (upper limit)
-4	0.619	0.578	0.661	0.697	0.645	0.747
-3	0.571	0.536	0.607	0.674	0.62	0.729
-2	0.522	0.486	0.561	0.642	0.591	0.695
-1	0.545	0.511	0.579	0.624	0.577	0.672
0	0.518	0.485	0.553	0.58	0.539	0.62
1	0.439	0.399	0.481	0.472	0.425	0.521
2	0.282	0.241	0.324	0.443	0.398	0.491
3	0.226	0.189	0.264	0.44	0.397	0.483
4	0.199	0.159	0.242	0.4	0.358	0.443
5	0.17	0.131	0.211	0.414	0.371	0.459
6	0.155	0.119	0.192	0.39	0.347	0.434
7	0.135	0.101	0.169	0.405	0.36	0.453
8	0.146	0.108	0.185	0.321	0.277	0.366
9	0.097	0.067	0.129	0.325	0.283	0.368
10	0.104	0.075	0.136	0.314	0.274	0.354
11	0.097	0.067	0.131	0.315	0.274	0.355
12	0.063	0.04	0.089	0.254	0.216	0.294
13	0.039	0.022	0.059	0.301	0.258	0.344
14	0.013	0.004	0.023	0.241	0.203	0.279
15	0.003	0	0.006	0.256	0.221	0.293
16	0	0	0	0.221	0.186	0.257
17	0	0	0.001	0.225	0.191	0.261
18	0	0	0	0.21	0.175	0.246
19	0	0	0	0.218	0.181	0.256
20	0	0	0	0.201	0.165	0.237

A22. *Statistical information of absolute calcium bursting parameters at 5 µmol/l TTA-P2 in WT slices (Fig. 32A, C, E).*

	WT			**WT control**			
	Mean	95% CI (lower limit)	95% CI (upper limit)	Mean	95% CI (lower limit)	95% CI (upper limit)	p-value
Activity (1/s)	0.078	0.037	0.125	0.310	0.257	0.362	$3.248x10^{-05}$, ***
Intra-burst frequency (1/s)	1.022	0.867	1.171	0.762	0.685	0.848	0.006, **
Active cells per slice (%)	16.611	8.989	25.094	63.003	52.350	73.262	$2.371x10^{-07}$, ***
n(animals)	6			9			
n(slices)	10			10			
n(cells)	246			213			

A23. *Statistical information of absolute calcium bursting parameters at 5 µmol/l TTA-P2 and 300 nmol/l isradipine in WT slices (Fig. 32C, E).*

	WT			**WT control**			
	Mean	95% CI (lower limit)	95% CI (upper limit)	Mean	95% CI (lower limit)	95% CI (upper limit)	p-value
Activity (1/s)	0	0	0	0.208	0.153	0.262	$2.839x10^{-13}$, ***
Active cells per slice (%)	0	0	0	48.541	35.409	62.104	$5.572x10^{-09}$, ***

A24. *Statistical information of calcium bursting parameters relative to control in WT slices (Fig. 32B, D)*

	5 µmol/l TTA-P2			5 µmol/l TTA-P2 and 300 nmol/l isradipine		
	Mean	95% CI (lower limit)	95% CI (upper limit)	Mean	95% CI (lower limit)	95% CI (upper limit)
Activity (1/s)	0.250	0.12	0.402	0.001	0	0.002
Intra-burst frequency (1/s)	1.341	1.137	1.536	—	—	—

A25. *Statistical information of absolute intra-burst frequency without inhibitors of WT and WT control ZG cells that remained active during 5 µmol/l TTA-P2 and 0 nM isradipine (Fig. 32E)*

	0 µmol/l TTA-P2 and 0 nmol/l isradipine						
	WT			WT control			
	Mean	95% CI (lower limit)	95% CI (upper limit)	Mean	95% CI (lower limit)	95% CI (upper limit)	p-value
Intra-burst frequency (1/s)	0.651	0.572	0.755	0.896	0.782	1.034	0.018, *

A26. *Mean $[Ca^{2+}]_i$ during perfusion with 5 µmol/l TTA-P2 and 300 nmol/l isradipine at various Ang II concentrations in nmol/l in WT cells and WT control (no inhibitors) (Fig. 34A).*

	WT			**WT control**		
Bins (min)	$[Ca^{2+}]_i$	95% CI (lower limit)	95% CI (upper limit)	$[Ca^{2+}]_i$	95% CI (lower limit)	95% CI (upper limit)
-4	864.549	836.929	892.926	888.099	854.841	922.111
-3	865.652	838.906	893.437	891.308	858.863	924.363
-2	869.298	841.805	897.773	885.136	853.188	916.859
-1	868.608	840.997	896.654	898.190	865.840	930.566
0	867.532	840.128	895.610	898.049	866.559	929.423
1	870.386	842.817	898.588	930.176	894.131	966.837
2	902.025	871.246	933.615	983.125	939.729	1027.534
3	954.147	917.252	991.973	1000.043	960.741	1040.524
4	977.727	940.114	1016.438	1032.237	988.984	1076.662
5	983.641	946.009	1022.706	1036.660	991.294	1082.005
6	973.729	939.878	1008.134	1108.969	1058.135	1159.981
7	971.776	939.103	1005.421	1058.114	1011.845	1107.226
8	998.934	960.843	1037.959	1036.406	993.498	1080.996
9	983.862	943.155	1026.580	1043.866	1004.186	1085.725
10	1006.429	966.100	1049.140	1023.154	978.285	1070.870
11	973.993	938.483	1010.298	1027.249	981.977	1075.130
12	909.260	881.889	936.394	1034.765	989.021	1083.589
13	871.519	845.934	897.578	980.283	943.726	1017.967
14	862.802	836.559	888.990	998.539	963.245	1035.649
15	850.449	824.585	876.181	1000.975	964.852	1038.451
16	846.927	821.062	872.230	975.663	935.696	1017.947
17	841.812	817.417	865.882	996.340	954.660	1038.854
18	843.909	819.944	867.792	1000.799	963.758	1040.706
19	842.062	818.451	865.552	953.245	917.400	989.815
20	838.415	815.881	861.054	971.624	933.894	1010.200
21	832.643	810.607	855.098	986.278	948.122	1024.644
22	847.909	824.713	871.310	1046.175	1008.910	1083.971
23	854.322	831.536	877.100	1050.743	1010.929	1090.409
24	852.572	830.638	874.356	1053.052	1016.071	1090.860
25	842.792	821.377	863.782	1099.930	1063.676	1136.284
26	834.369	813.755	855.144	1079.310	1043.213	1115.221
27	823.902	804.253	843.816	1067.017	1030.410	1103.287
28	817.811	798.443	837.846	1075.528	1042.072	1109.497
29	816.627	798.123	835.755	1069.909	1037.969	1102.267
30	793.104	765.087	824.458	1057.602	1024.909	1090.494

A27. *Mean baseline $[Ca^{2+}]_i$ during perfusion with 5 µmol/l TTA-P2 and 300 nmol/l isradipine at various Ang II concentrations in nmol/l in WT cells and WT control (no inhibitors) (Fig. 34A).*

	WT			**WT control**		
Bins (min)	Baseline $[Ca^{2+}]_i$	95% CI (lower limit)	95% CI (upper limit)	Baseline $[Ca^{2+}]_i$	95% CI (lower limit)	95% CI (upper limit)
-4	859.876	831.604	888.505	873.027	841.843	903.763
-3	859.027	832.326	885.803	881.753	851.764	912.312
-2	861.425	834.133	889.481	881.066	848.904	912.596
-1	858.330	831.529	885.791	892.199	860.664	923.614
0	857.752	830.754	885.190	891.762	860.330	922.837
1	862.609	834.929	891.073	911.551	877.542	944.952
2	879.763	850.252	910.233	939.589	900.227	978.250
3	900.661	867.702	934.623	949.212	914.233	985.023
4	897.787	865.578	930.691	950.418	912.135	987.185
5	905.287	872.870	938.693	943.250	908.057	978.630
6	908.940	876.583	941.743	946.982	905.857	987.722
7	908.073	875.425	941.506	947.290	910.585	984.288
8	890.809	859.109	923.233	929.640	893.946	965.165
9	881.171	851.287	912.028	928.225	894.580	962.347
10	885.196	852.928	917.900	930.274	895.200	965.148
11	895.400	865.839	925.796	935.826	900.910	969.836
12	875.110	847.987	902.721	923.621	890.759	955.517
13	862.243	836.134	888.658	920.755	887.167	954.410
14	856.032	829.443	882.551	922.507	891.196	954.264
15	848.399	822.093	874.735	930.808	897.592	964.449
16	846.078	820.242	871.507	924.076	891.323	957.127
17	841.812	817.417	865.882	922.972	889.397	956.285
18	843.909	819.944	867.792	930.758	899.708	961.392
19	842.062	818.451	865.552	926.340	893.172	960.548
20	838.415	815.881	861.054	931.187	895.798	966.774

A28. *Absolute mean $[Ca^{2+}]_i$ during perfusion with 5 µmol/l TTA-P2 and 300 nmol/l isradipine at various Ang II concentrations in WT cells compared to control (no blocker) (Fig. 34B).*

		WT			**WT control (no blocker)**			
Ang II (pmol/l)	**Blocker**	$[Ca2+]_i$	95% CI (lower limit)	95% CI (upper limit)	$[Ca2+]_i$	95% CI (lower limit)	95% CI (upper limit)	p-value
0	**-**	841.533	747.795	915.955	903.262	885.679	925.200	0.274, ns
100	**-**	951.938	822.231	1077.177	1024.507	967.314	1096.333	0.391, ns
100	**+**	817.096	733.205	900.988	968.964	917.150	1000.945	0.015, *
500	**+**	806.556	751.552	857.652	1072.202	1067.126	1077.279	$1.109*10^{-05}$, ***
n(animals)		5			3			
n(slices)		5			4			
n(cells)		117			69			

A29. *. Percentage of time spent bursting during perfusion with 5 µmol/l TTA-P2 and 300 nmol/l isradipine at various Ang II concentrations in WT and untreated control cells (no blocker) (Fig. 34C).*

		WT			**WT control (no blocker)**		
Ang II (pmol/l)	**Blocker**	%	95% CI (lower limit)	95% CI (upper limit)	%	95% CI (lower limit)	95% CI (upper limit)
0	**-**	5.953	2.642	9.800	4.101	1.382	7.683
100	**-**	44.323	40.082	48.493	39.547374	33.858	45.371
100	**+**	-	-	-	27.025	20.822	33.775
500	**+**	-	-	-	51.571	43.432	59.649

Cacna1h KI data

A30. *Mean $[Ca^{2+}]_i$ in ZG cells of Cacna1h WT and KI adrenal slices (Fig. 35A)*

		***Cacna1h* WT**			***Cacna1h* KI**			
K^+	Ang II(pmol/l)	Mean (nmol/l)	SD (nmol/l)	n(cells)	Mean (nmol/l)	SD (nmol/l)	n(cells)	p-value
3	0	767.8	262.0	125	936.5	181.3	139	0.0255, *
3	20	749.9	229.4	125	905.6	156.2	109	0.0058, **
3	1000	763.0	199.5	125	1098.2	291.0	124	< 0.0001, ***
5	0	805.1	192.1	105	1219.6	266.2	125	0.0002, ***
5	20	769.5	164.2	105	1163.2	269.9	125	0.0003, ***
5	1000	921.2	231.1	105	1484.4	441.2	138	0.0015, **

A31. *Spiking activity in ZG cells of Cacna1h WT and KI adrenal slices (Fig. 35B)*

		***Cacna1h* WT**			***Cacna1h* KI**			
K^+	Ang II(pmol/l)	Mean (1/s)	SD (1/s)	n(cells)	Mean (1/s)	SD (1/s)	n(cells)	p-value
3	0	0.001	0.005	88	0.002	0.013	106	Not Tested
3	20	0.005	0.016	88	0.001	0.007	92	0.05709
3	1000	0.041	0.045	88	0.028	0.044	99	0.0442, *
5	0	0.000	0.002	79	0.002	0.011	117	Not Tested
5	20	0.018	0.035	79	0.015	0.039	117	0.9542
5	1000	0.146	0.095	79	0.100	0.087	128	0.0313, *

A32. *Intraburst-Frequency in ZG cells of Cacna1h WT and KI adrenal slices (Fig. 35C)*

		***Cacna1h* WT**			***Cacna1h* KI**			
K^+	Ang II	Mean (1/s)	SD (1/s)	n(cells)	Mean (1/s)	SD (1/s)	n(cells)	p-value
3	20	0.36	0.12	52	0.36	0.12	9	0.8695
3	1000	0.36	0.11	295	0.28	0.08	165	0.0026, **
5	20	0.35	0.09	101	0.31	0.08	170	0.0114, *
5	1000	0.34	0.09	756	0.29	0.08	773	0.0013, **

A33. *Burst length in ZG cells of Cacna1h WT and KI adrenal slices (Fig. 35D)*

		***Cacna1h* WT**			***Cacna1h* KI**			
K^+	Ang II	Mean (s)	SD (s)	n(cells)	Mean (s)	SD (s)	n(cells)	p-value
3	20	17.18	20.72	52	26.43	24.91	9	0.2245
3	1000	23.19	25.90	295	23.34	32.11	165	0.9562
5	20	29.84	39.45	101	25.27	37.93	170	0.3430
5	1000	33.70	50.07	756	27.99	43.09	773	0.0428, *

A34. *Number of burst in ZG cells of Cacna1h WT and KI adrenal slices (Fig. 35E)*

		***Cacna1h* WT**			***Cacna1h* KI**			
K^+	Ang II	Mean (1/s/cell)	SD (1/s/cell)	n(cells)	Mean (1/s/cell)	SD (1/s/cell)	n(cells)	p-value
3	20	0.0011	0.0036	100	0.0001	0.0008	92	0.0414 (*)
3	1000	0.0066	0.0075	100	0.0033	0.0048	99	0.0152 (*)
5	20	0.0023	0.0045	98	0.0021	0.0059	117	0.8464
5	1000	0.0166	0.0115	98	0.0125	0.0114	128	0.0334 (*)

A35. *Baseline $[Ca^{2+}]_i$ in ZG cells of Cacna1h WT and KI adrenal slices (Fig. 36)*

		***Cacna1h* WT**			***Cacna1h* KI**			
K^+	Ang II	Mean (nmol/l)	SD (nmol/l)	n(cells)	Mean (nmol/l)	SD (nmol/l)	n(cells)	p-value
3	0	767.1	261.2	125	927.8	157.3	139	0.0260, *
3	20	748.1	229.1	125	904.7	156.0	109	0.0056, **
3	1000	739.1	203.9	125	1077.3	291.2	124	<0.0001, ***
5	0	804.9	191.5	105	1216.5	269.3	125	0.0003, ***
5	20	760.1	161.6	105	1159.8	269.5	125	0.0003, ***
5	1000	845.2	232.9	100	1445.2	481.4	135	0.0015, **

A36. *Peak $[Ca^{2+}]_i$ in ZG cells of Cacna1h WT and KI adrenal slices (Fig. 36)*

		***Cacna1h* WT**			***Cacna1h* KI**			
K^+	Ang II	Mean (nmol/l)	SD (nmol/l)	n(cells)	Mean (nmol/l)	SD (nmol/l)	n(cells)	p-value
3	0	1101.6	443.4	7	1386.2	654.9	10	Not tested
3	20	897.1	289.1	17	1263.9	135.5	6	0.0150, *
3	1000	941.5	206.4	90	1433.3	396.1	79	<0.0001, ***
5	0	1206.8	254.6	3	1531.8	475.7	12	Not tested
5	20	1064.6	191.2	46	1505.1	332.5	28	0.0084, **
5	1000	1080.4	216.2	88	1702.8	542.9	111	0.0040, **

A37. *Mean activation time constants of a calcium spike events in ZG cells of Cacna1h WT and KI adrenal slices (Fig.37B)*

		***Cacna1h* WT**			***Cacna1h* KI**			
K^+	Ang II(pmol/l)	Mean (s)	SD (s)	n(cells)	Mean (s)	SD (s)	n(cells)	p-value
3	1000	0.024	0.010	104	0.029	0.012	126	0.1235
5	1000	0.023	0.007	141	0.039	0.013	325	0.2373

A38. *Mean deactivation time constants of a calcium spike events in ZG cells of Cacna1h WT and KI adrenal slices (Fig.37C)*

		***Cacna1h* WT**			***Cacna1h* KI**			
K^+	Ang II(pmol/l)	Mean (s)	SD (s)	n(cells)	Mean (s)	SD (s)	n(cells)	p-value
3	1000	0.810	0.378	102	0.609	0.160	126	0.3705
5	1000	0.813	0.406	141	0.771	0.359	323	0.9008

Cacna1d KI data

A39. *Mean overall and baseline $[Ca^{2+}]_i$ in ZG cells of Cacna1d WT and KI adrenal slices treated with different isradipine concentrations(Fig. 39).*

	***Cacna1d* WT**				***Cacna1d* KI**			
Isradipin (nmol/l)	n (slices)	n (cells)	$[Ca^{2+}]_i$ ± SD (nmol/l)		n (slices)	n (cells)	$[Ca^{2+}]_i$ ± SD (nmol/l)	
			Mean	Baseline			Mean	Baseline
0	12	143	986.8 ± 164.6	851.5 ± 139.7	9	85	1119.1 ± 204.7	1014.0 ± 184.5
50	12	143	997.0 ± 142.5	863.4 ± 132.6	9	85	998.0 ± 153.3	948.2 ± 151.2
300	12	143	946.7 ± 184.4	885.2 ± 170.3	9	85	975.0 ± 184.4	918.3 ± 167.6

A40. *Time spent on rotating rod of Cacna1d WT and KI mice treated with isradipine or placebo (Fig. 40A).*

	***Cacna1d* WT**		***Cacna1d* KI**	
	Control	Treated	Control	Treated
Mean ± SD (s)	96.1 ± 47.0	88.1 ± 43.7	10.4 ± 9.7	17.5 ± 16.3
n(animals)	11	11	9	9

A41. *Tracklength of Cacna1d WT and KI mice treated with isradipine or placebo during the open field test (Fig. 40B).*

	***Cacna1d* WT**		***Cacna1d* KI**	
	Control	Treated	Control	Treated
Mean ± SD (m)	43.43 ± 7.43	44.89 ± 4.84	45.48 ± 16.26	42.27 ± 11.69
n(animals)	11	11	9	9

A42. *Nest score of Cacna1d WT and KI mice treated with isradipine or placebo during the nest building test (Fig. 40C).*

	***Cacna1d* WT**		***Cacna1d* KI**	
	Control	Treated	Control	Treated
Mean ± SD (score)	3.8 ± 1.03	4.09 ± 0.77	1.56 ± 0.39	1.89 ± 0.78
n(animals)	11	11	9	9

A43. *Absolute aldosterone concentrations in blood serum samples of Cacna1d WT and KI mice treated with isradipine or placebo (Fig. 40D-E).*

	***Cacna1d* WT**		***Cacna1d* KI**	
	Control	Treated	Control	Treated
Mean ± SD (pg/ml)	286.75 ± 128.97	522.26 ± 628.92		917.58 ± 973.37
n(animals)	11	10	9	9

List of Abbreviations and Acronyms

A44. *List of Abbreviationsand Acronyms*

Abbreviations and acronyms	Meaning
ACE	Angiotensin-converting enzyme
Agtr1a	Gene name of the angiotensin II type 1a receptor in mice
AM	Acetoxymethyl group
Ang II	Angiotensin II
APA	Aldosterone-producing adenoma
AT1R	Angiotensin II receptor type 1
ATP1A1	Gene name of the α1-subunit of the Na^+/K^+-ATPase in humans
ATP2B3	Gene name of the Plasma membrane Ca^{2+}-transporting ATPase 3 in humans
BBS	Bicarbonate bufferd solution
$[Ca^{2+}]_i$	Intracellular calcium concnetration
CACNA1A-I, S/ Cacna1a-i, s	Gene names of the α1-subunits of VGCCs in humans (upper-case letters) and mice (lower-case letters)
Ca_V	α1-subunits of VGGCs
CI	Confidence Interval
CLCN2/Clcn2	Gene name of the ClC-2 chloride channel in humans (upper-case letters) and mice (lower-case letters)
CYP11B2/Cyp11b2	Gene name of the Aldosterone synthase in humans (upper-case letters) and mice (lower-case letters)
Cytopl.	Cytoplasmatic
DAG	Diacylglycerol
DEG	Differentially expressed genes
DHP	Dihydropyridine
DI-DIV	Homologous domains I-IV in VGCCs
ELISA	Enzyme-linked immunosorbent assay
ER	Endoplasmatic reticulum
Extracell.	Extracellular
f	Female
FH	Familial hyperaldosteronism
Het	Heterozygous
HVA	High-voltage-activated
IP_3	Inositol 1,4,5-trisphosphate
IVF	In vitro fertilization

A44. *List of Abbreviationsand Acronyms*

Abbreviations and acronyms	Meaning
KCNJ5	Gene name of the G protein-activated inward rectifier potassium channel 4 (GIRK-4, Kir3.4) in humans
KI	Knockin
KO	Knockout
LFC	Log_2-fold change
LVA	Low-voltage-activated
m	male
NMD	Nonsense-mediated decay
PA	Primary (hyper)aldosteronism
PASNA	Primary aldosteronism, seizures, and neurologic abnormalities
PIP_2	Phosphatidylinositol 4,5-bisphosphate
PLC	Phospholipase C
RAAS	Renin-Angitensin-Aldosterone-System
RT	Room temperature
S1-S6	Transmembrane helices 1-6 in VGCCs
SD	Standard deviation
StAR	Steroidogenic acute regulatory protein
TASK	TWIK-related acid-sensitive K^+ channels
TM	Transmembrane
TWIK	Weak Inward rectifying K^+ channel.
VGCC	Voltage-gated calcium channels
WT	Wild-type
y	years
ZF	Zona fasciculata
ZG	Zona glomerulosa
ZR	Zona fasciculata

Publications

- Seidel, E., Schewe, J., Zhang, J., **Dinh, H. A.**, Forslund, K., Markó, L., Hellmig, N., Peters, J., Müller, D., Lifton, R. P., Nottoli, T., Stölting, G. & Scholl, U. I. (2021). Enhanced Ca^{2+}signaling, mild primary aldosteronism, and hypertension in a familial hyperaldosteronism mouse model (*Cacna1h*$^{M1560V/+}$). *Proceedings of the National Academy of Sciences of the United States of America, 118(17).* doi.org/10.1073/pnas.2014876118
- **Dinh, H. A.***, Stölting, G.* & Scholl, U. I. (2023). $Ca_V3.2$ (*CACNA1H*) in primary aldosteronism. *In Handbook of experimental pharmacology (S. 249–262).* doi.org/10.1007/164_2023_660
- Stölting, G.*, **Dinh, H. A.***, Volkert, M.*, Hellmig, N., Schewe, J., Hennicke, L., Seidel, E., Oberacher, H., Zhang, J., Lifton, R. P., Urban, I., Long, M., Rivalan, M., Nottoli, T. & Scholl, U. I. (2023). Isradipine therapy in *Cacna1d*$^{Ile772Met/+}$ mice ameliorates primary aldosteronism and neurologic abnormalities. *JCI insight.* doi.org/10.1172/jci.insight.162468
- **Dinh, H. A.**, Volkert, M., Secener, A. K., Scholl, U. I. & Stölting, G. (2023). T- and L-type calcium channels maintain calcium oscillations in the murine zona glomerulosa. *bioRxiv [Preprint].* doi.org/10.1101/2023.06.09.544326

* shared first authorship

Oral presentations at scientific conferences

- "$Ca_V3.2$ knock-out mice still exhibit calcium oscillations in the zona glomerulosa", Europhysiology 2022, Copenhagen
- "$Ca_V3.2$ knock-out mice still exhibit calcium oscillations in the zona glomerulosa", Progress in Primary Aldosteronism 7, 2022, Munich
- "T- and L-type calcium channels maintain calcium oscillations in the murine zona glomerulosa", 12th Symposium of the Young Physiologists, 2023, Kiel
- "T- and L-type calcium channels maintain calcium oscillations in the murine zona glomerulosa", 102nd Annual Meeting of the German Physiological Society, 2023, Berlin

Acknowledgement

I would like to take the opportunity to express my gratitude to all the people whose support and guidance have been instrumental in the completion of this dissertation. Their contributions have enriched my academic journey and shaped the outcome of this research.

Foremost among these contributors is Professor Dr. Thomas Friedrich to whom I extend my sincere appreciation for graciously undertaking the role of supervising my Ph.D. project. I am grateful for his insightful input and guidance at every stage of this dissertation, from project initiation to its completion.

I also express my profound gratitude to Professor Dr. Ute Scholl for welcoming me into her research group and providing me with the opportunity to contribute to diverse projects. I am grateful for her invaluable advice and support, especially in experimental design, as well as her constructive criticism during publication processes.

Moreover, I would like to express my gratitude to Prof. Dr. Andrew Plested for graciously agreeing to join my doctoral committee.

Special acknowledgment is due to Dr. Gabriel Stölting for his mentorship throughout my Ph.D. His tireless support, constant availability, and trust in my abilities have played a crucial role in my academic growth. I am thankful for his mentorship across various domains, including physiology, fluorescence microscopy, electrophysiology, and data presentation and analysis.

My gratitude extends to the members and alumni of AG Scholl, including Marina Volkert, Nicole Hellmig, Luise Hennicke, Iana Lukianova, Janek Haus, Kieu Nhi Tran Vo, Dr. Julia Schewe, Dr. Eric Seidel, Sarah Döring, Nico Brüssow, Marie Cotta, and Ana Lucía Huitrón for fostering a collaborative environment in the lab. Their support throughout this project, including animal breeding, genotyping, and various laboratory tasks, has been invaluable. Their camaraderie has made our lab a unique space filled with joy and a collective enthusiasm for research.

A heartfelt note of appreciation goes to Marina Volkert for sharing both office and lab space, and for navigating the challenges of a Ph.D. journey alongside me. Her support, particularly in providing research animals during the early morning hours, has been indispensable.

I would like to express my sincere gratitude to my family, particularly my parents, for their constant support. Finally, I extend my heartfelt thanks to my husband, Jasper, whose continuous encouragement and perspective have been essential throughout this period.